Study of the interaction between the oligomers from bio-oil heavy fraction and a catalyst in hydrotreatment process

Raiza Johanna Manrique Waldo

Study of the interaction between the oligomers from bio-oil heavy fraction and a catalyst in hydrotreatment process

Raiza Johanna Manrique Waldo

Thesis submitted in partial fulfillment of the requirements for the degree of:

Doctor of Philosophy

Advisor:

Ph.D. Farid Chejne Janna

Co-advisor:

Ph.D. Manuel García-Pérez

Research topic:

Valorization of the pyrolytic lignin

Research group:

Applied Thermodynamics and Alternative Energies - TAYEA

Universidad Nacional de Colombia

Facultad, Departamento de procesos y energía

Medellín, Colombia

2023

To the one and only, Camilo Uribe
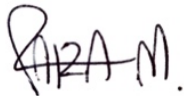
Declaración de obra original

Yo declaro lo siguiente:

He leído el Acuerdo 035 de 2003 del Consejo Académico de la Universidad Nacional. «Reglamento sobre propiedad intelectual» y la Normatividad Nacional relacionada al respeto de los derechos de autor. Esta disertación representa mi trabajo original, excepto donde he reconocido las ideas, las palabras, o materiales de otros autores.

Cuando se han presentado ideas o palabras de otros autores en esta disertación, he realizado su respectivo reconocimiento aplicando correctamente los esquemas de citas y referencias bibliográficas en el estilo requerido.

He obtenido el permiso del autor o editor para incluir cualquier material con derechos de autor (por ejemplo, tablas, figuras, instrumentos de encuesta o grandes porciones de texto).

Por último, he sometido esta disertación a la herramienta de integridad académica, definida por la universidad.

_____

Raiza Manrique

Fecha 25/01/2023

Acknowledgments

The author wishes to thank:

Abstract

Study of the interaction between the oligomers from bio-oil heavy fraction and a catalyst in hydrotreatment process

Biomass fast pyrolysis bio-oil is a promising alternative to be used as a source of fuels and chemicals. It hosts a wide variety of compounds and comes from renewable sources. Pyrolysis oil is formed by water, light organics (GC/MS detectable compounds), Oligomeric fractions derived from lignin and holocellulose. This dissertation focusses on the identification of oligomeric molecules in the pyrolytic lignin fraction and its catalytic hydro-deoxygenation. This fraction can potentially be used to produce fuels and chemicals via hydrodeoxygenation. The chemical structure of pyrolytic lignin oligomeric molecules is poorly known. In this study, quantum mechanical simulation was used to propose the structures based on calculations of the electronic structure. The DFT calculations were used to identify the thermodynamically most probable chemical structures of pyrolytic lignin molecules resulting from lignin pyrolysis followed by demethylation. The structure of new molecules of dimer, trimer and tetramer oligomers from pyrolytic lignin were proposed. The pyrolytic lignin fraction was further fractionated by solid-liquid extraction and the resulting subfraction thoroughly characterized using FTIR, UV-fluorescence and HSQC-NMR. Ethyl acetate subfractions was characterized by phenolic compounds with methoxyl substituents while acetone and isopropanol subfractions showed more aliphatic characteristics. Pyrolytic lignin fraction from BTG was hydrotreated with a sulfided NiMo/Al$_2$O$_3$ catalyst. Hydrotreating experiments were carried out with mixtures of pyrolytic lignin and yellow grease to obtain liquid fuels. All blends induced coke formation values between 0.7 and 2.5 wt. %, indicating that pyrolytic lignin has potential to reduce coke formation during the process. The results obtained in this thesis will allow the definition of strategies for the design of biorefineries including pyrolytic lignin to obtain products.

Keywords: Pyrolysis bio-oil, pyrolytic lignin, oligomers, structures, fractionation, bio-oil upgrading

Resumen

Estudio de la interacción entre los oligómeros de la fracción pesada del bioaceite de pirólisis rápida y un catalizador en el proceso de hidrotratamiento

El bioaceite de pirólisis rápida de biomasa es una alternativa prometedora para ser utilizada como fuente de combustibles y productos químicos. Alberga una amplia variedad de compuestos y proviene de fuentes renovables. El aceite de pirólisis está formado por agua, compuestos orgánicos ligeros (compuestos detectables por GC/MS), fracciones oligoméricas derivadas de la lignina y holocelulosa. Esta tesis se centra en la identificación de moléculas oligoméricas en la fracción pirolítica de lignina y su hidrodesoxigenación catalítica. Esta fracción se puede utilizar potencialmente para la producción de combustibles y productos químicos a través de la hidrodesoxigenación. La estructura química de las moléculas oligoméricas de lignina pirolítica es poco conocida. En este estudio, se utilizó simulación mecánica cuántica para proponer las estructuras basadas en cálculos de la estructura electrónica. Los cálculos DFT se utilizaron para identificar las estructuras químicas termodinámicamente más probables de las moléculas de lignina pirolítica resultantes de la pirólisis de lignina seguida de desmetilación. Se propuso la estructura de nuevas moléculas de oligómeros dímeros, trímeros y tetrámeros a partir de lignina pirolítica. La fracción de lignina pirolítica se fraccionó adicionalmente mediante extracción sólido-líquido y la subfracción resultante se caracterizó minuciosamente usando FTIR, UV-fluorescencia, HSQC-NMR. Las subfracciones de acetato de etilo se caracterizaron por compuestos fenólicos con sustituyentes metoxilo, mientras que la subfracción de acetona e isopropanol mostró características más alifáticas. Se realizó el hidrotratmiento de la fracción de lignina pirolítica de BTG con un catalizador de NiMo/Al$_2$O$_3$ sulfurado. Se realizaron experimentos de hidrotratamiento con mezclas de lignina pirolítica y grasa amarilla para obtener combustibles líquidos. Todas las mezclas obtuvieron valores de formación de coque entre 0,7 y 2,5 en peso. %, lo que indica que la lignina pirolítica tiene potencial para reducir la formación de coque durante el proceso. Los resultados obtenidos en esta tesis permitirán definir estrategias para el diseño de biorrefinerías que incluyan lignina pirolítica para la obtención de productos.

Palabras clave: Bioaceite de pirólisis, lignina pirolítica, oligómeros, estructuras, fraccionamiento, mejoramiento del bioaceite.

Index

List of figures

List of tables

Pág.

1. Introduction

1.1 Background

Petroleum fuels have contributed to 4 % in the early 20th century to 40% of the world's energy demand. Additionally, 96 % of transportation fuels are also derived from crude petroleum reserves [1]. Petroleum-based fuels are non-renewable and bear an environmental challenge due to the generation of carbon dioxide and other pollutants. Fossil-based CO_2 emissions reached 37.5 Gt in 2018 and have been growing at a 1.5 % per year over the past decade. Additionally, the global population will reach 9 billion by 2050, which will, in turn, increase the energy demand and potentially exacerbate these problems. The mentioned factors, among others, have created an urgency to identify sustainable feedstocks for the generation of energy, fuels, and chemicals [2].

Biomass can reduce dependence on fossil fuels and thereby contribute to the decarbonization of the economy [3]. Green technologies have the potential to generate clean energy and other value-added products. In countries with agricultural economies, the development and implementation of green technologies should be relevant for the proposition of public energy policies. For example, in Colombia the energy potential of coffee crop residues is around 46000 TJ per year [4].

Lignocellulosic biomasses consist of 40-50 % cellulose, 25-35 % hemicellulose, 15-20 % lignin, and small amount of ash and other biopolymers [5]. Cellulose is present in the cell wall of the plant cells and is a polymer composed of repeating D-glucose units, a six-carbon ring (pyranose). Hemicellulose is a heterogeneous group of branched polysaccharides, which surrounds the cellulose fibers and stands as a connecting link between cellulose and lignin. Lastly, lignin is an aromatic three dimensional and cross-linked phenol polymer, mainly present in the outer layer of the fibers which provides the rigidity the cell wall. Lignin consists of phenylpropane units joint by hydroxyl- and methoxy- substituents [6].

1.2 Bio-oil from pyrolysis of biomass

Pyrolysis is a thermal process that depolymerizes biomass in an inert atmosphere. Fast pyrolysis works at temperatures between 450-800 °C and short residence time of 0.5-10 s. These conditions prevent volatiles from participating in the secondary reactions and inhibit the primary products taking part in cracking reactions, this increasing bio-oil yields [2].

Bio-oil has some undesirable properties such as corrosiveness, thermal instability, high oxygen content, low heating value, low viscosity, and low pH. These challenges are important for the development of bio-oil refineries. The major objectives of bio-oil upgrading are to reduce the oxygen content and molecular weight of the molecules from the moisture, to increase the H/C ratio and to improve thermal stability [7]. Several upgrading processes have been proposed, such as high-pressure thermal treatment, zeolite cracking and

hydrotreatment [8]–[11]. Hydrotreatment, also known as hydrodeoxygenation (HDO), has become a promising technology which consists in subjecting the bio-oil to a heterogeneous system with hydrogen at medium temperature and high-pressure conditions (350°C and 10-30 MPa) for the elimination of the oxygen reactive functionalities. Hydrotreated bio-oil is valorized in an integrated process to produce heat, power, biofuels and chemicals.

Pyrolytic lignin can be the water-insoluble fraction of pyrolysis bio-oil, the hydrophobic compounds are mainly fragments derived from the lignin [12]. Compounds derived from lignin have less oxygenated compounds [13] compared to the other biomass building blocks, making the HDO process a more attractive upgrading option. However, one of the main challenges of analytical chemistry and engineering in the characterization of bio-oil is the structure identification of the pyrolytic lignin. Additionally, pyrolytic lignin requires further depolymerization to be used as a source of biobased chemicals (such as adhesives and antibacterial [14], [15]) and fuels [16], because it has a low number of monomers and is chemically heterogeneous.

In general, the utilization of pyrolytic lignin is a difficult task because there is a lack of understanding of many process variables, such as the pyrolytic lignin oligomers structures, efficient fractionation methods to separate pyrolytic lignin, and the coke formation during the upgrading of bio-oil fractions and its potential for the extraction of high value chemicals.

1.3 Objectives

The thesis "Study of the interaction between the heavy fraction oligomers from pyrolysis bio-oil and the catalyst in the hydrotreatment process" has the general objective to evaluate the hydrotreatment of the pyrolytic lignin fraction of bio-oil from fast pyrolysis.

The development of this objective was based on proposing a different oligomer structure (dimer, trimer, tetramers) using two different pathways where the molecules take hydrogen from the media or from themselves to achieve a mass balance. Afterwards, demethylation occurs. These two pathways were analyzed through DFT modeling based on the electronic structure calculations. Additionally, the FTIR and NMR spectra of the oligomers were obtained through Gaussian simulations and the thermophysical properties were estimated using several group contribution methods. All the collected information could be used for the design of pyrolysis equipment such as condensers and reactors.

Then, pyrolytic lignin was subjected to separation and isolation of the heavy fraction of bio-oil using liquid-liquid extraction and solid-liquid chromatography. Pyrolytic lignin and four subfractions: ethyl acetate, acetone, isopropanol, and methanol, were characterized to identify characteristics of each subfraction using FTIR (Fourier Transform Infrared Spectroscopy), NMR (Nuclear Magnetic Resonance), UV-fluorescence, and HSQC (Heteronuclear Single Quantum Coherence) – NMR techniques.

Finally, mixtures of pyrolytic lignin and yellow grease were co-processed to analyze the effect of pyrolytic lignin concentration on the coke formation in the hydrotreating process

over a NiMo/Al$_2$O$_3$ catalyst. The hydrotreatment process was run in a Parr reactor at 7.6 MPa and 380 °C. We also evaluated properties and characteristics of the organic phase and fuels.

1.4 Dissertation structure

The thesis is divided by chapters according to Figure 1-1. The second chapter contains an overview of pyrolysis and hydrotreatment reactions. The third chapter focuses on identification of pyrolytic lignin structures using DFT calculations. The fourth chapter shows the fractionation process to obtain pyrolytic lignin and its subfractions using liquid-liquid extraction and solid-liquid chromatography. The fifth chapter presents the evaluation of co-hydrotreatment of pyrolytic lignin and yellow grease blends at different concentrations. Finally, the sixth chapter contain the conclusions and recommendations for this research.
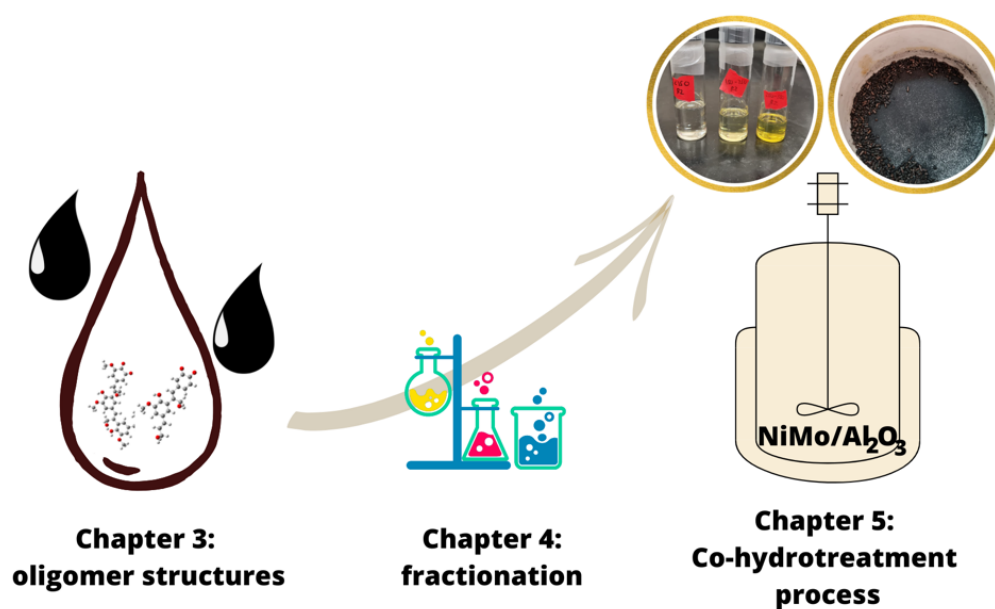
Figure 1-1. Graphical abstract of this research.

1.5 Publications

The following papers have been published or are being prepared for publication based on the work of this thesis:

o   Raiza Manrique, Evan Terrell, Pavlo Kostetskyy, Farid Chejne, Mariefel Olarte, Linda Broadbelt and Manuel García Pérez. Elucidating biomass-derived pyrolytic lignin structures from demethylation reactions through density functional theory calculations. Submitted to Energy and Fuels 2022.

o   Raiza Manrique, Farid Chejne and Manuel García-Pérez. A review of lignin reactions involved during pyrolysis and hydrotreatment process. To be submitted to Energy and Fuels.

o   Raiza Manrique, Marwan Gagaa, Myriam Rojas, Farid Chejne, Mariefel Olarte, Manuel García-Pérez and Eid Alsbou. Fractionation by liquid-liquid extraction and solid-liquid chromatography of the pyrolytic lignin from pyrolysis bio-oil. To be submitted to Energy and Fuels.

o   Raiza Manrique, Farid Chejne, Mariefel Olarte and Manuel García-Pérez. Co-hydrotreatment of pyrolytic lignin and yellow grease: effect of pyrolytic lignin concentration on coke formation yield. To be submitted to Energy and Fuels.

o   Camilo Uribe, Raiza Manrique and Farid Chejne. Fractional condensation of coffee husk pyrolysis vapor son three different surfaces. To be submitted to Brazilian Journal of Chemical Engineering.

o   Yinglei Han, Anamaria Pinheiro, Raiza Manrique, Kalidas Mainali, Sohrab Haghighi, Melba Denson, Mariefel Olarte and Manuel García-Pérez. Co-hydrotreatment of yellow greases and lignin-rich bio-oil: two-steps hydrotreatment to reduce coke and with different bio-oils. To be submitted to Energy and Fuels.

1.6 Scientific contributions

The proposed 6 dimer, 6 trimer and 6 tetramer structures (see Figure 1-2) of pyrolytic lignin oligomers based on Density Functional Theory calculations aid to elucidate how is the shape and chemical characteristics of pyrolytic lignin oligomers. Also, the determination of oligomers properties using group contribution methods is relevant for the design of pyrolysis equipment and process. Additionally, the pathways for the pyrolytic lignin could broaden the study of mechanism involved during pyrolysis of lignin.

a)

b)

c)
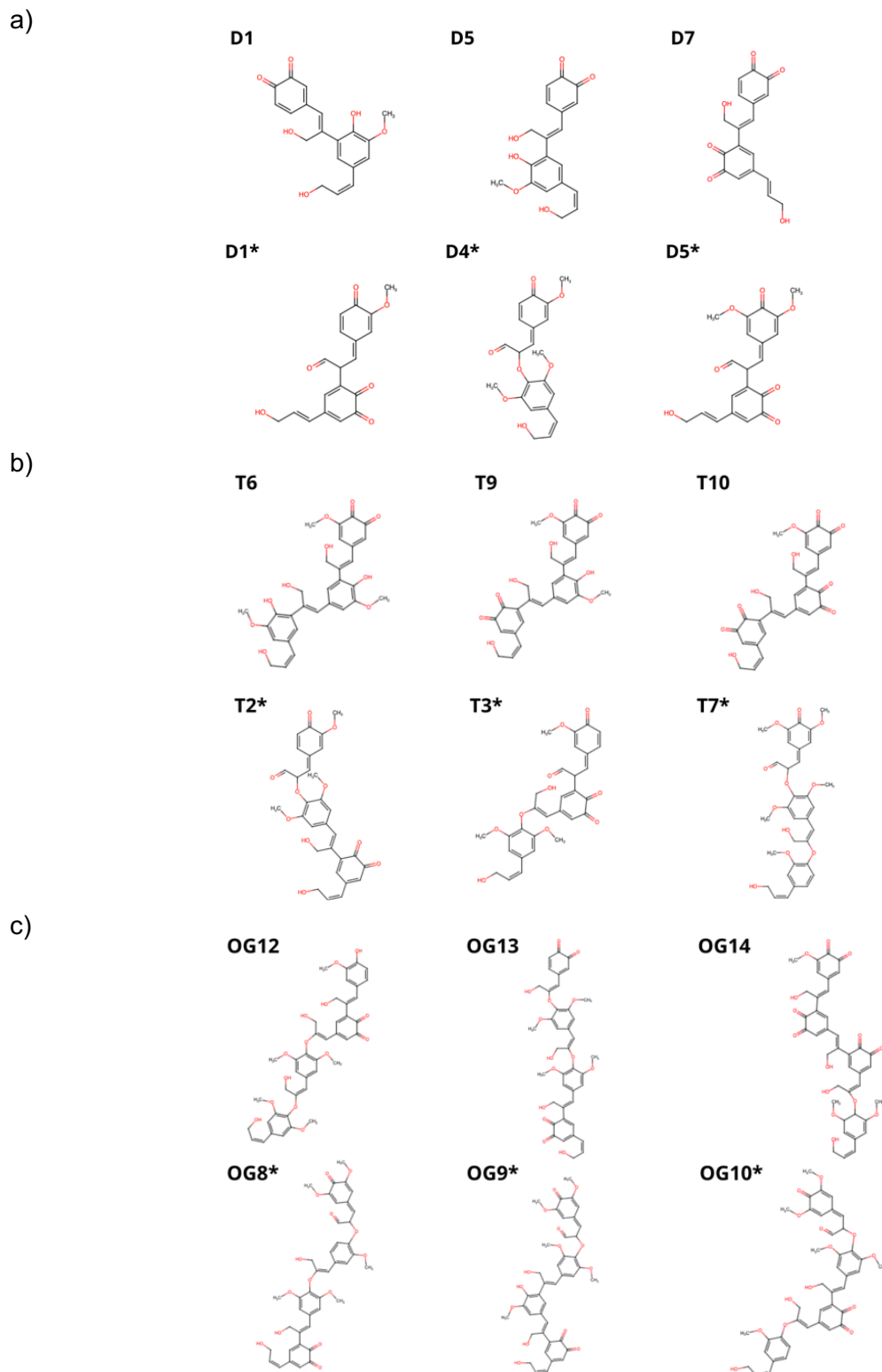
Figure 1-2. Proposed oligomers, a) dimers, b) trimers, and c) tetramers.

This work contributed to upgrade high concentrations of pyrolytic lignin (up to 40%) to produces fuels advancing the technology to produce sustainable fuels from pyrolysis oils

through co-hydrotreatment of pyrolytic lignin and yellow grease. Furthermore, we expanded the biorefinery concept to include the production of chemical, with an efficient utilization of pyrolytic lignin from pyrolysis bio-oil.

2. Lignin reactions involved during pyrolysis and hydrotreatment process

Lignocellulosic biomass is a renewable resource that can be used for the production of fuels, chemicals and materials[17]. Fast pyrolysis is a well-known process to produce bio-oil from biomass. Bio-oil obtained from fast pyrolysis of biomass is a multicomponent mixture formed mainly by oxygenated organic compounds: acids, water, alcohols, ethers, anhydrosugars, furans, phenols, aldehydes and ketones, covering a wide range of molecular weight and functionalities [18], [19]. Oxygen present in the bio-oil comes from fragments of cellulose, hemicellulose and lignin, grants unfavorable properties like high acidity, high viscosity and lower heating value; generating negative effects like corrosion and promoting soot formation when it is used as a fuel through direct combustion [20]. The high oxygen content of pyrolysis bio-oil is the principal cause of the differences in terms of properties and behavior when compared to other fuels [20]–[22]. High water and oxygen content produces in low energetic density, while the content of carbonyl and sugar molecules contribute to thermal instability during its storage and coke production during its heating [7].

2.1 What is lignin?

Lignin is the second most abundant natural polymer (after cellulose) in plants cell walls. It provides strength to plant tissues and rigidity to the cells walls because it is cross-linked with cellulose and hemicellulose via ester and ether linkages. Lignin is essential for plant defense, seed dispersion, and the formation of a diffusion barrier in the roots and mechanical support to xylem cells [23]. Lignin is different in structure and composition from cellulose and hemicellulose in biomass sources, being the only aromatic and containing (less oxygen accounting for 20-40 wt.% of the total oxygen in most biomass sources). The extracted lignin from lignocellulose biomass retains high calorific value, due to the lower oxygen-to-carbon (O/C) ratio than both cellulose and hemicellulose [24]. Lignin is a good candidate to be consider as a fuel source since its O/C ratio value is lower as compare to other sources according to Table 2-1.

Table 2-1. Comparison of the O/C and H/C ratios of various energy sources [25], [26].

	O/C ratio	H/C ratio
Crude oil	0-0.03	1.60-2.10
Lignin	0.32-0.46	1.1-1.3
Wood	>0.61	>1.4

The lignin structure is complex and still to this day not fully resolved, it is known to be amorphous and polyaromatic. It is composed of three hydroxycinnamoyl alcohol monomers: coumaryl alcohol (H), sinapyl alcohol (S) and coniferyl alcohol (G), which are

the precursors of the three lignin units in the lignin polymer chain. These units are composed by phenylpropane units, and the difference between them is the presence or absence of methoxy group (H vs. S, G) and the number and location of the methoxy group (that can be in the carbon three or five and two methoxy groups in the sides to the molecules for S unit, see Figure 2-1). However, besides these units, several phenolic compounds are also known to behave as true lignin monomers in many plants, thus increasing the complexity of the lignin polymer [27], for example lignins derived exclusively from caffeyl alcohol (C-lignin) were discovered in seed coats of vanilla orchid. The composition and structure of lignin varies among taxonomy and cell type, environmental conditions, and maturity stage [28]. In general, G-unit dominates softwood, while G and S-unit dominate hardwood plants (generally derived 50 % from G and 50 % from S units). Grass contained all three types of lignin monomers in a 40:40:20 proportion of G, S and H units [29]. Figure 2-1 shows the 3 basic units of lignin.
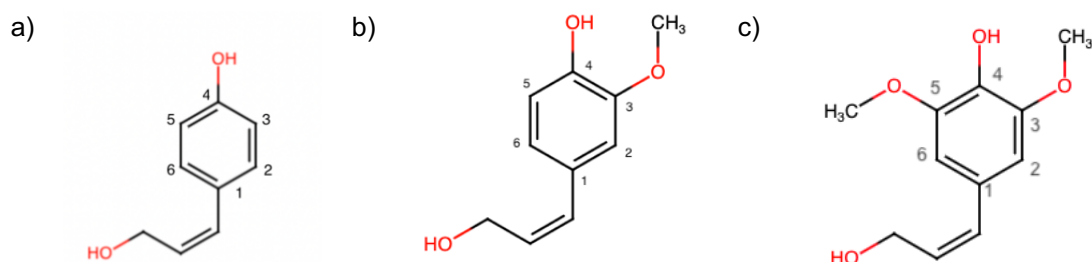
Figure 2-1. Lignin basic units a) H b) G and c) S units.

These units are the most predominant and comprise around through different bonds. There are two major linkages between these monomers: carbon-carbon linkage, also known as condensed linkages, and an ether linkage. The most predominant linkage in the lignin polymer is ether linkage representing 56 % or more of the total bonds [30]. Among these type of bonds, β-O-4 alkyl-aryl ethers represents around 50-80 % of total linkages in native lignins. Other linkages are β-5/phenylcoumarans, β-β/resinols, 5-5/dibenzodioxocins, 5-O-4/biphenyl ethers, and β-1/spirodienones [31]. Due to the different ratios of the monomers in different sources of lignin, the exact ratios of linkages are also different in various species. The distributions of these bonds in hardwood and softwood are shown in Table 2-2.

Table 2-2. Proportion of different types of linkages connecting the lignin units [30].

Linkage type	Softwood	Hardwood
β-O-4	43-50	50-65
α-O-4	6-8	4-8
4-O-5	4	6-7
β-5	9-12	4-6
5-5	10-25	4-10
β-β	2-4	3-7
β-1	3-7	5-7

The FTIR analysis presented by Wang *et al.* [32] showed that peaks related to lignin corresponded to O-H stretching vibration, C-H stretching vibration, unconjugated C=O stretching vibration, aromatic or aliphatic skeletal vibrations, aromatic ring breathing with C-O and C=O stretching vibration, conjugated C=O stretching vibrations in ester groups and carbonyl/carboxyl C=O stretching vibrations [33]–[35]. Lignin has abundant aromatic groups and can act as precursor for synthesizing fuels, chemicals, and advanced materials. These special characteristics, as compared to those of cellulose and hemicellulose, makes the lignin valorization a challenge for feasibility lignocellulosic biorefineries. In biorefineries, the aromatic structures of lignin could make of this product a great precursor aromatic compounds that could be useful for the production of related chemicals.

2.2 Pyrolysis of lignin

Pyrolysis is one of the most studied methods for lignin or biomass depolymerization and conversion [36]. Biomass fast pyrolysis has been extensively investigated in recent years to produce liquids, evidencing that it is a low-cost technology with high efficiencies compared to other processes, and on a small scale it has low investment costs, high efficiency, and environmental acceptance [37]. Pyrolysis is a thermal degradation process that occurs in the absence of oxygen, which generates solid, liquid and gas products. The operating conditions can be modified and a slow, fast or flash pyrolysis regime can be implemented, depending on the composition and proportion of the product of interest respectively [38]. The mass balance obtained for the different modes of pyrolysis is presented in Table 2-3.

Table 2-3. Main products in pyrolysis.

Pyrolysis	Conditions	Liquids (%)	Solids (%)	Gases (%)
Slow	Reactor temperature ~300°C, heating rate <1°C/s, residence time of solids ~30 min.	0-5	77	23
Intermediate	Reactor temperature 400-500°C, heating rate 1-1000°C/s, residence time of gases ~10-30s.	50	25	25
Fast	Reactor temperature 500°C, heating rate >1000°C/s, short residence time for vapor ~1s.	75	12	13

Lignin is more difficult to decompose since it decomposes slower over a broader temperature range (150-500 °C) than cellulose and hemicellulose, weight loss usually occurs at temperatures above 400°C according to [34]. This broad temperature can be explained by the several oxygen functional groups from its structure have different thermal stabilities, hence their cleavage occurs at different temperatures. During pyrolysis, lignin can be gasified and produces gas containing hydrogen, carbon dioxide, carbon monoxide and methane. The hydrogen and carbon monoxide mixed in the gasses can be further processed to produce syngas for other applications [39], [40]. Lignin depolymerization through pyrolysis usually starts with the cleavage of weak bonds at low temperatures. The cleavage of the aryl-ether linkages results in the formation of highly reactive and unstable free radicals that may further react through rearrangement and radical-radical interactions to form products with increased stability [41].

2.2.1 First step of lignin pyrolysis

Lignin pyrolysis can be divided into two different stages: primary pyrolysis (150–400 ◦C) and secondary pyrolysis (400–800 °C) [42]. The first-stage destroys most ether linkages with the weakest bond energies; such as the α-O-4 and β-O-4 links, which are some of the most abundant linkages within the lignin molecule. During this stage, the aromatic methylated groups and the condensed linkage are stable, therefore the depolymerized lignin fragments are the basic unit of lignin, like 4-methylguaiacol, syringol, coniferyl alcohol and some lignin-derived chemicals like vanillin, isoeugenol or some unsaturated alkyl [42], [43]. Under pyrolysis conditions and without hydrogen supply from hydrogen donors, the amount of hydrogen is not enough for the depolymerized lignin fragments and other intermediates to form a stable chemical molecule. Therefore these intermediates undergo the repolymerization and form dimers or oligomers. Furthermore, the repolymerization process tends to form the condensed bonds instead of ether bonds. Thus, the repolymerized products are often more resistant to the depolymerization and increase the challenge for further conversion. However, when the temperature reaches 350 °C or higher, the hydrogen radicals released from the lignin molecule can be sufficient to stabilize the

intermediates or depolymerized fragments, thus the yield of lignin-derived monomers could be increased [36], [44]–[46].

Homolytic and heterolytic cleavage*.* Pyrolytic cleavage of the C-O aryl ether bonds and C-C bonds can be considered in terms of both homolytic and heterolytic mechanisms because these mechanisms have the same products. The lack of reliable mechanism evidence has given rise to a long-standing controversy concerning which of the homolytic and heterolytic mechanisms take place [42].

2.2.2 Second step of lignin pyrolysis

In the secondary pyrolysis step, the temperature is higher than 400 °C (usually up to 800°C). The cleavage of C–C links usually leads to on increase the monomers yield. At around 450 °C, the methoxyl groups in lignin aromatic compounds undergo homolytic cleavage leading to their hydrogenation or methylation, towards phenols and o-cresols [47]. Therefore, the major products from the first stage such as syringol are further converted into o-vanillin, guaiacol and o-quinone methide [48]. Further temperature rise >550 °C benefits the cleavage of the aromatic rings, producing non-condensable gas. The second stage pyrolysis product catechol can be degraded into carbon monoxide and cyclopentadienone which can be further decomposed into carbon monoxide and acetylene. Higher temperatures, such as 600 °C, facilitates the formation of polycyclic aromatic (PAHs) compounds showing an accelerated production of carbon content in the residue and lower the yields of monomers when the reaction reaches temperatures >700 °C [36], [49]; despite this rise, phenols and o-cresols are stable [50].

Char formation. The formation of char from lignin-derived compounds is an important process in biomass pyrolysis however, the involved molecular mechanism is not clear. The first stage of coke formation occurs at 450 °C. Hosoya *et al.* [51] indicated that the methoxyl group from guaiacol is responsible for the significant amount of coke formation and proposed the researchers to consider methyl o-quinone as an intermediate compound in the formation of char. The second stage of coke formation happens when the temperature is higher that 550°C and various products are involved, including catechols, pyrogallols, and cresols [36]. Bio-oil yield is affected by the functional groups of lignin such as methoxyl and hydroxyl since the radicals that these groups polymerize rapidly and are the cause of the low melting point of lignin, facilitating the formation of coke.

2.3 Bio-oil and pyrolytic lignin composition

Bio-oil is a multicomponent organic liquid made of mixture of more than 300 compounds, covering a range of molecular weights and functionalities [52]. Figure 2-2 shows the description of the bio-oil composition by families and functional groups.
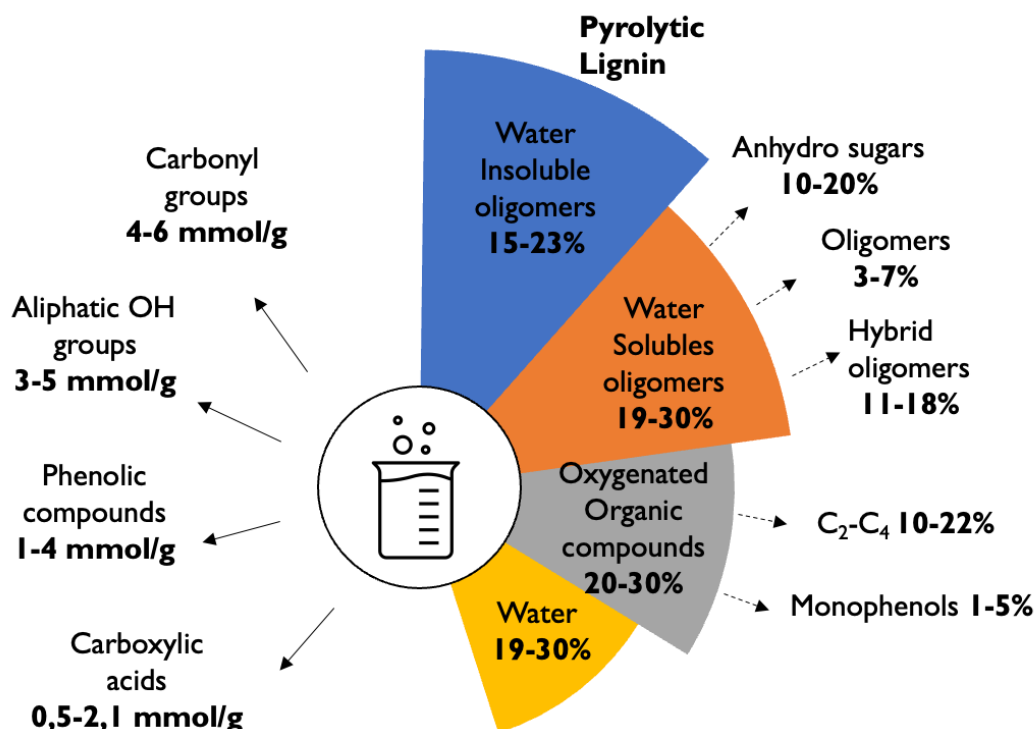
Figure 2-2. Description of the bio-oil composition based on [53].

Bio-oil is composed of a mixture of water (19-30%w), organic compounds can be identify using in gas chromatograph coupled with mass spectrometer (GC/MS), 20-30%w, oligomers soluble in water (28-36%) and water-insoluble oligomers (15-23%) known as pyrolytic lignin [54]–[58]. The organic compounds detectable in GC/MS can be divided into C2 to C4 oxygenated compounds derived from cellulose and hemicellulose fragmentation and monophenols derived from lignin depolymerization reactions [56], [57]. Water-soluble oligomers such as levoglucosan come from cellulose depolymerization reactions. This oligomers may come from dehydration reactions of oligomeric products such as pyrolytic humins and may be a combination of cellulose and lignin primary products such as hybrid oligomers [37]–[41]. The water-insoluble fraction is formed by lignin oligomeric products and is known as pyrolytic lignin [56], [57].

The pyrolytic lignin fraction mainly derives from the fragments of lignin pyrolysis and has a significant influence on the properties of bio-oil, such as increasing the instability of bio-oil [59]. To make better use of bio-oil, separating pyrolytic lignin from the liquid bio-oil becomes increasingly important. On the other hand, pyrolytic lignin has high carbon content and natural aromatic structures, so it is a renewable resource to be used as a source of biobased chemicals and fuels [60], [61], [16].

2.3.1 Organic solvent extraction

Extraction and fractionation of bio-oil through solubility properties (also known as liquid–liquid extraction) has been widely studied and reported using physical and chemical solvents [62]. The organic solvent is dependent on its selectivity towards targeted compounds/chemicals which in turn relies on their molecular structure. Instead, the extracted or fractionated chemicals from bio-oil are highly dependent on the polarity and classification of the used solvent. It operates based on the relative solubilities in two immiscible liquids or phases. In organic solvent extraction, organic soluble components will dissolve and distribute themselves in the solvent and the distinct denser phase of organic fraction can settle and be separated easily. The organic solvent will then be removed by evaporation, leaving the extracted products.

2.3.2 Solid phase extraction

The solid phase extraction is a form of adsorption which is found to be a technique for separation of selected compounds from a mixture using a solid adsorbent. During the process, bio-oil compounds are bound to the surface of a solid adsorbent, either by physisorption or chemisorption. The principle of adsorption lies essentially on the surface chemistry of adsorbent and adsorbate, as well as the molecular size of the adsorbate that influences the diffusion and mass transfer into the pores of the adsorbent. Due to its unique advantages, e.g., lower energy requirement, better economic viability, lower waste generation omitting the use of large quantities of solvent, etc., extensive research have been exploited in finding specific adsorbents that can selectively adsorb the desired by-products or pollutants to enhance the quality of bio-oil [62].

2.3.3 Distillation

These systems separate light and heavy fractions of bio-oil from differences in temperature gradients using countercurrent condensers operating at high temperatures. Light fractions such as water, C_1-C_4, monophenols and mono-sugars are in the vapor phase and heavy oligomeric fractions are in the form of aerosols. Temperature, residence time, condensation surface, among others are factors that have a strong influence on the final composition of the fractions [18].

2.4 Upgrading techniques

The major objective of bio-oil upgrading is to reduce the oxygen content and molecular weight, to increase the H/C ratio and to improve thermal stability [7]. Several upgrading processes have been proposed to realize the conversion of pyrolytic lignin to light aromatics (intense depolymerization reactions are required) [63], such as high-pressure thermal treatment, zeolite cracking and hydrotreatment [8]–[11]. Even though there are many studies related to catalytic hydrotreatment, there is a lack of understanding on many

process variables, such as the reaction mechanisms involved in the HDO process and its potential for the extraction of high value chemicals.

Several reactions have been proposed for HDO and the reactions that accompany HDO. Understanding of these reaction networks has emerged from investigations of model compounds with different catalysts and operational conditions [25]. More than one pathway has been inferred for oxygen removal by reactions with H_2 from compounds such as guaiacol. One pathway is direct hydrodeoxygenation (direct deoxygenation, DDO), which leads to the formation of aromatics and water. Another is hydrogenation of the phenolic ring followed by dehydration to form cyclohexene derivatives and rehydrogenation to produce cyclohexane derivatives [64]. Furthermore, removal of methoxy groups from phenolic compounds can proceed by demethylation (DME) and by demethoxylation (DMO), which involve C–O bond breaking and respectively produce methane and methanol [65].

Hydrodeoxygenation

Hydrotreatment, also known as hydrodeoxygenation (HDO), has become a promising technology which consists in subjecting the bio-oil to a catalyst with hydrogen at medium temperature and high-pressure conditions (350°C and 10-30 MPa) for the elimination of the oxygen is reactive functionalities. Hydrotreated bio-oil can be valorized in an integrated process to produce: heat, power, biofuels and chemicals.

He *et al.* [66] studied the effects of reaction time, reactant concentration, hydrogen pressure and H_2 supply to optimize the HDO process and to deduce an HDO reaction network. At 150°C, the oxygenation of the aromatic ring, yielding 90mol% 1-methyl-1,2-cyclohexanediol, is the kinetically relevant step, while at high temperatures (>300°C), the kinetically relevant step is the complete deoxygenation of the oxygen-containing functional groups, mainly yielding cyclohexane. However, the experiments were carried out at 7 MPa, a lower pressure than the other reported works involving higher hydrodeoxygenation levels.

Auersvald *et al.* [67] evaluated the conditions reactions of the composition and properties of products obtained by hydrotreating the bio-oil originating from the ablative fast pyrolysis of straw over a commercial sulphided $NiMo/Al_2O_3$ catalyst. The acidity expressed by total and carboxylic acid number decrease to less than 2 mg KOH/g and water content dropped to less than 1 wt.% in products obtained at 360°C and 8 MPa. Moreover, two methods to characterize the hydrotreatment quality were proposed: one estimating the degree of deoxygenation and other based on the principal component analysis. Nevertheless, the authors did not suggest which one is the better method for the prediction of the hydrotreated bio-oil quality.

A recent study by Figueiredo *et al.* [68] investigated the effect of different feedstocks on the final bio-oil product composition, particularly on the amount of alkyl phenolics and aromatics. Pyrolytic lignin was hydrotreated with Pd/C, resulting in a depolymerized product mixtures of products with monomer yields up to 39.1 wt.%. However, this study did not

suggest a reaction mechanism obtain high value compounds derived from alkyl phenolics and aromatics.

Hydrocracking

The cracking of lignin catalyzed by solid acids to produce aromatic hydrocarbons has been widely investigated in recent years. Pyrolytic lignin cracking usually starts by scission of the weak C-C and of the polar C-O bonds on an acid center followed by a radical mechanism [69]. The obtained aromatic compounds can then be converted into aromatic hydrocarbons by secondary cracking, such as decarboxylation, decarbonylation, or inter/ intra-molecular alkyl transfer reactions [70].

Hydrogenolysis

The conversion of gas-phase phenol in the presence of a metal sulfide catalyst can take places by hydrogenolysis route. The hydrogenolysis produces benzene and water by removing of a hydroxyl group.

Hydrogenation

The conversion of gas-phase phenol in the presence of a metal sulfide catalyst can take place by the hydrogenation route. Phenol is converted to cyclohexanone, which is hydrogenated to form cyclohexanol.

2.5 Conclusions and outlooks

Due to the complex lignin structure, its depolymerization is not an easy step. However, the conversion of lignin into compounds can be achieved by diverse reaction combined with the addition of solvents and catalyst that improves the cleavage of lignin. All the techniques used for depolymerization have many advantages and drawbacks that need to be considered, such as the equipment required, industrial scalability, the time and temperature required the need for solvents and catalyst. The main challenges for the use of pyrolytic lignin is the identification of its chemical structure, since this will allow an in-depth analysis of the reaction mechanisms involved during the lignin pyrolysis processes and improvement processes such as hydrotreatment. Understanding these mechanisms with oligomers will allow us to go into detail about how the deoxygenation routes, the use of catalysts and coke formation could be improved.

3. Elucidating biomass-derived pyrolytic lignin structures from demethylation reactions through density functional theory calculations

Pyrolytic lignin is a fraction of pyrolysis oil that contains a wide range of phenolic compounds that can be used as intermediates to produce fuels and chemicals. However, the characteristics of the raw lignin structure make it difficult to establish a pyrolysis mechanism and determine pyrolytic-lignin structures. This study proposes dimer, trimer, and tetramer structures based on their relative thermodynamic stability for a hardwood lignin model in pyrolysis. Different configurations of oligomers were evaluated by varying the positions of the guaiacyl (G) and syringyl (S) units and the bonds βO4 and β5 in the hardwood model lignin through electronic structure calculations. The homolytic cleavage of βO4 bonds is assumed to occur and generate two free radical fragments. These can stabilize taking hydrogen radicals that may be in solution during the intermediate liquid (pathway 1) formation before the thermal ejection. An alternative pathway (pathway 2) could happen when the radicals use intramolecular hydrogen, turning themselves into stable products. Subsequently, a demethylation reaction can take place, thus generating a methane molecule and new oligomeric lignin-derived molecules. The most probable resulting structures were studied. We used FTIR and NMR spectra of selected model compounds to evaluate our calculation approach. Thermophysical properties were calculated using group contribution methods. The results give insights into the lignin oligomer structures and how these molecules are formed. They also provide helpful information for the design of pyrolysis oil separation and upgrading equipment.

Keywords: Lignin model, pathway, radical fragments, pyrolytic lignin, DFT calculations.

3.1 Introduction

Biomass pyrolysis is an extensively studied thermochemical process transforming raw biomass into fuels and chemicals [71]. Small lignocellulosic material particles (less than 2 mm) are subjected to rapid heating rates up to temperatures in the vicinity of 500 °C to produce vapors/gases and char. The vapors need to stay in the reactor less than 2 s to avoid secondary reactions [72]. Pyrolysis oil comprises hundreds of chemical monomeric and oligomeric compounds and between 10 and 30 wt.% of water [73]. The aromatics oligomers found in this heavy fraction, often called pyrolytic lignin, are an important bio-oil fraction [74], coming mainly from the depolymerization of lignin during the pyrolysis process under rapid heating rates and a short hot vapor residence time (<1 s). These compounds are valuable platform chemicals that can contribute to the profitability of biomass pyrolysis with economic separations.

Lignin is a tridimensional aromatic polymer composed of three basic units: p-hydroxyphenyl (H), guaiacyl (G), and syringyl (S). The proportion of these units depends on the biomass species. Softwood lignin mainly comprises G units while hardwood lignin is a mixture of G and S units, and grass lignin contains the three moieties [75]. The bonds of basic units can be divided into three types: ether bonds ($\beta O4$, $\alpha O4$, $\gamma O4$) are the most prevalent and represent 60-70% of the lignin bonds; carbon-carbon bonds ($5-5$, $\beta 5$, $\beta 1$), 30-40 % and ester bonds are few and exist mainly in herbaceous plants [76]. In addition, the methoxyl (O-CH$_3$) and phenolic hydroxyl (Ph-OH) groups in the aromatic rings are the two most important functional groups in lignin units [77]. All these characteristics of the lignin polymer structure makes it difficult to establish a pyrolysis mechanism and to know the features of the pyrolytic lignin structure.

A chain reaction mechanism can explain lignin depolymerization during the pyrolysis process. An important study by Hosoya *et al*. [78] studied the char formation of various lignin compounds during this process using monophenols as model compounds. The products were identified through Ion-Gas Chromatography Mass Spectrometry and Gas Chromatography-Mass Spectrometry (GCMS). They proposed that the o-quinone methide — initiated from the H-abstraction of the phenolic hydroxyl groups — is an important intermediate for lignin char formation during pyrolysis. Jiang *et al.* [79] studied the model compound Phenethyl Phenyl Ether (PPE), four other lignin-derived radicals and two primary products (G and S units) to confirm the possible interactions between lignin pyrolysis primary and secondary reactions using Density Functional Theory (DFT) calculations combined with analytical experiments performed using a Py-GC/MS (Pyrolysis Gas Chromatography Mass Spectrometry). They used the homolysis radical mechanism and bond dissociation energies to estimate the interactions during the lignin pyrolysis process. Results showed that the formed radicals can be stabilized by lignin, and it's derived pyrolytic products while the G and S units and the cellulose products act as hydrogen donors to form stable hydrogenated products. Later, Hu *et al.* [80] studied hydroxyl-assisted hydrogen transfer interaction in lignin pyrolysis through quantum mechanics calculations and pyrolysis experiments. They concluded that hydroxyl-assisted hydrogen could exist in the pyrolysis of lignin. Recent researchers have found that the methoxyl groups on GS-type products can quickly lose -CH$_3$ radicals via homolytic mechanisms, and then through H-abstraction to form CH$_4$ [17, 18]. DFT calculations and analytical techniques suggest that lignin pyrolysis happens through a homolysis radical mechanism.

In addition, Terrell *et al*. [83] studied raw lignin and pyrolysis lignin products with Fourier Transform Ion Cyclotron Resonance Mass Spectrometry (FT-ICR-MS) to propose a lignin fragmentation mechanism. They suggested potential trimer and tetramer structures based on the basic three units and four kinds of bonding between them, losing different functional groups. Fu *et al.* [84] studied the composition and structure of pyrolysis oligomers from different biomasses using Electrospray Ionization-Mass Spectrometry (EI-MS) and Sequential Mass Spectrometry (MS[n]). They classified pyrolysis bio-oil oligomers and concluded that lignin-derived oligomers are formed by dehydration, decarboxylation, and demethylation. This is consistent with lignin pyrolysis products, namely the formation of gas

products such as CO, CO_2, and CH_4 [13, 16], which can be obtained via decarboxylation, decarbonylation, and demethylation, respectively.

To understand lignin pyrolysis mechanisms, it is important to study their properties, e.g., boiling point, the heat of vaporization, Hansen solubility parameters, standard enthalpy, and Gibbs free energy. Group contribution methods are widely used to estimate the thermophysical properties of pure compounds that may be very difficult to measure experimentally. This method consists of dividing the molecule into known small groups and calculating their properties to obtain those of the original molecule through addition rules. Fonts *et al.* [87] proposed a chemical composition of pyrolysis bio-oil obtained from biomass and determined its thermophysical properties through *ab initio* calculations and estimation methods. High Molecular Mass (HMM) and Low Molecular Mass (LMM) pyrolytic lignin were used to calculate the heavy fraction properties; however, the calculated critical temperature had a very low negative value, which is irregular. This inconsistency could be due to difficulty selecting the property's calculation method. This study recommends isolating some oligomers to determine the thermophysical properties experimentally. Terrell [88] estimated the Hansen solubility parameters for biomass conversion products using an adaptable group contribution method. The solubility parameter was calculated for 35 lignin-derived oligomers.

This manuscript aims to evaluate different lignin-oligomer structure representations from fast pyrolysis based on their relative stabilities estimated by electronic structure calculations. Oligomers' physicochemical properties are calculated by applying the group contribution method.

3.2 Methodology

3.2.1 Assignmment of pyrolytic lignin-oligomers

A model hardwood lignin was used to evaluate the assignment of pyrolytic lignin-oligomers. In this manuscript, we studied the most probable demethylation mechanism (see Figure 1). The demethylation reaction pathway of the oligomer-lignin structure was applied to model oligomers, and the reaction pathways were produced by three-step reactions. First, the ether bond $O-CH_3$ ruptures to form a free radical and methyl; this homolytic cleavage absorbs energy. Then, the intermediate radical undergoes dehydrogenation to form the quinone product. Finally, hydrogen and methyl bond to form methane [86]. First and sequential demethylations (up to 3) of these assignments were completed at a gas phase, a typical fast pyrolysis temperature of 773.15 K, and a pressure of 101325 Pa. Homolysis of the $O-CH_3$ bond can occur after fragment stabilization by increasing the temperature to 450 °C approx. [42].
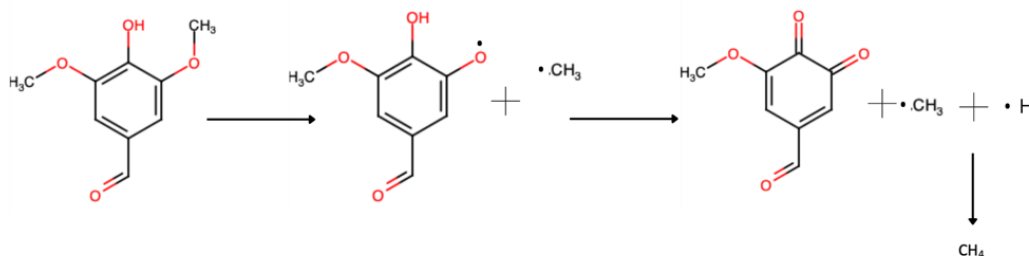
Figure 3-1. Description Demethylation mechanism reproduced with permission from [86]. Copyright 2023 Elsevier.

A chain reaction mechanism can explain pyrolytic lignin depolymerization [42], [89]. **Error! Reference source not found.** shows the proposed mechanism of the first assignment of dimers presented in

Table 1.. Under pyrolysis conditions (rapid heating up 500 °C and inert atmosphere), a model lignin composed by S and G units bonds with βO4 and β5-G(β5)G(βO4)G(β5)G- depolymerizes through βO4 and breaks the bonds between its dimers units (Figure 2-a). This bond is one of the weakest and can be thermally cleaved at 200-250 °C. Therefore, the chain mechanism is primarily initiated by direct βO4 homolysis of the model lignin to generate two or more free radical fragments [90], [91] i.e., dimers, trimers, or tetramers. Figures S1 and S2 show the mechanism when the radical fragments are trimer and tetramers, respectively. The radicals are in the oxygen and carbon where the βO4 bond were located as shown in Figure 2-b. These radical fragments can stabilize taking hydrogen radicals that may be in solution during the formation of the intermediate liquid before thermal ejection [92] (pathway 1). In this way, the hydrogen lost due the homolytic rupture is recovered and the structure in this case is G(β5)G. An alternative pathway could happen when the radicals use intramolecular hydrogen and turn themselves into stable products (pathway 2). The assignment of this pathway is named (G(β5)G -H_2) because the structure loses two hydrogens due to the homolytic rupture. Both pathways are shown in detail in Figure 2-c. The above are the initial structures we propose to evaluate the demethylated structures of pyrolytic lignin at subsequent stages of the pyrolysis process. Table 1 presents all initial assignments for dimer, trimer, and tetramer for both pathways. Then, homolysis of the O-CH_3 bond can occur by increasing the temperature to 450 °C approx. [42]. Figure 2 shows the proposed mechanism of the first assignment of dimers presented in

Table 1.. Figures S1 and S2 show the mechanism when the radical fragments are trimer and tetramers, respectively.
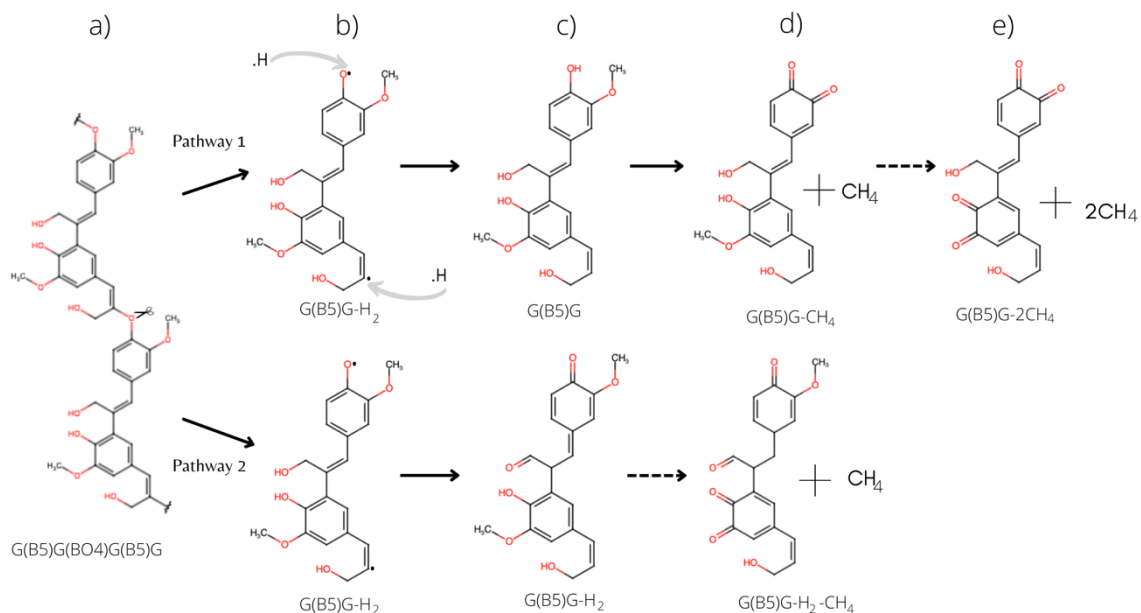
Figure 3-2. Proposed dimer decomposition mechanism: a) model lignin; b) radical fragments; c) balanced step; and d) and e) demethylation reaction.

Letters G and S represent its syringyl and guaiacyl monomers, respectively. Linkages $\beta O4$ and $\beta 5$ connecting two monomers. These bonds are evaluated at different configurations because they are the most relevant in the lignin structure. Recent studies by Fan *et al.* [93] and Lei *et al.* [94] observed free radicals *in situ* and mentioned a pathway that can originate from the $\beta O4$ bond cleavage and be transformed into a quinone structure. The scission of the $\beta O4$ bond is generally the initial step for the model lignin decomposition. As a result of this reaction, radical fragments are generated, which can be stabilized by hydrogen molecules as suggested elsewhere [79]. After this balanced step, the demethylation reaction could happen with the temperature increase. Table 1 shows the assignments based on the permutations of two monomer units and two bonds to single, double, and triple demethylation in the pyrolitic lignin structures through two different pathways. They differ in the way they stabilize the radical fragments of the model hardwood lignin after the homolytic cleavage in the first stage of pyrolysis (discussed in detail in the next section). The assignments were based on the lignin oligomers proposed elsewhere [83].

Table 1. Initial assignments of the oligomers studied through pathway 1 and 2.

Dimers		Trimers		Tetramers	
Pathway		Pathway		Pathway	
1	2	1	2	1	2
G(β5)G	G(β5)G -H$_2$	G(β5)G(βO4)S	G(β5)G(βO4)S- H$_2$	G(β5)G(βO4)S(βO4)S	G(β5)G(βO4)S(βO4)S- H$_2$
G(βO4)G	G(βO4)G- H$_2$	G(βO4)G(βO4)S	G(βO4)G(βO4)S- H$_2$	G(βO4)S(β5)G(βO4)	G(βO4)S(β5)G(βO4)S- H$_2$
G(βO4)S	G(βO4)S- H$_2$	S(βO4)S(β5)G	S(βO4)S(β5)G- H$_2$	G(βO4)S(βO4)S(β5)G	G(βO4)S(βO4)S(β5)G- H$_2$
S(β5)G	S(β5)G- H$_2$	G(βO4)S(βO4)G	G(βO4)S(βO4)G- H$_2$	S(β5)G(β5)G(βO4)	S(β5)G(β5)G(βO4)S- H$_2$
S(βO4)G	S(βO4)G- H$_2$	S(β5)G(β5)G	S(β5)G(β5)G- H$_2$	S(β5)G(βO4)G(βO4)	S(β5)G(βO4)G(βO4)S- H$_2$
S(βO4)S	S(βO4)S- H$_2$	S(β5)G(βO4)G	S(β5)G(βO4)G- H$_2$	S(β5)G(βO4)S(β5)G	S(β5)G(βO4)S(β5)G- H$_2$
		S(βO4)G(β5)G	S(βO4)G(β5)G- H$_2$	S(β5)G(βO4)S(βO4)G	S(β5)G(βO4)S(βO4)G- H$_2$
		S(βO4)G(BO4)G	S(βO4)G(BO4)G- H$_2$	S(βO4)G(β5)G(βO4)S	S(βO4)G(β5)G(βO4)S- H$_2$
				S(βO4)G(βO4)S(β5)G	S(βO4)G(βO4)S(β5)G- H$_2$
				S(βO4)S(β5)G(β5)S	S(βO4)S(β5)G(β5)S- H$_2$
				S(βO4)S(β5)G(βO4)G	S(βO4)S(β5)G(βO4)G- H$_2$
				S(βO4)S(βO4)G(β5)G	S(βO4)S(βO4)G(β5)G- H$_2$

The data set comprises 16 dimer, 98 trimer, and 46 tetramer structures for pathway 1 because the different positions in which the methoxy groups could be in the molecule were evaluated by assignment. The data set in the second pathway comprises 6 dimer, 8 trimer, and 12 tetramers because only the most stable structures per assignment in the first pathway were used to evaluate the structures. All structures were evaluated based on their relative thermodynamic stability through electronic structure calculations. The link between any unit and an S unit trough β5 bonding was not considered because the S unit has two methoxy groups in the 3 and 5 carbon (these spaces are unavailable) according to Figure 1-b.

3.2.1 DFT computational details

Most thermodynamically stable product. Geometry optimization and frequency calculations of all reagents, intermediates, and products were performed using DFT with the Gaussian 16 program suite at M06-2X functional, and the 6-311++G(d,p) basis set for the O, C and H atoms [95]. Each equilibrium geometry for all calculations was verified to have no imaginary frequency. The most thermodynamically stable product structure was then assessed based on the reaction that yields the lowest Gibbs free energy change, i.e.,

this reaction is the most favorable structure. It should be noted that only close-shell calculations were performed to assess the stability of the demethylation products (oligomer-CH_3 or oligomer-H_2-CH_3) and the stabilities of the radical intermediates in the proposed mechanism were not assessed.

Estimation of FTIR and NMR spectra of most stable molecules. Once the thermodynamically stable molecule was identified, the Fourier Transform Infrared Spectroscopy (FTIR) spectra were calculated. The frequency scale factor of the functional and basis set was 0.9567 according to available literature [96]. Later, we calculated the theoretical Proton Nuclear Magnetic Resonance (^{1}H-NMR) and Carbon-13 Nuclear Magnetic Resonance (^{13}C-NMR) spectra using the Gauge-Independent Atomic Orbital (GIAO) method. It is necessary to understand the NMR since spectra strongly depend on the molecule structure because they are constantly in motion. Thus, we made sure to use the lowest energy structure of the molecule of interest. Vibrational frequencies, calculated at the M06-2X functional and 6-311++G(d,p) level of theory were used to generate the FTIR and NMR spectra of the stable products. Also, NMR spectra of the typically used reference molecule —tetramethylsilane (TMS)— was calculated and the shielding value was subtracted from the stable products spectrum to obtain the relative shifts. Generating information on the FTIR and NMR spectra of the new oligomeric molecules is of great practical importance because many of them are not available commercially. Thus, the calculated spectra information will help assigning structures once the appropriate bio-oil separation strategies have been implemented and that the experimental spectra of these molecules will have been obtained. Theoretical results may slightly differ among types of functional and basis sets and the type of reference molecule employed in FTIR and NMR estimations.

Estimation of FTIR and NMR spectra of model compounds. Our calculation method was validated by comparing the estimated FTIR and NMR spectra with known phenolic molecules (vanillin, hydroquinone, and benzoquinone) with qualitative agreement observed for a number of peaks. Dimethyl sulfoxide d6 (DMSO-d6) solvent was used for the simulated NMR spectra of model compounds to match the experimental results. HPLC analytical grade of the model compounds were used to validate the method used in the simulations. The calculated spectra of oligomers were compared with those of pyrolytic lignin as another strategy to evaluate the validity of our FTIR estimations. The latter was obtained by cold water precipitation and dichloromethane (DCM) extraction from commercial bio-oil (BTG, The Netherlands). The NMR results for model compounds were scaled to be plotted and compared with the experimental results using a factor of 100000 and 200000 for vanillin, 30000 and 200000 for hydroquinone, and 80000 and 300000 for benzoquinone for proton and carbon-13 NMR.

FTIR spectra were obtained using a Shimadzu IRPrestige 21 spectrometer equipped with MIRacleTM single reflection ATR Ge probe. A drop of oil was applied to cover the crystal window, and the spectra were determined with 64 scans —600 to 4000 cm-1— with a resolution of 4 cm-1. The spectra were baseline corrected and band fitted between 1490 and 1850 cm-1 using 9 Gaussian bands according to [97]. The results were scaled to be

plotted and compared with the simulated results using a factor of 10000 for vanillin, hydroquinone, benzoquinone, and pyrolignin.

The ^{1}H-NMR and ^{13}C-NMR spectra were determined on a Bruker 500 Neo spectrometer equipped with a 5mm Prodigy broadband cryoprobe with Z-axis gradients. Model compounds (30 mg each) proton spectra were obtained at 500.13MHz in DMSO-d6 (0.6 mL), 30 °C with 16 scans, 90° pulse (12μs), 3s relaxation delay, and acquisition time of 4.4 s, 32768 points, and a spectral width of 7463 Hz. Proton data were apodized with 1.3 Hz of line broadening. 13C-NMR spectra were acquired at 125.77 MHz with 90° pulse angle (10.0 μs), 1.08s acquisition time, 2 s relaxation delay d1, and inverse-gated 1H composite pulse decoupling using 4000 scans, a spectral width of 30120.5 Hz, and 32768 points. The FID was apodized with 8 Hz exponential line broadening of the model compounds.

3.2.2 Group contribution to estimate thermophysical properties

Group contribution methods for thermophysical property estimation rests on the assumption that forces between atoms in the same or different molecules have short ranges. Quantitative Property-Property Relationships (QPPR) and Quantitative Structure-Property Relationships (QSPR) were applied to estimate the relevant thermophysical properties of the compounds. The parameters estimated in this study are the physical change, ideal gas, and condensed gas properties. For the physical change properties, normal boiling point (Stein and Brow method [98], M. Satou et al. method [99], and Yuan et al. method [100]), critical temperature (Lydersen method [101] and Joback method [102]), critical volume (Lydersen method [101] and Joback method [102]), critical pressure (Lydersen method [101]) enthalpy of vaporization temperature (Joback and Reid [102] and QPPR methods) were estimated. The Hansen solubility parameters were calculating using the Stefanis & Panayiotou method [103]. The condensed gas properties consist of liquid heat capacity was calculated using the Chueh & Swanson method [104], and solid heat capacity (Hurst & Harrison method [105]). Lastly, the Harrison & Seaton method [106] was also employed to determine gas heat capacity. The ideal gas properties included gas heat capacity, standard Gibbs free energy, change in enthalpy, and change in entropy; they were calculated using electronic structure calculations. Complete equations and procedures are described elsewhere (Fonts et al. [107] 2021). Briefly, the functional groups of the different elements comprising the molecule were identified, their numbers of frequency were summed up, and then multiplied by their group contribution. The information collected is very important for engineering calculations.

3.3 Results and Discussion

3.3.1 Simulated structures

This study focused on the evaluation of pyrolytic-lignin structures after demethylation reaction, as it is assumed to be one of the primary reactions that could happen after depolymerization [108]. Some studies also mentioned methane as one of the main gaseous

products during lignin pyrolysis [40, 41]. Homolysis of the O-CH$_3$ bond occurs at temperatures above 400 °C, the radical induces a rearrangement by substitution, and methylated aromatics are produced from subsequent reactions [13, 42]. Additionally, the released methyl group reacts with hydrogen at the phenol position and forms methane (see Figure 2-d), the resulting structure following pathways 1 and 2 are G(β5)G-CH$_4$, (G(β5)G - H$_2$-CH$_4$), respectively. Demethylation through pathway 2 cannot be given in all evaluated structures because a phenol group was used to stabilize the molecule in the last step. This reduces the availability of groups to form methane (dotted line). Lastly, different types of demethylations can occur through pathway 1 (see Figure 2-e). These possibilities were also simulated when performed once, twice, and thrice depending on the type of oligomer configuration. Hence, more than one demethylation can occur (dotted line) depending on the O-CH$_3$ available in the molecule for pathway 1. The formation of G(β5)G-2CH$_4$ (double demethylation) through pathway 1 could happen since O-CH$_3$ groups are available. Twice and thrice demethylations can be found in trimer and tetramer mechanisms.

The methylated aromatic oligomer structures become quinone products according to the mechanism used in this study, as shown in Figure 1-c. They were specifically benzoquinones, which can be an intermediate compound or a final product in lignin thermal decomposition in the biomass pyrolysis process, as suggested in earlier work [43, 44]. These types of compounds have been found to be intermediate products during biomass pyrolysis [45, 46]. This mechanism is also proposed for trimers and tetramers, their difference lies in the methoxy groups available for demethylation reactions once the molecule is balanced. The mechanism of trimers and tetramers can be observed in Figure S1 and S2 of the supplementary material.

Dimers. Table 2 shows the most thermodynamically stable dimer products per assignment of both pathways (those with lower Gibbs free energies out of the simulated molecules). The most probable oligomers in the pathway 1 (see Figure 2) are structures D1 (Gβ5G-CH$_4$), D5 (SβO4S-CH$_4$), and D7 (D-Gβ5G-2CH$_4$). They have a β5 bond and are conjugated, containing alternating double bonds that allow overlapping between adjacent π bonds. The selected dimers (Sβ5G) have an S and G unit connected by a β5 bond; thus, the stable structures have a conjugated C-C double bond. The molecular formulas of the proposed dimers present some difference in hydrogen loss related to methanol formation. These molecular formulas for oligomers are consistent with results obtained in previously reported work [83]. The dimers' Gibbs free energies are -29.5 and -44.6 kJ/mol for single and double demethylation, respectively. Kotake *et al.* [114] report that the formation of the quinone methides could be attributed to the reduction of the stability of G units caused by conjugated C-C double bond.

Table 3-1. Most thermodynamically stable structures of demethylated lignin dimers.

Structure	Label	Molecular formula	Molecular weight (amu)	ΔG_{rnx} (kJ/mol)	ΔH_{rxn} (kJ/mol)	ΔS_{rxn} (J/mol-K)
			Pathway 1			

GB5G-CH$_4$	D1	C$_{19}$H$_{18}$O$_6$	342.84	-29.51	86.59	150.16
GBO4G- CH$_4$	D2	C$_{19}$H$_{18}$O$_6$	342.84	-10.77	108.02	153.66
GBO4S- CH$_4$	D3	C$_{20}$H$_{20}$O$_7$	372.69	-6.21	107.11	146.56
SB5G- CH$_4$	D4	C$_{20}$H$_{20}$O$_7$	372.69	-21.92	82.35	143.32
SBO4S- CH$_4$	D5	C$_{21}$H$_{22}$O$_8$	342.84	-27.14	86.32	146.75
SBO4G- CH$_4$	D6	C$_{20}$H$_{20}$O$_7$	372.12	-23.67	90.67	147.89
GB5G- 2CH$_4$	D7	C$_{18}$H$_{14}$O$_6$	326.69	-44.63	176.13	285.52
Pathway 2						
GB5G-H$_2$- CH$_4$	D1*	C$_{19}$H$_{16}$O$_6$	340.01	-4.77	116.83	157.29
GBO4G-H$_2$- CH$_4$	D2*	C$_{20}$H$_{20}$O$_6$	356.13	-	-	-
GBO4S-H$_2$- CH$_4$	D3*	C$_{21}$H$_{22}$O$_7$	386.14	-	-	-
SB5G-H$_2$- CH$_4$	D4*	C$_{20}$H$_{18}$O$_7$	370.10	0.74	116.13	149.25
SBO4S-H$_2$- CH$_4$	D5*	C$_{22}$H$_{24}$O$_8$	416.15	-	-	-
SBO4G-H$_2$- CH$_4$	D6*	C$_{21}$H$_{22}$O$_7$	386.14	-	-	-

In the case of pathway 2, the initial radical structures were balanced using its intramolecular hydrogen. In this pathway, quinones are formed by the location of the radical in the upper part of the structure, and the other radical is balanced with the double bond in the aliphatic chain of the first unit. After that, the structures react to form methane and quinones through demethylation. However, in the evaluated structures, only D1* (Gβ5G-H$_2$-CH$_4$) and D4* (Sβ5G-H$_2$-CH$_4$) could continue the reactions (see Figure 3-2) because they contain the G units, which indicates available methoxy and OH groups in the ring of the basic lignin unit, unlike the other structures balanced through pathway 2. The Gibbs free energy values were -4.77 and 0.74 KJ/mol, respectively. The molecules with unreported values indicate that after the chemical balance, those structures could not continue subsequent reactions due to lack of OH and O-CH$_3$ groups (a representation of these structures can be seen in Table S1). D1* (Gβ5G-H$_2$-CH$_4$) is the most stable structure, probably because it is a conjugated one, as happens in the first pathway. Additionally, when the structures take the first route, it is possible that a second demethylation takes place due to the availability of methoxy and OH groups. On the contrary, in the second pathway balancing process, the structures lose that availability by forming quinones during stabilization. A detail representation of the most stable dimers through pathways 1 and 2 are shown in Figure 3-3.
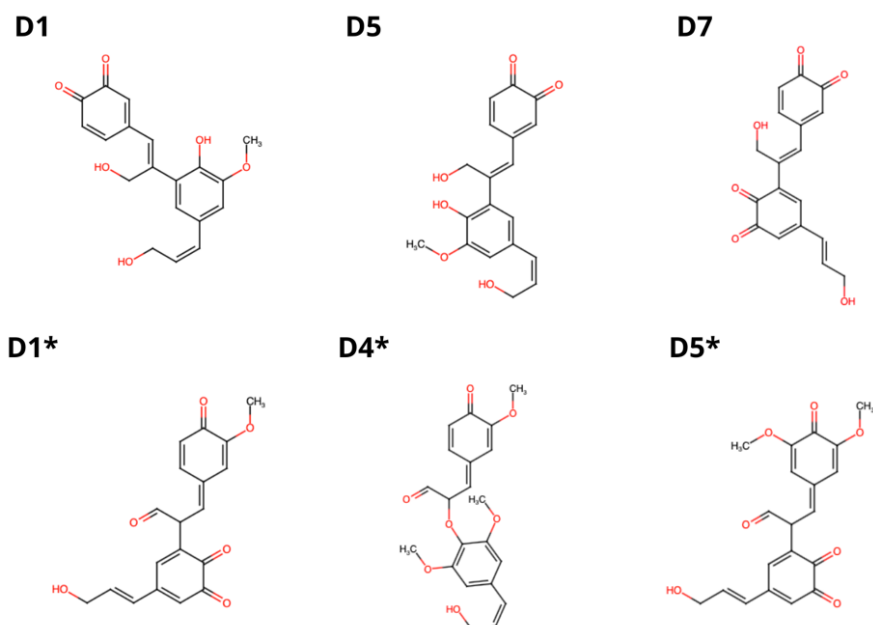
Figure 3-3. Detailed representation of the most stable dimers.

Trimers. Table 3-3 shows the information of molecular formula and weight, Gibbs free energy, enthalpy, and entropy of the most stable trimers per assignment. These that take pathway 1 (see Figure S1) are structures T6 (Sβ5Gβ5G-CH₄), T9 (Sβ5Gβ5G-2CH₄), and T10 (Sβ5Gβ5G-3CH₄) with Gibbs free energies of -53.3, -66.4, and -119.9 kJ/mol for a single, double, and triple demethylation, respectively. These trimers are isomers (Sβ5Gβ5G) and have one S, and two G units linked by two β5 bonds. The molecular formulas of the proposed trimers are $C_{30}H_{30}O_{10}$, $C_{29}H_{26}O_{10}$, and $C_{28}H_{22}O_{10}$, their difference lies in the hydrogen loss related to methanol formation more than once. These molecular formulas are similar to the structures proposed by Terrell *et al*. [115] for lignin oligomers.

Table 3-2. Most thermodynamically stable structures of demethylated lignin trimers.

Structure	Label	Molecular formula	Molecular weight (amu)	ΔG_{rnx} (kJ/mol)	ΔH_{rxn} (kJ/mol)	ΔS_{rxn} (J/mol-K)
			Pathway 1			
SBO4GB5G-CH₄	T1	$C_{30}H_{30}O_{10}$	550.55	-26.69	87.21	147.31
GBO4SB5G-CH₄	T2	$C_{30}H_{30}O_{10}$	550.55	-35.72	79.63	149.20
GB5GBO4S-CH₄	T3	$C_{30}H_{30}O_{10}$	550.55	-38.21	60.89	128.17
SB5GBO4G-CH₄	T4	$C_{30}H_{30}O_{10}$	550.55	-25.83	115.83	147.69
SBO4GBO4G-CH₄	T5	$C_{30}H_{30}O_{10}$	550.55	-31.74	87.47	154.18
SB5GB5G-CH₄	T6	$C_{30}H_{30}O_{10}$	550.55	-53.35	5.71	178.26

GBO4SBO4G-CH$_4$	T7	C$_{30}$H$_{30}$O$_{10}$	550.55	-45.67	107.36	147.98
GBO4GBO4S-CH$_4$	T8	C$_{30}$H$_{30}$O$_{10}$	550.55	-33.71	76.39	142.40
SB5GB5G-2CH$_4$	T9	C$_{29}$H$_{26}$O$_{10}$	534.51	-66.37	114.67	344.41
SB5GB5G-3CH$_4$	T10	C$_{28}$H$_{22}$O$_{10}$	518.47	-119.96	325.93	465.03
Pathway 2						
SBO4GB5G-H$_2$-CH$_4$	T1*	C$_{30}$H$_{28}$O$_{10}$	548.16	13.51	96.16	141.85
GBO4SB5G-H$_2$-CH$_4$	T2*	C$_{30}$H$_{28}$O$_{10}$	548.16	12.95	107.82	156.21
GB5GBO4S-H$_2$-CH$_4$	T3*	C$_{30}$H$_{28}$O$_{10}$	548.16	11.29	106.81	152.77
SB5GBO4G-H$_2$-CH$_4$	T4*	C$_{30}$H$_{28}$O$_{10}$	548.16	30.67	78.86	141.68
SBO4GBO4G-H$_2$-CH$_4$	T5*	C$_{31}$H$_{32}$O$_{10}$	564.20	-	-	-
SB5GB5G-H$_2$-CH$_4$	T6*	C$_{30}$H$_{28}$O$_{10}$	548.16	15.33	106.75	157.9
GBO4SBO4G-H$_2$-CH$_4$	T7*	C$_{31}$H$_{32}$O$_{10}$	564.20	-	-	-
GBO4GBO4S-H$_2$-CH$_4$	T8*	C$_{31}$H$_{32}$O$_9$	548.20	-	-	-

Trimers in pathway 2 have more structures after balancing, and it is possible that demethylation occurs if compared to the dimers due to the additional monomer providing available methoxy and OH groups depending on the assignment of the structure. In this route, trimers are balanced by their own atoms, thus producing quinones in the depolymerization stage of the pyrolysis process before the demethylation reaction; hence, a double quinone can be found in this oligomer structures (see Figure S1). Some of these balanced trimers can go through demethylation reactions due to the availability of methoxy and OH groups in the molecule (the structures can be seen in Table S2). For this reason, trimers T5* (SβO4GβO4G-H$_2$-CH$_4$), T7* (GβO4SβO4G-H$_2$-CH$_4$), and T8* (GβO4GβO4S-H$_2$-CH$_4$) do not have the energy, enthalpy, and entropy properties of reaction. Although the reaction energies are positive in these structures, the most probable trimers are T2* (GβO4Sβ5G-H$_2$-CH$_4$) and T3* (Gβ5GβO4S-H$_2$-CH$_4$) because they have values of 11.3 and 12.9 kJ/mol. Figure 3-4 shows a detail representation of the most stable structure and T7* (GβO4SβO4G-H$_2$-CH$_4$) as an example of the trimer structure that could not undergo the demethylation reactions.

T6   **T9**   **T10**

T2*   **T3***   **T7***
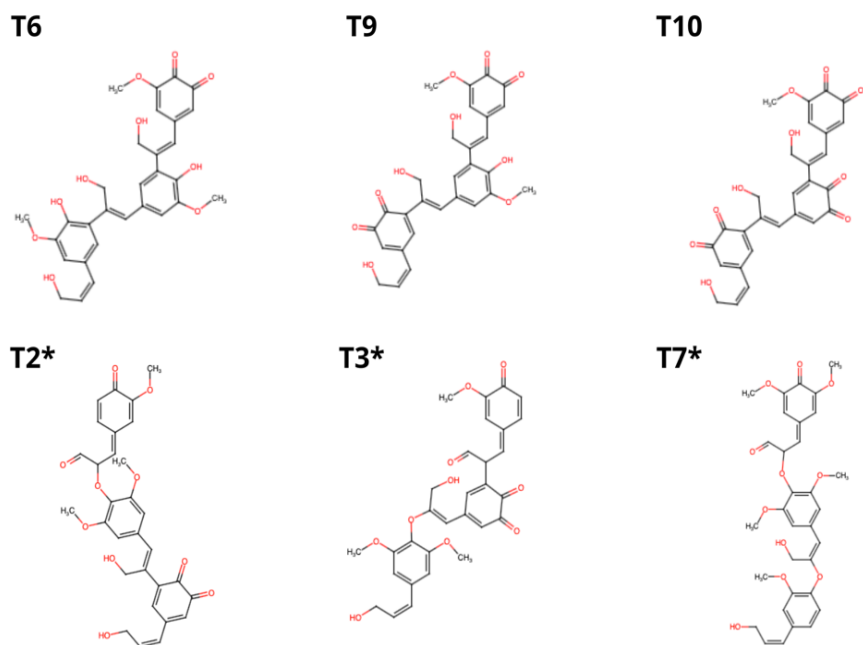
Figure 3-4. Detailed representation of the most stable trimers.

Tetramers. Table 3-4 shows the values of thermodynamic properties of most stable tetramers per assignment according to the proposed trimer mechanism in Figure S2. The ones that take pathway 1 are structures OG12 (Gβ5GβO4SβO4S-CH$_4$), OG13 (GβO4SβO4Sβ5G-2CH$_4$) and OG14 (Sβ5Gβ5GβO4S-3CH$_4$) with Gibbs free energies of -31.0, -49.4, and -52.8 kJ/mol for a single, double, and triple demethylation, respectively. These oligomers have four monomeric units, therefore, a greater possibility of subsequent demethylation reactions. For this reason, tetramers that have undergone more than one demethylation reaction are observed. The most probable tetramer-structure for a single demethylation is the assignment Gβ5GβO4SβO4S. The latter has two G and two S units linked by one β5 and βO4 bonds. Again, the β5 bonds are relevant in these oligomers because they facilitate the conjugated effect in this type of molecule.

Table 3-3. Most thermodynamically stable structures of demethylated lignin tetramers.

Structure	Label	Molecular formula	Molecular weight (amu)	ΔG_{rnx} (kJ/mol)	ΔH_{rxn} (kJ/mol)	ΔS_{rxn} (J/mol-K)
			Pathway 1			
GBO4SB5GBO4S-CH$_4$	OG1	C$_{41}$H$_{42}$O$_{14}$	758.26	-10.26	101.37	144.38
GBO4SBO4SB5G-CH$_4$	OG2	C$_{41}$H$_{42}$O$_{14}$	758.26	-29.16	78.67	144.38
SB5GB5GBO4S-CH$_4$	OG3	C$_{41}$H$_{42}$O$_{14}$	758.26	-24.93	84.47	145.38
SB5GBO4GBO4S-CH$_4$	OG4	C$_{41}$H$_{42}$O$_{14}$	758.26	-17.80	102.63	155.77

SB5GBO4SB5G-CH$_4$	OG5	C$_{41}$H$_{42}$O$_{14}$	758.26	-25.36	94.01	154.41
SB5GBO4SBO4G-CH$_4$	OG6	C$_{41}$H$_{42}$O$_{14}$	758.26	-30.14	92.69	158.86
SBO4GB5GBO4S-CH$_4$	OG7	C$_{41}$H$_{42}$O$_{14}$	758.26	-29.19	82.13	143.99
SBO4GBO4SB5G-CH$_4$	OG8	C$_{41}$H$_{42}$O$_{14}$	758.26	-15.50	96.24	144.53
SBO4SB5GB5G-CH$_4$	OG9	C$_{41}$H$_{42}$O$_{14}$	758.26	-23.00	21.69	147.16
SBO4SB5GBO4G-CH$_4$	OG10	C$_{41}$H$_{42}$O$_{14}$	758.26	-29.72	52.78	154.29
SBO4SBO4GB5G-CH$_4$	OG11	C$_{41}$H$_{42}$O$_{14}$	758.26	-18.78	99.71	153.25
GB5GBO4SBO4S-CH$_4$	OG12	C$_{41}$H$_{42}$O$_{14}$	758.26	-31.00	87.47	149.89
GBO4SBO4SB5G-2CH$_4$	OG13	C$_{40}$H$_{38}$O$_{14}$	742.22	-49.37	42.10	291.70
SB5GB5GBO4S-3CH$_4$	OG14	C$_{39}$H$_{34}$O$_{14}$	726.19	-52.81	76.48	482.24
Pathway 2						
GBO4SB5GBO4S-H$_2$-CH$_4$	OG1*	C$_{41}$H$_{40}$O$_{14}$	756.24	24.85	101.43	163.35
GBO4SBO4SB5G-H$_2$-CH$_4$	OG2*	C$_{41}$H$_{40}$O$_{14}$	756.24	21.52	97.63	154.12
SB5GB5GBO4S-H$_2$-CH$_4$	OG3*	C$_{41}$H$_{40}$O$_{14}$	756.24	17.36	100.54	152.50
SB5GBO4GBO4S-H$_2$-CH$_4$	OG4*	C$_{41}$H$_{40}$O$_{14}$	756.24	17.92	100.32	152.94
SB5GBO4SB5G-H$_2$-CH$_4$	OG5*	C$_{41}$H$_{40}$O$_{14}$	756.24	16.39	102.32	153.54
SB5GBO4SBO4G-H$_2$-CH$_4$	OG6*	C$_{41}$H$_{40}$O$_{14}$	756.24	16.96	105.58	158.51
SBO4GB5GBO4S-H$_2$-CH$_4$	OG7*	C$_{41}$H$_{40}$O$_{14}$	756.24	24.64	101.37	162.98
SBO4GBO4SB5G-H$_2$-CH$_4$	OG8*	C$_{41}$H$_{40}$O$_{14}$	756.24	11.75	101.71	146.77
SBO4SB5GB5G-H$_2$-CH$_4$	OG9*	C$_{41}$H$_{40}$O$_{14}$	756.24	13.12	102.87	150.03
SBO4SB5GBO4G-H$_2$-CH$_4$	OG10*	C$_{41}$H$_{40}$O$_{14}$	756.24	12.35	100.07	145.42
SBO4SBO4GB5G-H$_2$-CH$_4$	OG11*	C$_{41}$H$_{40}$O$_{14}$	756.24	19.08	99.87	153.86
GB5GBO4SBO4S-H$_2$-CH$_4$	OG12*	C$_{41}$H$_{40}$O$_{14}$	756.24	20.20	102.44	158.63

In pathway 2, the most stable structures are OG8* (SβO4GβO4Sβ5G-H$_2$-CH$_4$), OG9* (SβO4Sβ5Gβ5G-H$_2$-CH$_4$), and OG10* (SβO4Sβ5GβO4G-H$_2$-CH$_4$) with Gibbs free energies of 11.75, 13.12, and 12.35 kJ/mol, respectively. After balancing the structures, all tetramers can continue the demethylation reaction due to the greater number of OH and methyl groups available for their total amount of monomers. Figure 3-5 shows a detailed representation of the most stable tetramers through pathways 1 and 2.
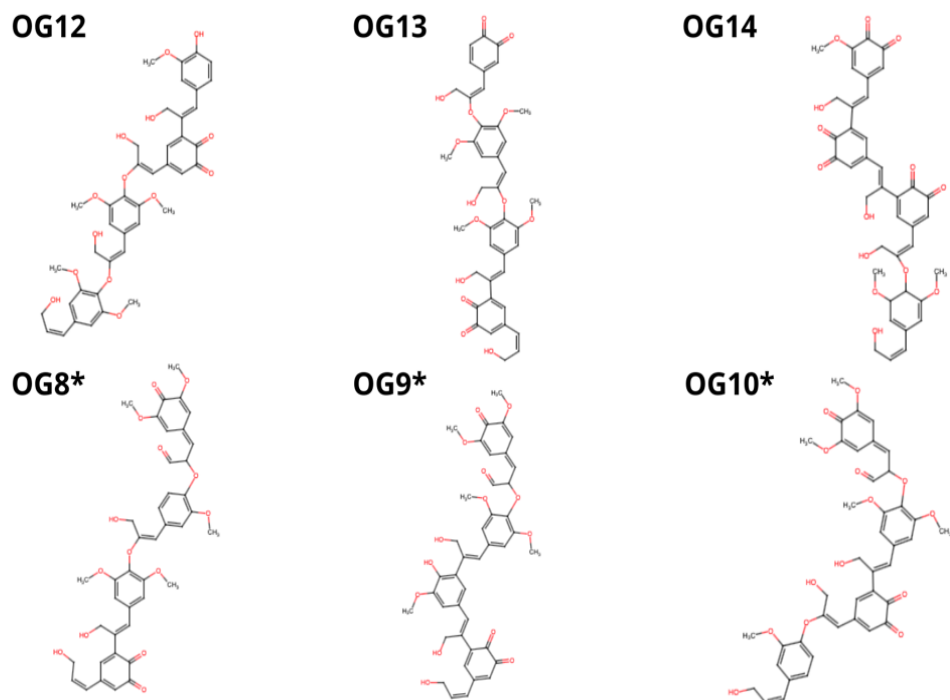
Figure 3-5. Detailed representation of the most stable tetramers.

In all the oligomers, the most stable structures contain a greater number of β5 bonds. This type of bond connecting the lignin units facilitates the stability of the molecule due to the conjugated C-C bonds. Table S1-S3 shows a detailed representation of all the lignin oligomers. In addition, the coordinates corresponding to all optimized structures in their ground states can be found in the supporting information document.

3.3.2 FTIR and NMR Spectra Calculations

Model compound validation. To validate the FTIR and NMR spectra obtained from electronic structure calculations, we decided to compare the calculated and experimental values of phenolic model compounds: vanillin, hydroquinone, and benzoquinone. To the best of our knowledge, samples of the oligomers listed in Figures 3-3, 3-4 and 3-5 are not available in literature. Figure 3-6 and Figure 3-7 show the FTIR spectra fingerprint regions and the ^{13}C and ^{1}H - NMR of the model compounds' spectra, respectively. The model compounds are dotted lines, and the simulated spectra are solid lines. The spectra in the fingerprint region of the compounds are similar. The peaks that are clearly identified in the experimental spectrum can be observed in the simulated spectrum for vanillin, hydroquinone, and benzoquinone.
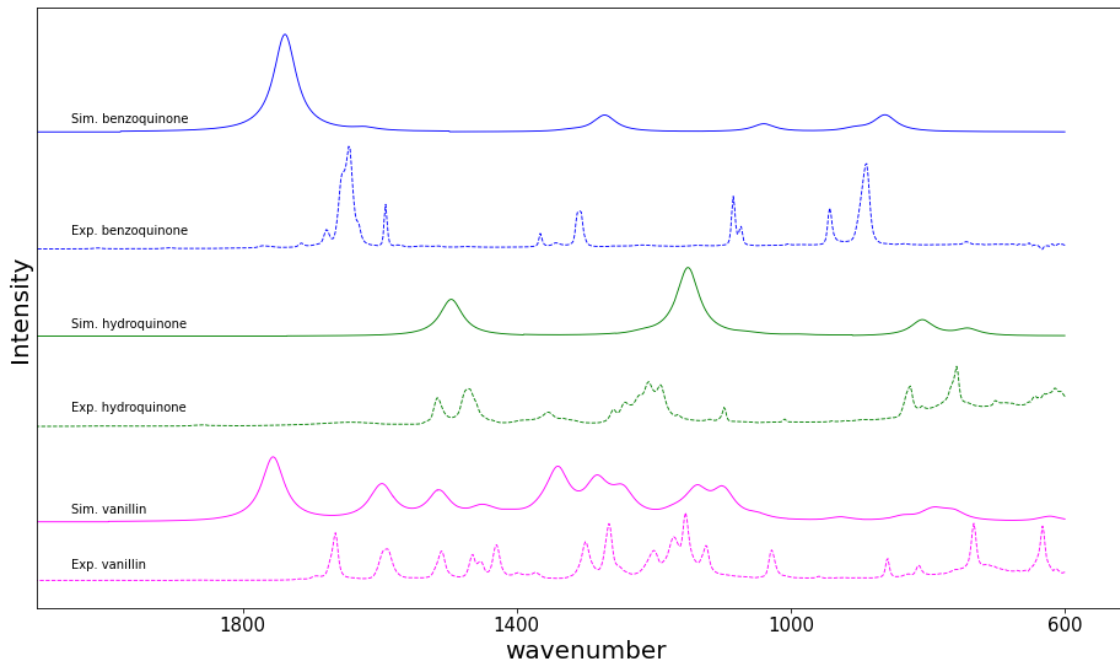
Figure 3-6: Fingerprint region of the FTIR spectra of model lignin compounds.

Additionally, the obtained spectra were compared to the FTIR spectra reported in the literature for these compounds, resulting a similar spectrum to those found in previous studies [49, 50]. The simulation parameters show good fitting of the model compounds and can be used to simulate these kinds of molecules. Although the peak locations present qualitative agreement, electronic structure calculations still lack accuracy due to the harmonic oscillator approximation. Figure 3-7 shows the ^{13}C and ^{1}H NMR spectra of the model compounds to compare the experimental and simulated ones.

a)

b)
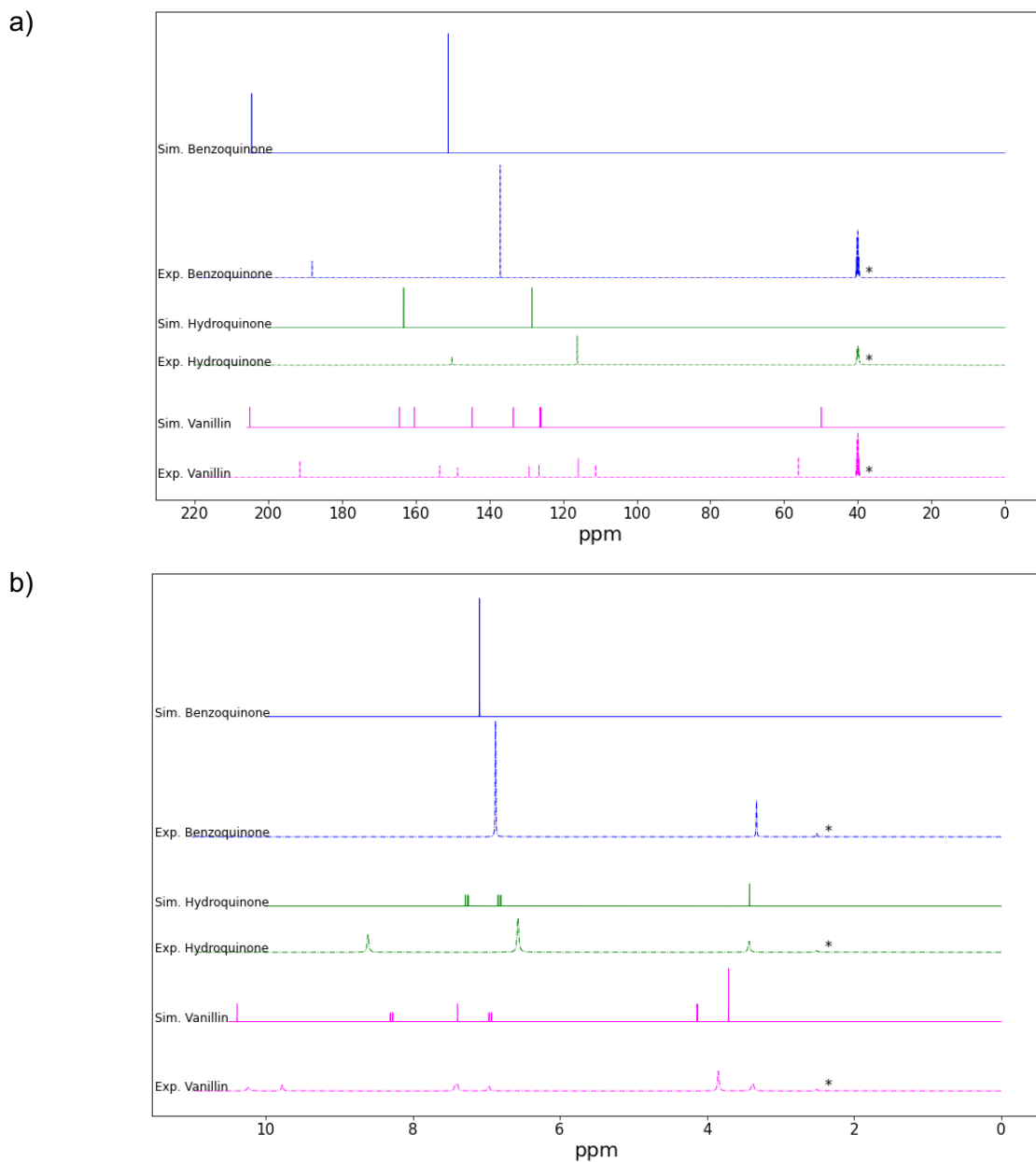
Figure 3-7:NMR spectra of model compounds a) ^{13}C NMR and b) ^{1}H NMR; *(asterisk

correspond to solvent peak).

Bars of the simulated model compounds tend to be located to the right of the experimental peaks for carbon and hydrogen for vanillin, hydroquinone, and benzoquinone as model compounds. The peaks around 40 ppm for experimental ^{13}C-NMR and 2.3 ppm for the experimental ^{1}H-NMR correspond to the solvent DMSO-d6 used during the experiment. In addition, the simulated FTIR and NMR spectra were calculated in a gas phase simulation, while the experimental FTIR and NMR spectra were obtained at liquid phase. This also justifies the difference in the experimental and simulated FTIR and NMR peaks even though the fitting between the simulated and experimental data is close enough to use the simulated FTIR and NMR spectra to characterize the proposed oligomer structures.

Although peak locations present qualitative agreement, electronic structure calculations still lack accuracy due to the harmonic oscillator approximation. This does not capture anharmonic vibrational modes; therefore, it could disagree with experimental measurements. The adjustment value has not been extensively discussed in the literature; then, a new value could allow a greater similarity between the spectra.

Information on resulting oligomers. The FTIR spectrum of the 3 most probable simulated compounds for dimers, trimers, and tetramers are shown in Figure 3-8. The rest of the FTIR spectra of the proposed oligomers are presented in Figures S3-S7. These spectra can be compared with the experimental pyrolignin based on the spectra of water-insoluble fraction of biomass pyrolysis bio-oil that is report in literature. Figure 3-8 shows the FTIR spectra of lignin oligomers. The absorption peaks at 2971 and 2870 cm^{-1} correspond to methyl groups. In this band, the intensity is lower in the dimers and trimers that have undergone a complete demethylation of the molecule, since they have a limited amount of methyl groups, as would be expected for such compounds. In addition, the structure with more than once demethylation (like D7, T9, T10, OG13 and OG14) demonstrated lower intensity in these peaks. The shoulders in 1712 and 1673 cm^{-1} indicates unconjugated and conjugated carbonyl group, respectively. The former can be attributed to unconjugated carbonyl from ester groups and the latter to conjugated aryl ketones. The peak at 1673 cm^{-1} is more intense for dimers because it present conjugated carbonyl in its structure. This is the case of the trimer T10 and tetramer OG14, which shows this intense peak since all the carbonyl group in its structure are conjugated.
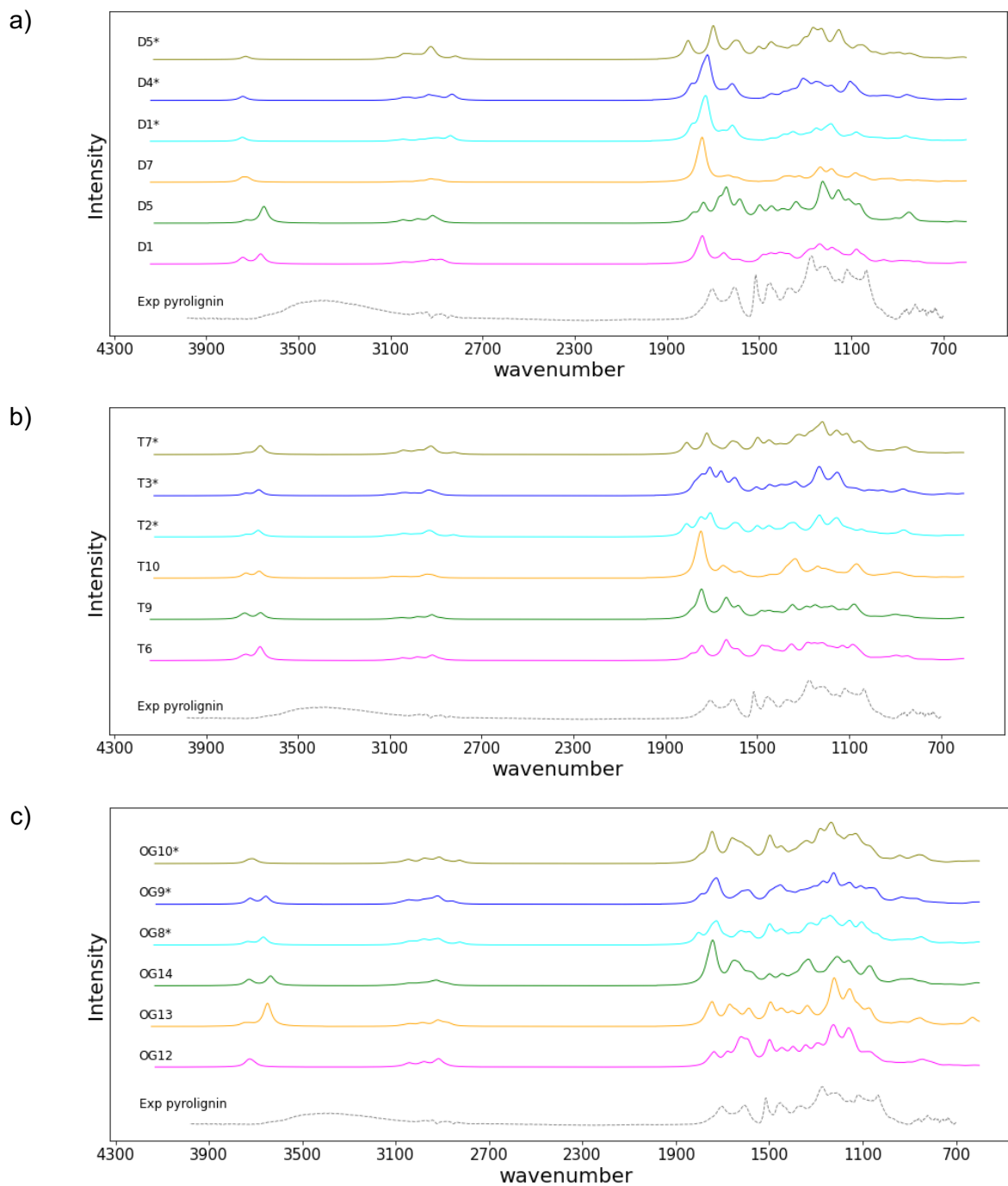
Figure 3-8: FTIR spectra of the proposed lignin oligomers: a) dimers, b) trimers, and c) tetramers.

Peaks around 1606–1336 cm^{-1} are related to aromatic skeletal vibration caused by C=O stretching, C-H deformations, and asymmetry in -CH$_3$ and -CH$_2$, the chemical groups that conform the lignin oligomers. The skeletal vibration of C-O present on syringyl units was identified at 1332 and 1116 cm^{-1}, while in the guaiacyl units it is in the 1275 and 1154 cm^{-1} peaks, thus confirming the presence of S and G units in those oligomers because of the high thermal stability of methoxyl groups attached to the aromatic rings [48]. Finally, the peaks at 1366, 1216, 1035, and 989 cm^{-1} could be related to the aliphatic side chains, carbonyls, and unsaturated double bonds as has been suggested in other reports [118]. The experimental pyrolytic lignin spectrum report in Figure 3-9 was obtained using pyrolignin powder obtained from cold-water precipitation of pyrolysis bio-oil.
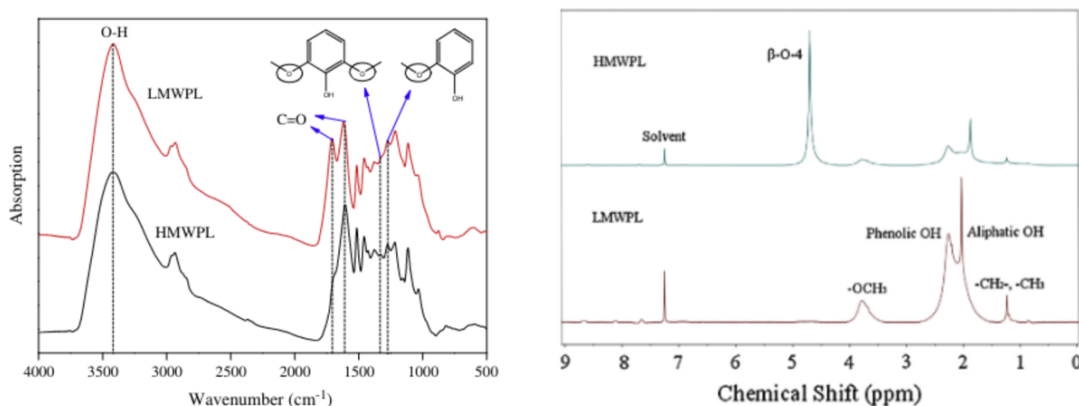
Figure 3-9. FTIR and ^{1}H NMR experimental spectra of low (red line) and high (black and blue line) molecular weight of pyrolytic lignin. Reprinted from ref [119] with permission from Elsevier.

This spectrum is compared with the spectrum report by Wang *et al.* [119] in Figure 3-9, obtained by separating bio-oil using solvents to get high-molecular-weight and low-molecular-weight pyrolytic lignin. In contrast, peaks at 1700 cm^{-1} can be identified in the pyrolytic lignin. They are related to the vibration of the aromatic bonds caused by C=O at 1400 cm^{-1} that may have to do with the deformations and asymmetries of the CH$_3$ and CH$_2$ chemical groups. These peaks were also identified in the benzoquinones reported in this study. However, in pyrolytic lignin, there is a peak at 3450 cm^{-1} related to the O-H bonds, which was not observed in the spectra of the benzoquinones reported in this study. According to the FTIR results, oligomers D5 (SβO4S-CH$_4$), T3* (Gβ5GβO4S-H$_2$-CH$_4$), and OG13 (GβO4SβO4Sβ5G-2CH$_4$) have a spectrum and therefore a more similar structure if compared with the experimental pyrolignin used in this study. Another simulated information that we can use to analyze is NMR spectra. These spectra were used to define the inter unit bonds of proposed oligomers structures. ^{1}H NMR simulated spectra of the pyrolignin are presented in Figure 3-10.
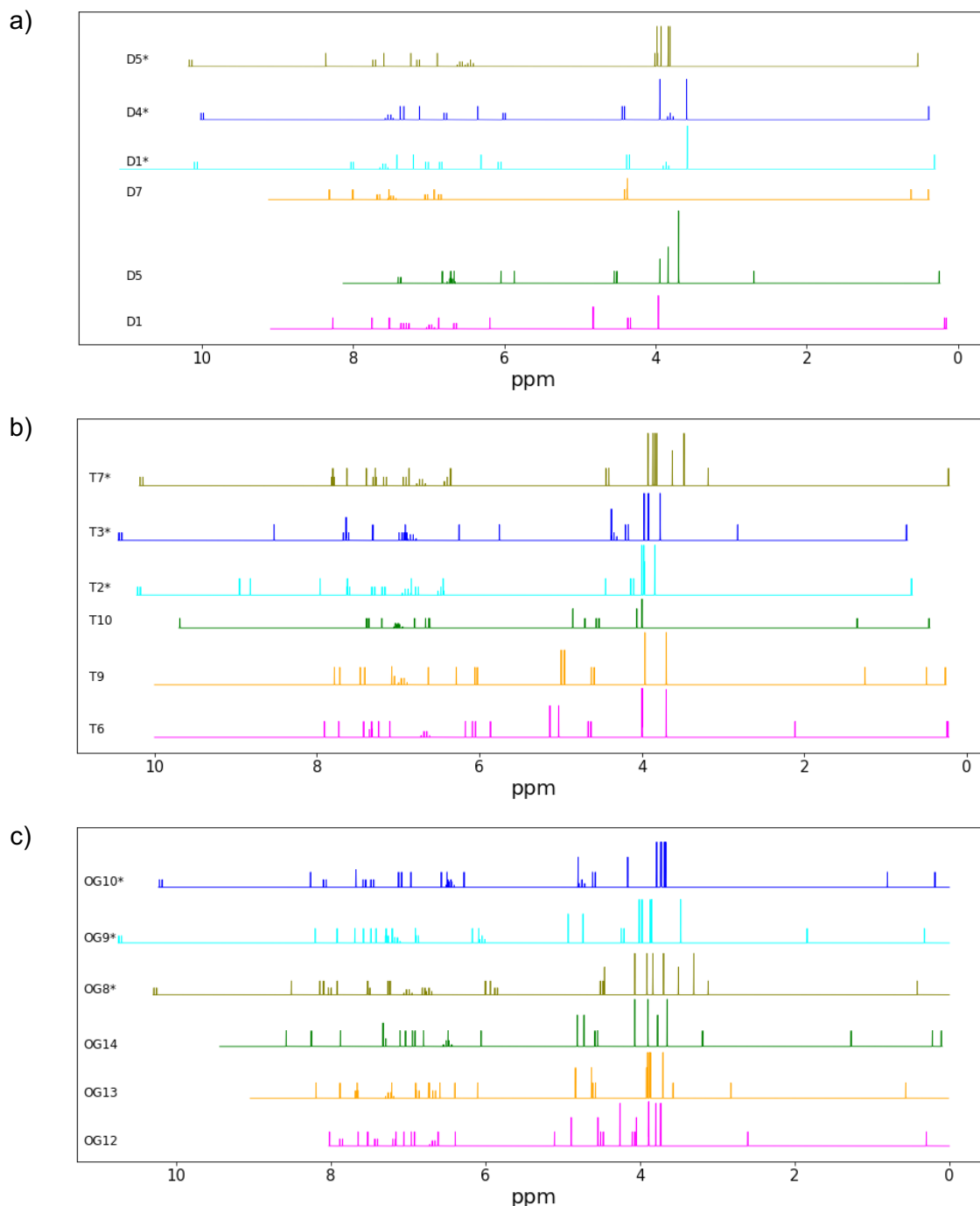
Figure 3-10: ^{1}H-NMR simulated spectra of the proposed lignin oligomers: a) dimers, b) trimers, and c) tetramers.

Signals at 8.0–6.0 ppm can be attributed to aromatic and double-bond protons. In contrast, dimers only have two aromatic rings compared to trimers and tetramers; explaining why they have strong signals in that range. Additionally, signals between 4.1–3.6 ppm are related to methoxy groups found in these oligomers due to the presence of G and S units; the signal intensity is proportional to the number of monomers in the lignin oligomers;

hence, it is possible to see more signals in tetramers than in dimers' spectra. Peaks between 3 and 0.5 ppm can be attributed to hydrogen in CH_2 and CH_3 groups; this signal is stronger as there are more monomers in the polymer chain. Also, in contrast with the different pathways, the most probable structures through pathway 2 have lower signals in this region because they balance using their own atoms and form quinones when reacting with CH_3 groups.

In the case of trimers and tetramers —since the structures can have a higher number of demethylations— the signal gets more intense because the methoxy bond is broken to produce methane and forms the quinone group. Peaks at 4.5–4.2 ppm, 9.3–8.1 ppm, and 1.5–0.5 ppm imply that the oligomers contain benzyl alcohol, phenolic and aliphatic groups, respectively. The results indicate that pyrolignin contains many unsaturated groups [118].

On the other hand, the ^{1}H NMR simulated spectrum for pyrolignin is similar to the one reported by Wang *et al.* [118] in Figure 3-9. The low-molecular-weight lignin is similar to dimers and trimers, and the high-molecular-weight pyrolignin is similar to tetramers simulated spectra, especially for the peaks between 4–3.5 ppm related to the hydrogen occurring on methoxy groups. Tetramers have a longer polymer chain with G and S units if we compare the simulated spectra is compared to the experimental one. In addition, lighter pyrolytic lignin has a more intense signal between 1 and 3 ppm, mainly related to the presence of aromatic and aliphatic OH groups because methyl groups are released to form methane. Benzoquinone molecules, that could represent pyrolytic lignin, bear a close resemblance to the spectrum of heavy pyrolytic lignin.
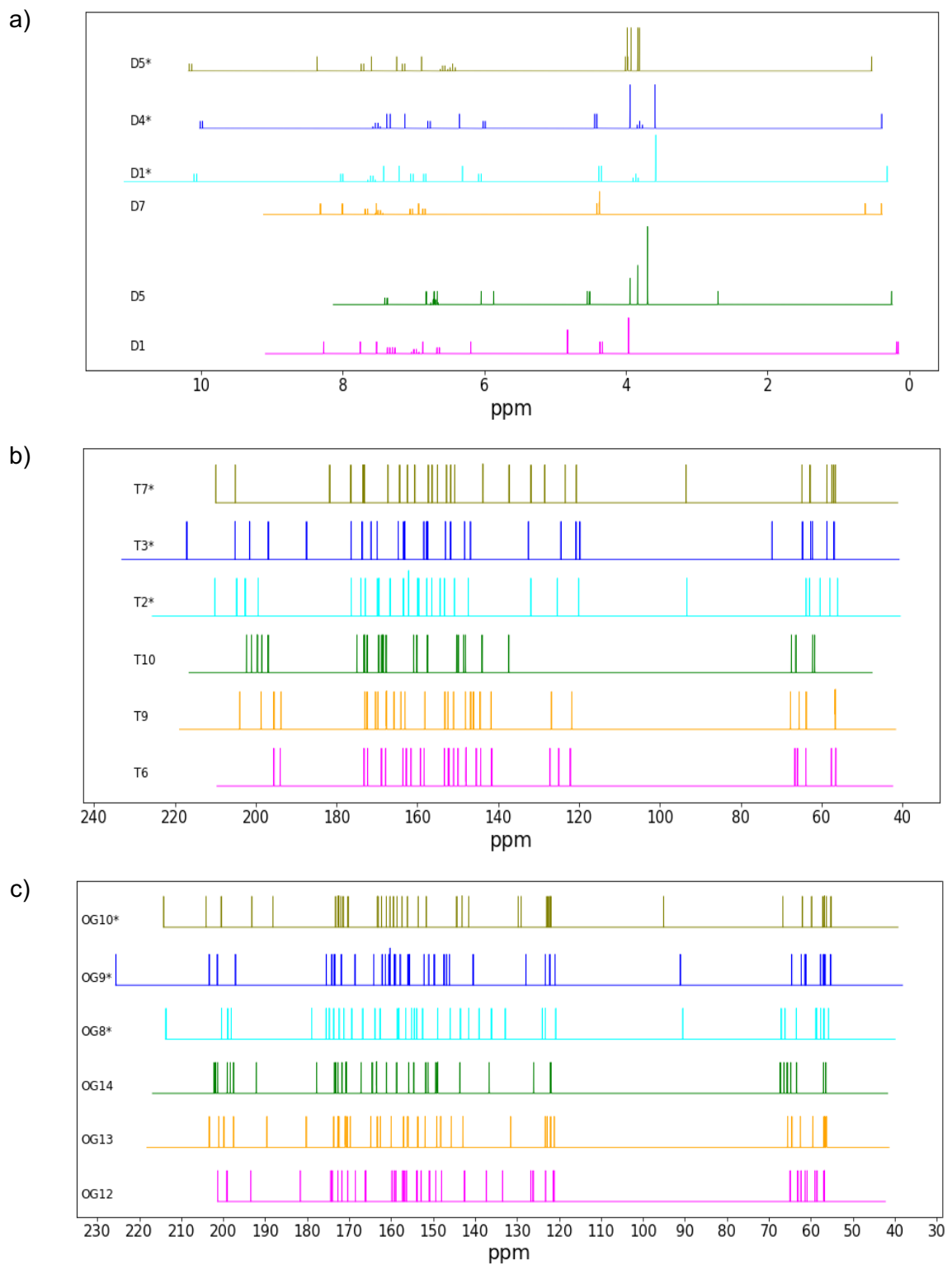
Figure 3-11:C-NMR simulated spectra of the proposed lignin oligomers: a) dimers, b) trimers, and c) tetramers.

The interunit bonds in each oligomer were calculated from the ^{13}C-NMR spectra, as shown in Figure 3-11. The aromatic region can be divided into oxygenated aromatic (166–142 ppm), condensed aromatic (142–125 ppm), and protonated aromatic (125–102 ppm) regions. In the first region, signals at 152 and 138 ppm originate from the βO4 structure in S-type carbon, which confirms the cleavage of βO4 linkage by the pyrolysis process in the OG oligomers. Some of them have peaks in the condensed aromatic region. These structures still have methoxy groups that could form new quinones. Moreover, signals around 60 ppm are related to the propane side chain of carbon in the βO4 structure [120]. This confirms the propane side chain located in the OG oligomers. Signals from syringyl residues (C_2/C_6 at 108/104 ppm) are not present in this spectrum, supporting that quinones form mainly through demethylation of the syringyl initial structure. Additionally, even if this spectrum is only a trimer representation of the pyrolytic lignin, its shape is similar to the NMR spectra found in the literature for the water insoluble fraction of the pyrolysis bio-oil or pyrolytic lignin [121]. The ^{13}C and ^{1}H - NMR spectra for all of the proposed oligomers are present in Figure S8-S17.

3.3.3 Thermophysical properties

The thermophysical properties to be estimated are shown in Table 3-5, Table 3-6 and Table 3-7. The molecular structures of the demethylated lignin oligomers were analyzed and distributed into sets of structural groups in accordance with the functional groups proposed in the literature. These properties could be relevant to design new bio-oil upgrading systems such as distillers and condensers.

Table 3-4 Estimated thermophysical properties of proposed lignin dimers.

Physical property	Symbol	Author	D1	D5	D7	D1*	D4*	D5*
Normal boiling point, K	T_b	Satou *et al.* [99]	748.6	790.0	736.1	747.1	769.0	798.6
		Yuan *et al.* [100]	636.4	658.3	624.6	636.4	647.6	668.4
		Stein and Brown [98]	713.7	782.1	552.5	632.3	754.7	676.6
Critical temperature, K	T_c	Joback and Reid [102]	4715.9	4764.6	3754.9	4925.1	4885.7	5058.5
		Lydersen [101]	936.6	981.8	918.5	928.4	917.7	918.7
Critical volume, m³K/mol	V_c	Joback and Reid [102]	1116	1190	1115	1095	1233	1233
		Lydersen [101]	1325	1293	828.0	631.0	763.0	737.0
Critical pressure, MPa	P_c	Lydersen [101]	19.7	15.9	21.8	19.2	14.2	19.8
Hansen solubility parameters, MPa$^{1/2}$	δ_d	Stefanis and Panayiotou [103]	22.1	21.1	25.1	24.8	20.9	24.9
	δ_h		19.9	21.3	25.7	25.5	21.7	27.2
	δ_{hb}		31.3	38.6	27.5	21.3	17.8	21.8
Liquid heat capacity at 293.15 K, J/mol.K	$C_{p,l}$	Chueh and Swanson [104]	166.5	181.3	158.2	161.1	184.4	175.9
Solid heat capacity at 293.15 K, J/mol.K	$C_{p,s}$	Hurst and Harrinson [105]	423.5	502.4	382.4	255	268.4	295.2
Gas heat capacity at constant pressure at 300 K, kJ/mol.K	$C_{p,g}$	Harrison and Seaton [106]	272.5	326.0	247.5	262.8	289.6	341.3
Gas standard enthalpy of formation, KJ/mol	$\Delta H_{f,G}^{\circ}$	Joback [102]	-2791	-3478	-2367	-2731	-3265	-3030
Gas standard Gibbs free energy, kJ/mol	$\Delta G_{f,G}^{\circ}$	Joback [102]	-1150	-1594	-757	-1278	-1455	-1270
Gas heat capacity at constant volume, J/mol.K	C_v	DFT calculation	720.2	851.6	646.9	692.1	829.9	758.7
Dipole moment, Debye	μ	DFT calculation	9.1	7.9	8.0	9.9	6.4	9.7

The calculated normal boiling points of the simulated oligomers were between 624 and 790 K for dimers, 720 and 908 K for trimers, and 800 and 1080 K for tetramers. Those results resemble those reported in the literature, where the upper calculated values correspond to larger oligomers. Additionally, the calculated ranges of values for the trimers and tetramers are higher than the typical fast pyrolysis temperatures (773 K). This supports the hypothesis that heavy lignin oligomers (trimers or bigger) are ejected as aerosols during the pyrolysis reaction rather than vaporized [55, 56]. As compared to the evaluated group additivity methods, the Yuan method presents lower values of the oligomers' normal boiling point, while the Satou *et al.* method presents the highest values, as shown in Table 3-5, Table 3-6 and Table 3-7. As the number of rings in the system increases, so does the normal boiling point. However, as the oligomers have a greater number of quinone groups (those that

undergo more than one demethylation) the boiling point values decreases. Although there are no reports of experimental values of this property, the theoretical values reported by E. Terrell *et al.* [83] for the boiling point depending on molecular weight coincide with the values presented in this work. However, the values reported in this work differ from those reported by Fonts et al. [87] for high and low molecular mass pyrolytic lignin, which are 3496 and 1637 K, respectively. This may be due to the fact that the Joback method (used by Fonts) is not adequate when large molecules such as lignin oligomers are involved. Stein and Brown [124] have shown previously that group contribution estimates for normal boiling point tend to diverge from experimental values around temperatures greater than 600 K. Therefore, this work used adjusted methods for this type of systems.

Table 3-5 Estimated thermophysical properties of the proposed lignin trimers.

Physical property	Symbol	Author	T6	T9	T10	T2*	T3*	T7*
Normal boiling point, K	T_b	Satou *et al.* [99]	908.6	900.8	893.1	907.6	907.67	915.3
		Yuan *et al.* [100]	736.2	728.8	721.1	736.2	736.2	743.3
		Stein and Brown [98]	949.9	881.2	795.3	894.4	881.5	973.2
Critical temperature, K	T_c	Joback and Reid [102]	5084.5	5172.2	4783.4	5473.3	5508.4	5367.0
		Lydersen [101]	970.9	1110.5	1064.0	875.6	880.8	884.2
Critical volume, m³K/mol	V_c	Joback and Reid [102]	1666	1602	1499	1657	1689	1712
		Lydersen [101]	1054	1042	1292	1061	1087	1090
Critical pressure, MPa	P_c	Lydersen [101]	10.6	11.9	13.7	11.2	11.4	10.2
Hansen solubility parameters, MPa$^{1/2}$	δ_d	Stefanis and Panayiotou [103]	22.8	25.6	29.6	27.9	26.0	22.6
	δ_h		29.8	32.4	37.9	36.4	33.7	29.7
	δ_{hb}		30.7	34.1	38.0	28.1	28.2	24.5
Liquid heat capacity at 293.15 K, J/mol.K	$C_{p,l}$	Chueh and Swanson [104]	257.7	251.6	243.2	232.7	249.8	255.9
Solid heat capacity at 293.15 K, J/mol.K	$C_{p,s}$	Hurst and Harrinson [105]	687.7	646.6	605.4	402.6	402.6	416.0
Gas heat capacity at constant pressure at 300 K, kJ/mol.K	$C_{p,g}$	Harrison and Seaton [106]	438.6	413.6	388.6	428.9	428.9	453.9
Gas standard enthalpy of formation, KJ/mol	$\Delta H_{f,G}^{\circ}$	Joback [102]	-3650	-5095	-3247	-4682	-4488	-4343
Gas standard Gibbs free energy, kJ/mol	$\Delta G_{f,G}^{\circ}$	Joback [102]	-1190	-2515	-662	-2132	-1906	-1686
Gas heat capacity at constant volume,	C_v	DFT calculation	1179.4	1106.9	1033.9	1150.0	1151.2	1122.4
Dipole moment, Debye	μ	DFT calculation	11.8	4.5	8.8	9.1	11.2	5.5

Hansen solubility parameters are useful in valorization processes of bio-oil fractions because they are related to the intermolecular forces between compounds. Therefore, they are relevant in liquid-liquid extraction systems to select the solvent in analytical and industrial scale applications. The Hansen solubility parameter considers dispersion forces

(δ_d), dipole-dipole forces (δ_{dh}), and hydrogen bonding (δ_h). The values reported in Tables 3-5, 3-6, and 3-7 show a similar behavior to that of the normal boiling point, as structures with more molecules (monomers) and quinones present higher solubility values. Ethyl acetate, dichloromethane and acetone may be suitable to extract the pyrolytic lignin fraction in bio-oil. The values in Tables 3-5, Table 3-6 and Table 3-7 are similar to those reported by I. Fonts; however, they are higher than those reported by E. Terrell [88], it could be explained because the group contribution method used were different. Liquid and solid heat capacity are used in the design of bio-oil upgrading systems and are reported in the tables.

Table 3-6 Estimated thermophysical properties of lignin tetramers.

Physical property	Symbol	Author	OG12	OG13	OG14	OG8*	OG9*	OG10*
Normal boiling point, K	T_b	Satou *et al.* [99]	1068.6	1056.7	1045.5	1051.7	1052.4	1053.1
		Yuan *et al.* [100]	804.4	799.1	793.5	804.4	804.4	804.4
		Stein and Brown [98]	1204.9	118.2	1040.9	1123.6	1132.9	1123.6
Critical temperature, K	T_c	Joback and Reid [102]	5719.5	5625.4	5765.9	5090.5	6078.2	5990.5
		Lydersen [101]	1026.4	968.1	1009.8	906.3	924.8	906.3
Critical volume, m³K/mol	V_c	Joback and Reid [102]	2208.0	2091.0	2100.0	2228.5	2167.5	228.5
		Lydersen [101]	2748.0	1294.0	1394.0	1519.0	1548.0	1519.0
Critical pressure, MPa	P_c	Lydersen [101]	8.2	9.8	8.7	7.6	7.9	7.6
Hansen solubility parameters, MPa$^{1/2}$	δ_d	Stefanis and Panayiotou [103]	23.8	26.1	28.9	26.5	27.6	25.9
	δ_h		34.9	39.2	42.6	40.4	39.4	39.0
	δ_{hb}		44.6	40.6	44.5	34.7	41.9	34.4
Liquid heat capacity at 293.15 K, J/mol.K	$C_{p,l}$	Chueh and Swanson [104]	348.8	340.4	329.0	340.9	340.3	340.9
Solid heat capacity at 293.15 K, J/mol.K	$C_{p,s}$	Hurst and Harrinson [105]	951.9	910.8	869.6	936.8	936.8	936.8
Gas heat capacity at constant pressure at 300 K, kJ/mol.K	$C_{p,g}$	Harrison and Seaton [106]	604.8	579.8	554.8	595.1	595.1	595.1
Gas standard enthalpy of formation, KJ/mol	$\Delta H_{f,G}^{\circ}$	Joback [102]	-6888	-7250	-7200	-6819	-6822	-6819
Gas standard Gibbs free energy, kJ/mol	$\Delta G_{f,G}^{\circ}$	Joback [102]	-3083	-3642	-3636	-3164	-3193	-3164
Gas heat capacity at constant volume,	C_v	DFT calculation	391.7	357.2	357.2	1610.2	1611.2	1610.8
Dipole moment, Debye	μ	DFT calculation	10.2	8.2	8.2	7.4	9.2	11.0

The enthalpy of formation is necessary to calculate the energy balance of the pyrolysis reaction and subsequent processes like distillation and hydrotreatment, while Gibbs free energy of the compounds is useful to analyze the spontaneity of a reaction. The dimers' results for these properties are consistent with the values reported by Fonts [87] for low molecular mass. The values are -1447.9 and -750.9 kJ/mol for the gas standard enthalpy of formation and gas standard Gibbs free energy for low molecular mass. The dimer molecular mass is around 370 amu, value close to 400 amu for the low molecular weight compounds that were used in the reference. On the contrary, the trimers and tetramers molecular mass are around 550 and 750 amu, far from the 1050 amu that the reference used as a surrogate bio-oil, thus indicating again that the Joback method is not adequate for the size of the lignin oligomers.

3.4 Conclusions

Based on the results of this study, the following insights are proposed. Structures for dimer, trimer, and tetramer oligomers are suggested based on the demethylation reaction, as it is assumed to be one of the primary reactions happening after depolymerization. Initial assignments were proposed starting with direct βO4 homolysis to generate two free radical fragments that can be either dimers, trimers, or tetramers. These radical fragments can stabilize, taking hydrogen radicals that may be in solution during the formation of the intermediate liquid (pathway 1) before the thermal ejection. Another pathway (pathway 2) could happen when the radicals use intramolecular hydrogen, turning themselves into stable products. Electronic structure calculations on model pyrolysis reactions show several structures of dimers, trimers, and tetramers depending on the Gibbs free energies of the reaction. The most probable oligomers have a β5 bond and are conjugated structures. These kinds of bonds reduce the stability of G and S units caused by conjugated C-C double bond and imply the formation of quinone methides. In addition, quinones can be an intermediate compound or a final product in lignin thermal decomposition in the biomass pyrolysis process, as suggested elsewhere [43, 44]. According to the FTIR results, oligomers D5 (SβO4S-CH$_4$), T3* (Gβ5GβO4S-H$_2$-CH$_4$), and OG13 (GβO4SβO4Sβ5G-2CH$_4$) have a comparable spectrum and therefore a more similar structure if compared with the experimental pyrolignin used in this study. The molecular structures of the demethylated lignin oligomers were analyzed and distributed into sets of structural groups according to the functional groupings proposed in the literature. These properties could be relevant in the design of new bio-oil upgrading systems such as distillers and condensers. The normal boiling points for both trimers and tetramers are higher than 773 K. This supports the hypothesis that heavy lignin oligomers are not vaporized but ejected during the pyrolysis reaction.

4. Separation and characterization of targeted pyrolytic-lignin fractions

The bio-oil generated through the process of pyrolysis is composed of a highly complex mixture of numerous organic compounds. This study utilized a combination of liquid-liquid extraction and column chromatography techniques to separate the different chemical compounds present in pyrolignin. The separated fractions were then analyzed using various analytical techniques, such as UV-fluorescence, FTIR, PyGC-MS, and 2D-HSQC NMR spectroscopy. The analysis showed that the ethyl acetate fraction was primarily composed of phenolic compounds with methoxyl substituents, while the acetone and isopropanol fractions mainly consisted of aliphatic compounds. These findings suggest that the ethyl acetate fraction could be a promising candidate for use in antibacterial applications. The results of this study provide valuable information for the development of strategies aimed at incorporating pyrolysis bio-oil feedstocks into the framework of a biorefinery.

4.1 Introduction

The increasing demand for raw materials, the depletion of fossil fuels, and the environmental consequences associated with their consumption have made it imperative to find alternative sources of energy. Pyrolysis bio-oil derived from lignocellulosic biomass is an attractive candidate in this regard as it is comprised of a mixture of various chemical compounds and has the potential to provide both energy and useful products. However, the high oxygen content, complex composition, and low calorific value of bio-oil present significant challenges for its utilization [1]. The heavy fraction of bio-oil has been identified as a potential source of non-fuel co-products due to its ease of separation from the rest of the mixture and its composition, which mainly consists of aromatic structures [2]. This fraction, referred to as pyrolytic lignin or pyrolignin, is formed through the depolymerization and recombination of lignin fragments during the pyrolysis process, and accounts for 13-27 wt.% of the bio-oil.

The utilization of pyrolytic lignin as a feedstock for renewable chemicals and components in bio-based materials, such as bio-asphalt, biopolymers, bio-binders, and phenolic resins, has been proposed [3]. The high molecular weight, viscosity, and reactivity of these lignin oligomers in the bio-oil contribute to its instability, making it challenging to process the oil into valuable products [4]. In a biorefinery framework, it is crucial to consider the content and structural characteristics of these oligomers. Hence, there is a pressing need to develop techniques to isolate these oligomers from the bio-oil to enhance its valorization and utilization as a high-value resource [1].

Bio-oil refinement aims to simplify its composition and concentrate its components with similar characteristics and structures, thereby improving its purity and making it easier to recover and utilize. Methods such as liquid-liquid extraction, distillation, centrifugation, membrane separation, and solid-liquid chromatography can be employed, but liquid-liquid extraction (organic solvent extraction) is particularly promising because the solvent can be recovered and reused and the process can be conducted at room temperature and atmospheric pressure, making it economically viable [5]. Solvent extraction capitalizes on the differences in solubility between polar and nonpolar compounds in the bio-oil to categorize them according to the solubility of specific solvents [6]. In comparison, solid phase extraction is a noteworthy technique as it eliminates the formation of an emulsion between the bio-oil and solvent, and it can effectively separate selected compounds from a mixture using a solid adsorbent [7].

Wang *et al.* [8] investigated the separation of monophenols and pyrolytic lignin using a multi-step method with acidic solution, basic solution, and organic solvents. They found that the phenolic fraction obtained through reactive extraction of the water-insoluble phase was rich in phenolic compounds, with a high concentration of 94.35 wt.%, and the guaiacol content reaching 48.27 wt.%. Both light and high-molecular weight pyrolignin were found to contain reactive phenolic compounds and polymers with molecular weights of 1000 g/mol and 1700 g/mol, respectively. In a recent study, Matos *et al.* [9] examined the fractionation of eucalyptus pyrolignin using aqueous acetone solutions. They analyzed the fractions using GPC (Gel Permeation Chromatography), NMR (Nuclear Magnetic Resonance), FTIR (Fourier Transform Infrared Espectroscopy, TGA (Temo Gravimetric Analysis), and GC-MS (Gas Chromatography – Mass Spectroscopy). The most soluble fraction produced a more homogeneous fraction, containing a concentration of phenolic, carboxylic, and lower molecular weight compounds. The antioxidant activity was mainly due to phenolic compounds with methoxy substituents.

Hertzog et al. [10] conducted a study on the fractionation of bio-oil using flash chromatography, which resulted in four different fractions. The achieved fractions were analyzed using FT-ICR MS and NMR spectroscopy. The stationary phase was silica gel, and to elute the bio-oil compounds, toluene, methanol, water, and formic acid were used. The authors concluded that fraction 1 was characterized by low-oxygenated and unsaturated compounds, fraction 2 consisted of more oxygenated unsaturated compounds, fraction 3 had some derivatives of cellulose and hemicellulose, and fraction 4 had more polar compounds from the pyrolysis of cellulose and hemicellulose.

The aim of this study is to perform a novel combination of liquid-liquid extraction and solid-liquid chromatography to separate pyrolytic lignin, in order to uncover valuable chemical characteristics that can aid in its valorization as part of a bio-oil-based biorefinery. This research is a critical step in advancing the industrial use of lignin and making pyrolysis oil biorefineries a practical reality. The findings from this study will provide a deeper insight

into the composition and structure of pyrolytic lignin fractions, which will aid in the design of biorefineries processes.

4.2 Methodology

Bio-oil fractionation by liquid-liquid extraction

The study utilized a sample of pyrolysis bio-oil procured from BTG (Netherlands) that was stored in a refrigerator at a temperature of 268 K. The method used was a multi-step solvent fractionation adapted from Garcia et al. (2007) with minor modifications as depicted in **Error! Reference source not found.** [24]. The bio-oil was thoroughly mixed by manual shaking and 300 mL of it was subjected to rotary evaporation at a temperature of 55 °C and a vacuum pressure of 28 in Hg to obtain the light fraction. The resulting bio-oil was then mixed with 25 wt.% of methanol and subjected to sonification and vortex agitation for an hour to homogenize the mixture. A 10 g sample of the mixture was taken for precipitation in cold water, following a previously reported procedure [11]. The resulting emulsion was then separated by vacuum filtration using Whatman filter #42, yielding the fractions that were insoluble and soluble in water.
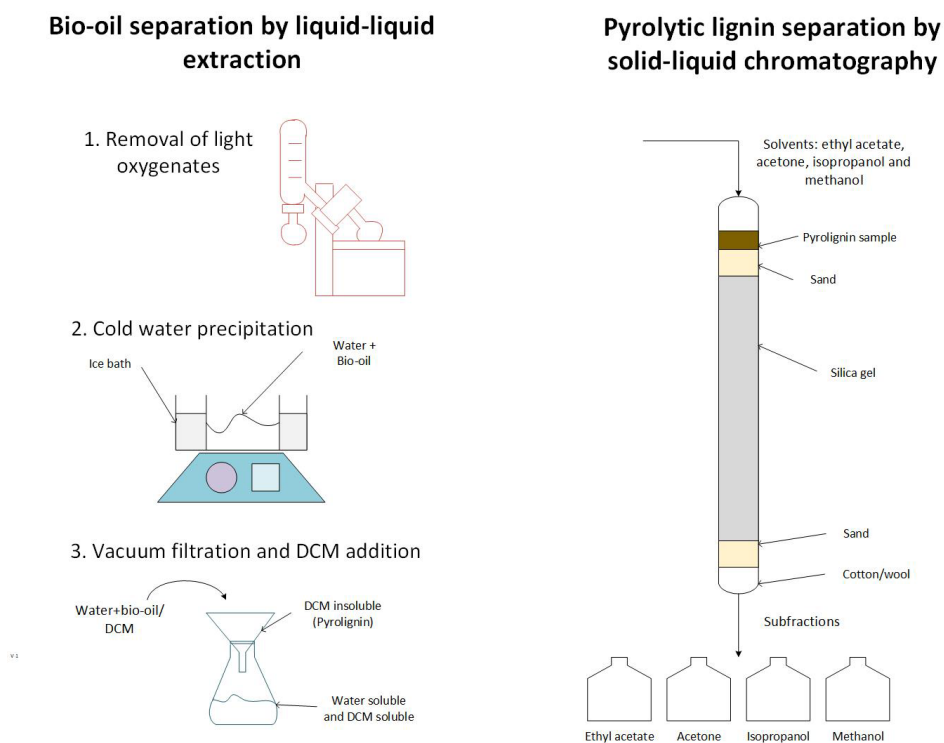
Figure 4-1. Solvent fractionation and column chromatography extraction for the pyrolytic lignin.

The water-insoluble portion was allowed to air dry on the Buchner filter for 4 hours. Then, dichloromethane (DCM) was passed through to separate the DCM-soluble and DCM-

insoluble components. The DCM-insoluble fraction, also known as pyrolytic lignin, was left to dry in a well-ventilated area overnight before being stored in the refrigerator. All chemical reagents used were of high-performance liquid chromatography (HPLC) grade (Supelco, Italy).

Pyrolytic lignin fractionation by solid-liquid chromatography

The separation of pyrolignin was performed in a 100 mL burette with a 17 mm outer diameter. The column was filled with 36 grams of silica gel for chromatography, which was ultra-pure with a particle size of 40-60 um and 60 Angstrom. At the bottom of the column, a small piece of loosely packed wool and cotton was added, followed by 2.7 grams of J.T. Baker sand placed at both the bottom and top of the column, as depicted in Figure 4-1.The retention volume of the column was 30 mL, with a residence time of 68 minutes. 150 mg of pyrolytic lignin were dissolved with 1 mL of methanol. The sample was loaded and after it was completely absorbed in the sand layer, the first 30 ml of the methanol were added and the collection process started. The other 30 mL were added at the end of the 68 minutes following the process until the four solvents were used. The solvents used were ethyl acetate, acetone, isopropanol and methanol for their different polarities. Four fractions were collected to eliminate the solvent through rotary evaporation process and subsequently store in the fridge. All the chemical reagents used were of HPLC grade (Supelco, Italy).

^{1}H NMR and HSQC studies

The ^{1}H-NMR and HSQC (Heteronuclear Single Quantum Coherence) spectra were determined to analyze chemical characteristics related to the structure of the subfractions. These experiments were determined on a Bruker 500 Neo spectrometer equipped with a 5mm Prodigy broadband cryoprobe with Z-axis gradients. Model compounds (30 mg each) proton spectra were obtained at 500.13MHz in DMSO-d6 (0.6 mL), 30 °C with 16 scans, 90° pulse (12 μs), 3 s relaxation delay, and acquisition time of 4.4 s, 32768 points, and a spectral width of 7463 Hz. Proton data were apodized with 1.3 Hz of line broadening. HSQC spectra were acquired at 125.77 MHz with 90° pulse angle (10.0 μs), 1.08s acquisition time, 2 s relaxation delay d1, and inverse-gated ^{1}H composite pulse decoupling using 4000 scans, a spectral width of 30120.5 Hz, and 32768 points. The FID was apodized with 8 Hz exponential line broadening of the model compounds.

ATR-FTIR studies

FTIR spectra were obtained using a Shimadzu IRPrestige 21 spectrometer equipped with MIRacle^{TM} single reflection ATR Ge probe. A drop of oil was applied to cover the crystal window, and the spectra were acquired with 64 scans, 600 to 4000 cm^{-1}, with a resolution of 4 cm^{-1}. The spectra were baseline corrected and band fitted between 1490 and 1850 cm^{-1} using 9 Gaussian bands.

UV Fluorescence (synchronized)

The subfractions were diluted in HPLC-grade methanol at 5000 ppm and analyzed on a Shimadzu RF 5301 pc (software: Panorama Fluorescence 2.1) spectrometer. Synchronous fluorescence spectra at a constant wavelength difference were set. The excitation wavelength was scanned from 250 to 700 nm, and emission wavelengths were recorded with a 15 nm difference (from 265 to 715 nm). The excitation slit width and emission slit width were set at 3 nm. Data were collected every 1 nm.

4.3 Results and Discussion

4.3.1 Bio-oil and pyrolytic lignin separation

The resulting fractionated chemicals depended on the polarity and classification of the solvent used in the liquid-liquid extraction. The solvent operates based on the relative solubilities of two immiscible liquids or phases. Organic soluble compounds dissolved and distributed themselves in the solvent and the distinct denser phase of the organic fraction settled and could be separated easily [125]. The first stage of the separation scheme was the removal of the light oxygenates compounds such as water, acetic acid, and acetaldehyde through rotary evaporation of the bio-oil. The percentage of these light compounds in this extraction was 26 wt. %. Later, the remaining bio-oil was mixed with 25 wt.% of methanol. The addition of methanol disrupted the heavy fraction, benefitting the precipitation of pyrolytic lignin upon subsequent addition of water [126]. Water was used as the first solvent in this separation scheme applying a cold-water precipitation method to dissolve and isolate water-soluble and water-insoluble phases to form an aqueous phase and pyrolytic lignin. Through water extraction, compounds with hydrophilic functional groups interact with water, creating a miscible and an immiscible phase due to the difference of water solubilities of pyrolytic lignin and sugars. The miscible phase (water-soluble) was a yellow solution consisting mainly of carbohydrate-derived polar compounds such as lower molecular weight phenols, acids, and ketones [127]. Sugars have strong hydrophilicity due to their polyhydroxyl moieties, whereas pyrolytic lignin has complex structures and many hydrophobic groups. Water soluble fraction had a recovery yield of 59.3 wt.%. The immiscible phase (water insoluble) was a brown solid, rich in monophenols and less polar phenolic oligomers with high molecular weight and bearing polyfunctional groups which remained cross-linked [41], [119]. The water-insoluble recovery index in this fraction was 14.69 wt.%, which is among the reported values of 13.5 and 27.7 wt.% according to [2] and [8]. Bio-oil contain various functional groups (hydroxyl, alkyl, alkoxy, carboxyl, carbonyl, etc.). The next step in the separation scheme was the addition of DCM where the monophenols and oligomers were separated into low and high molecular weight fractions with recovery yields of 8.7 and 6 wt.% respectively [129]. The recovery yield of each fraction is shown in Table 4-1.

Table 4-1. Recovery yield of liquid-liquid extraction for bio-oil.

Fraction	Content (wt. %)
Light	26.0
Water soluble	59.3
DCM soluble	8.7
DCM insoluble	6.0
Total	100.0

Solid phase extraction was used to separate and isolate the compounds in the pyrolytic lignin fraction. During the adsorption process, pyrolytic lignin compounds are adhered to the surface of the silica gel, either by physisorption or chemisorption. The adsorption principle lies on the surface chemistry of adsorbent and adsorbate, the molecular size of the adsorbate that influences the diffusion and mass transfer into the pores of absorbent [62]. In the column chromatography separation, 300 mg of this pyrolytic lignin fraction was dissolved in 1 ml of methanol and placed at the top of the packed column for solid-liquid separation according to Figure 4-2. The pyrolytic lignin subfractions yields are showed in Figure 4-2.
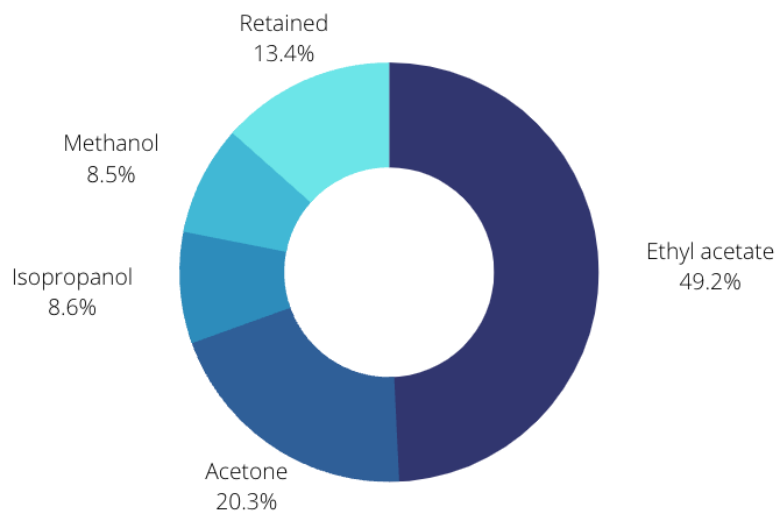
Figure 4-2. Solid-liquid chromatography yield.

Four solvents of different polarity (from high to medium polarity) were used to separate the highest test number of compounds from the initial matrix. The first solvent used was ethyl acetate with a yield of 49.2 wt.%, the second was acetone with 20.3 wt. %, the third isopropanol with 8.6 wt.% and finally methanol with 8.5 wt. %, in the column there was a remainder of 13.4 wt. % because part of the polar compounds were retained due to the great affinity of these compounds with the silica gel within the column.

4.3.2 Characterization of pyrolytic lignin subfractions

The distribution of the heavy molecules in the subfractions was also studied and is presented in the Figure 4-3, which shows the UV-fluorescence spectra for PL and the four subfractions. Three distinct regions can be observed: i) monophenols before 285 nm, ii) dimers and short conjugated systems around the range between 285 and 320 nm and iii) polycondensed structures after 320 nm [130]. Peaks of high intensity for the "monophenols region" are present in the pyrolignin, ethyl acetate and isopropanol subfractions, while the acetone and methanol subfractions show a lower intensity in this region, which indicates a separation during the column chromatography. Presence of dimers and short conjugated systems was not clear in these samples. Peaks in the multiaromatic and conjugated ring and systems area (>320 nm) are present in all samples. The polycondensed structures are found mostly in the ethyl acetate fraction, evidenced by two peaks with the highest intensity from 320 to 440 nm. These polycondensates are also present, although to a lesser extent, in the pyrolignin and 3-isopropanol subfraction, although its intensity is much lower. Nevertheless, the shape of the UV spectrum is preserved (first peak with more intensity than the second at the same wavelength). The fourth subfraction (methanol) shows a spectrum where the second peak is very small in proportion to the first, which shows that it could be chemical variations in these compounds. The 2-acetone subfraction presents an opposite spectrum, the first peak is smaller than the second, also, shows signal with more intensity than the other fractions between 440 and 620 nm evidencing that there are differences between the chemical composition of the polycondensates of this fraction, which is why they show important variations in their absorbance.
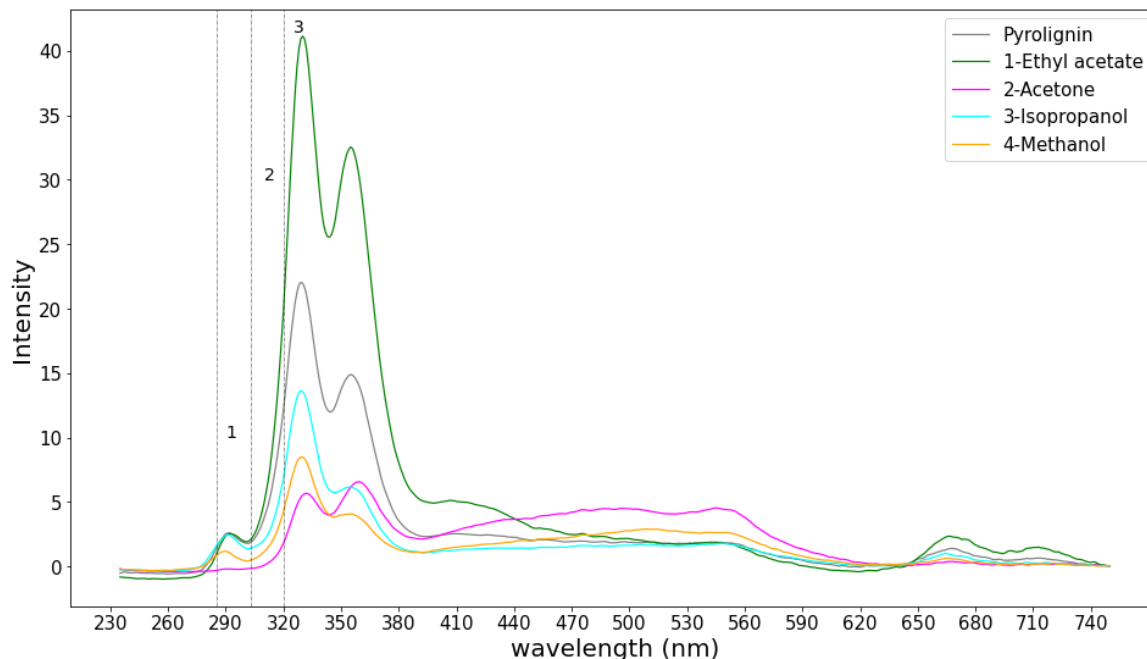
Figure 4-3. UV fluorescence spectra for pyrolytic lignin and its subfractions; region 1: monophenols, region 2: dimers and short conjugated systems and region 3: polycondensed structures.

The pyrolytic lignin and its subfractions were also subjected to FTIR spectroscopy tests. The obtained spectra for all the subfractions are presented in Figure 4-4. The peak at 1460 cm^{-1} is associated to C-H asymmetric deformations of the methylene group, from the $-CH_2$ and $-CH_3$ groups. Absorption bands at 1510 cm^{-1} are present in the pyrolignin and all its subfractions. This band results from carbonyl and aromatic skeletal vibrations [131]. The presence of these peaks shows that there was a permanence of S and G units after pyrolysis. This is probably due to the high thermal stability of methoxy groups when linked to aromatic rings. Peaks at around 1600 cm^{-1} are associated to conjugated C=O groups and are often broadened by aromatic skeletal vibrations [128], and bands of 1620-1610 cm^{-1} means C=C strain of the α,β-unsaturated ketone group.

Carbonyl groups are formed during pyrolysis due to thermal cleavage and high reactivity, they are also one of the factors that increase bio-oils instability [15]. Several peaks around 1700 cm^{-1} are present in the second subfraction when acetone was used as a solvent to separate the pyrolytic lignin. The band at 1700 cm^{-1} is attributed to the unconjugated C=O stretching vibrations, which refers to the unconjugated carbonyl of ketones and esters [126]. The presence of these peaks has been reported when acetone is used in the fractionation

process [15]. This suggests that the use of acetone allows its interaction with these compounds and flushes these compounds into the subfraction 2.
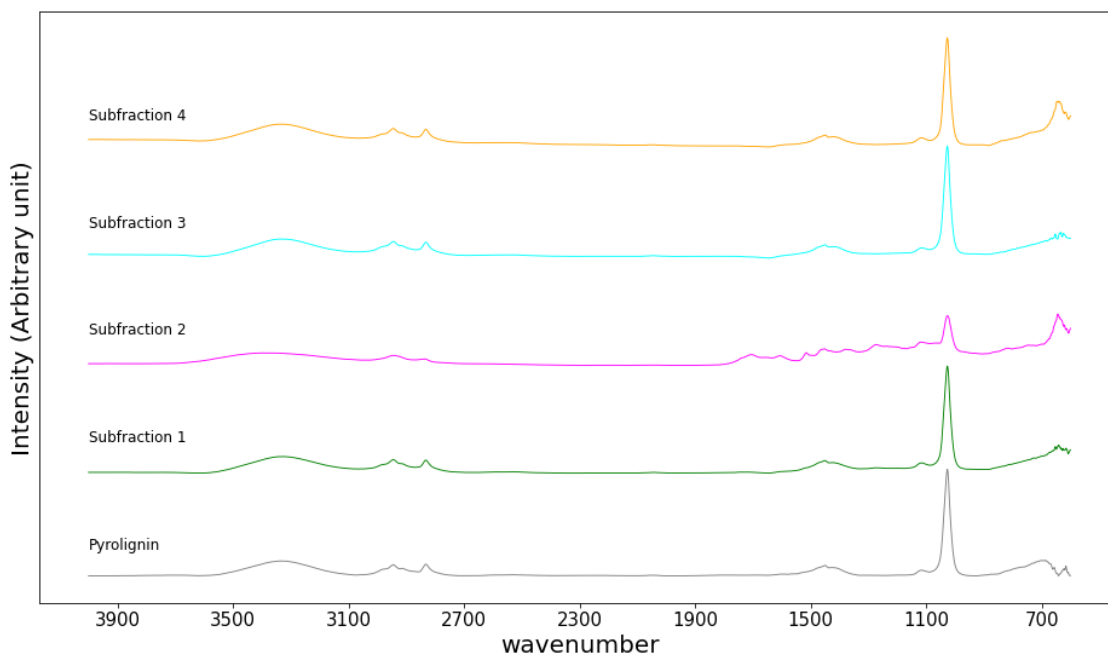
Figure 4-4. FTIR spectra of pyrolytic lignin and its subfractions.

NMR spectroscopy was performed on the samples in order to investigate the chemical structure of the pyrolytic lignin and its subfractions. The assigned numbers shown in Figure 4-5 are according to the Kishimoto *et al.* [132]. The pyrolignin spectrum showed a strong resonance between 2.2. and 2.5 ppm, traceable to the acetylated phenolic hydroxyl groups while the peaks between 3.4 and 4.0 ppm could be attributed to the H in -OCH_3 groups. Other peaks in the region between 0.7 to 1.6 ppm are related to the H in -CH_2 and -CH_3. The region between 1.7 and 2.2 ppm is associated to H in acetylated aliphatic OH. Both types of hydroxyl groups had high contents in the pyrolytic lignins, which is consistent with the FTIR results. The larger amount of hydroxyl groups in PL might be explained by the higher degree of degradation of the lignin during the pyrolysis process, because the functional groups were released by the breakage of ether linkages. Finally, signals between 6.8 and 8.7 ppm are present in the spectrum indicating the presence of aromatic H present in the pyrolignin rings.

The column chromatography process of PL shows an effective separation of the functional group signals related to H in -CH_2, -CH_3, acethylated aliphatic OH and acethylated phenolic OH that do not appear in the subfractions of PL. This signal lost intensity when the polarity of the organic solvent in the process was increased. This suggests these groups remain in the silica gel because of its polarity. It can be a good option to separate these compounds, making them more suitable for use in the synthesis phenolic resins [133].
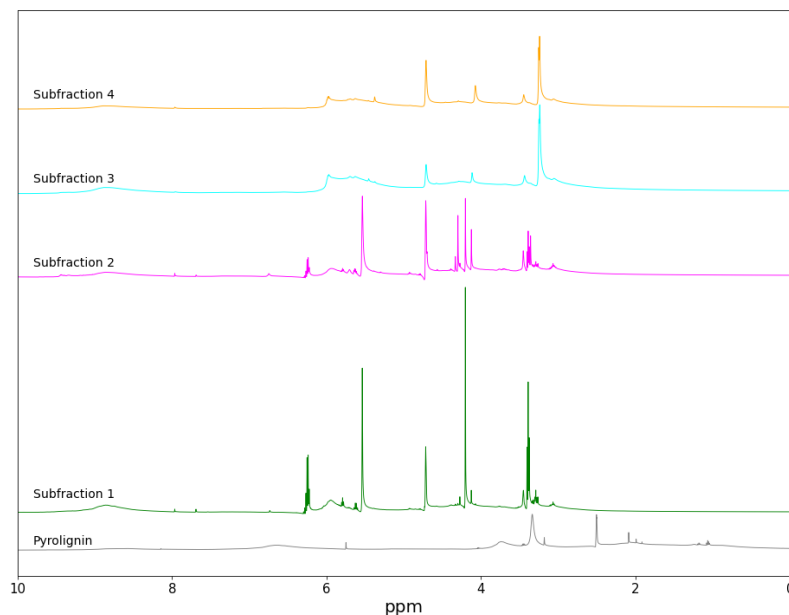
Figure 4-5. Proton NMR spectra achieved for the pyrolignin and four subfractions.

2D HSQC NMR was used to elucidate the structural characteristics of the pyrolignin subfractions. The spectra of the four samples are displayed in Figure 4-6. According to the chemical shift δ_C/δ_H, the HSQC spectrum can be divided into an aromatic region (δ_C/δ_H 90-160/5.5-9.0) and an aliphatic sidechain region (δ_C/δ_H 0-5/0-70) including C-O region and C-C region. For the ethyl acetate fraction, the aromatic region contains resonance signals of H, G and S units, among which G units are the most prevalent. These results are according to the FTIR spectrum for the ethyl acetate fraction that shows peaks related with the aromatic skeleton. Phenolic compounds are related to antibacterial activity [134]. In the aliphatic sidechain region, the resonance peaks at δ_C/δ_H 5-25/0.5-1.5 are attributed to -CH$_3$ or -CH groups and that in (δ_C/δ_H 25-40/0.5-3.5) are from CH$_2$ of sidechains groups [135]. The side chain (δ_C/δ_H 50-90/2.5-5.0 ppm) shows the presence of methoxyl groups in the ethyl acetate subfractions. Some studies [15], [134] have attributed antioxidant activity to phenolic compounds with methoxyl substituents, indicating the potential of this subfraction for this use.
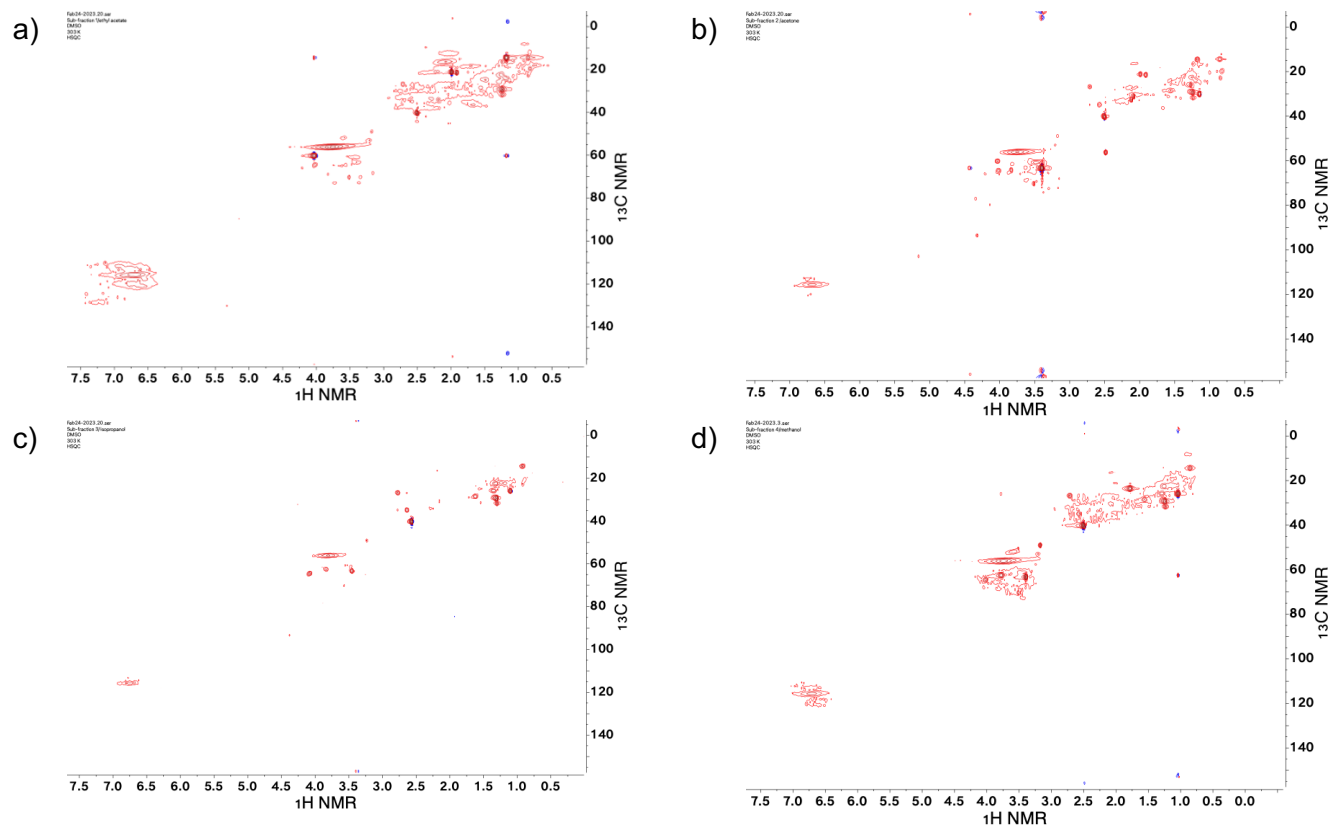
Figure 4-6. 2D HSQC NMR spectra of pyrolytic lignin subfractions, a) ethyl acetate, b) acetone, c) isopropanol and d) methanol.

The acetone and isopropanol subfraction spectra just show the presence of compounds in the aliphatic sidechain region. The cross signal at δ_C/δ_H 60-70/4.0-3.5 ppm is associated with β aryl-ether structures, these structures tend to be cleaved during pyrolysis. However, some of them may remain due to their high activation energies [136]. The other signal at δ_C/δ_H 55.5/3.7 ppm is attributed to C/H in methoxyl groups.

4.4 Conclusions

he findings of this research indicated that liquid-liquid extraction procedures combined with column chromatography are effective methods for separating fractions with varying chemical compositions. As such, once specific compounds or groups of compounds have been detected, these techniques can be utilized for their separation and subsequent utilization. The pyrolytic lignin subfractions were characterized using UV-fluorescence, FTIR, NMR and PyGC-MS. These methods demonstrated the charachteristics of each of the sub-fractions. Ethyl acetate subfraction (subfraction 1) was characterized by phenolic compounds with methoxyl substituents, acetone, and isopropanol subfraction (2 and 3) showed more aliphatic characteristics. The fractionation process also furnished pyrolytic lignin fractions that possess good biological activity, which can be used to develop alternative antibacterial agents [15]. However, given the intricate chemical composition of pyrolignin, the separation and purification of certain compounds demands the application

of multiple separation methods and a multi-step process, such as liquid-liquid extraction and column chromatography. Furthermore, it is suggested to enhance the separation process in column chromatography to isolate more fractions of desired compounds. This will help in formulating strategies for incorporating pyrolysis bio-oil feedstocks into a biorefinery.

5. Co-hydrotreatment of pyrolytic lignin and yellow grease: effect of pyrolytic lignin concentration on coke formation yield

Hydrotreatment is an effective approach to process vegetable oils into bio-fuels composed of straight and branched chain aliphatic hydrocarbons. The content of aromatics in these fuels is usually very low; co-hydrotreatment of pyrolytic lignin and yellow grease over NiMo/Al$_2$O$_3$ catalyst adds an aromatic structures to them. Co-hydrotreatment studies with different pyrolytic lignin/yellow greases blend ratios (0, 10, 20, 30, and 40 wt.%) were conducted. The coke formation value for yellow grease was 0.7 wt.% and ranged between 1.5 and 2.5 wt.% with the increase of pyrolytic lignin in the blend. It suggests that the formation of solids in the bio-oil hydrotreatment is strongly related to the oligomers from the sugar fraction and that PL has potential to reduce coke formation in the process. All blends are recommended for the co-hydrotreatment of these blends based on coke yield. The resulting organic phase was distilled into gasoline, kerosene, and diesel. The overall fuel distribution of the organic product was shown to be strongly dependent on the pyrolytic lignin concentration. The diesel yield was higher in the hydrotreated samples, with more than 20 % during distillation. Two-dimensional GCxGC was used to determine carbon distribution on the fuels. FTIR and UV fluorescence spectra showed that most of the feedstock was converted to biofuels after hydrotreatment. The fuel properties, such as density, viscosity, and surface tension, were reported and compared to transportation fuel properties. Fuel yields revealed the potential of co-hydrotreatment to upgrade pyrolytic lignin into valuable products.

Keywords: hydrotreatment, pyrolignin, yellow grease, coke, fuels.

5.1 Introduction

The increasing energy demand has raised concerns about the extraction of fossil fuels and environmental pollution and have led many researchers to investigate alternative energy sources. Lignocellulosic biomass is a renewable resource to produce fuels, chemicals, and materials that could eventually to replace part of the fossil fuels [17]. Fast pyrolysis is a well-known process to produce bio-oil from biomass. The latter being a multicomponent mixture formed mainly of oxygenated organic compounds such as acids, water, alcohols, ethers, anhydrous sugars, furans, phenols, aldehydes, and ketones which covers a wide range of molecular weight and functionalities [18], [19]. Pyrolytic lignin (PL) is the water-insoluble fraction of the pyrolysis bio-oil where the hydrophobic compounds are mainly fragments derived from it [12] and have less oxygenated compounds [13] compared to other biomass building blocks, thus making the hydrotreatment process a more attractive upgrading option. Additionally, pyrolytic lignin requires further depolymerization (because it

has a low number of monomers and is chemically heterogeneous) to be used as a source of biobased chemicals and fuels[16]. Yellow grease (YG) is considered a cost-effective feedstock for fuel production due to its lipid content and relatively low cost and abundance [137]. Triglycerides are the main components of all vegetable oils and fat structures and are formed from a single molecule of glycerol combined with three fatty acid molecules. The objectives of bio-oil upgrading is to reduce the oxygen content and molecular weight, to increase the H/C ratio, and to improve thermal stability [7]. Several upgrading processes such as high-pressure thermal treatment, zeolite cracking, and hydrotreatment have been proposed [10–13]. Hydrotreatment —also known as hydrodeoxygenation (HDO)— has become a promising technology; it consists in subjecting the bio-oil to a heterogeneous system with hydrogen at medium temperature and high-pressure conditions (350-400 °C and 10-30 MPa) to eliminate the oxygen reactive functionalities. However, rapid catalyst deactivation related to coke formation at elevated temperatures is a limiting factor in this process. Coke forms because the cracking and depolymerization of the abundant oxygen-containing organics in bio-oil —due to the benzene rings in pyrolytic lignin— are electron-rich and facilitate electrophilic substitution to form much heavier organics [14, 15].

Afshar Taromi and Kialiaguine [140] studied the deoxygenation of triglycerides from canola oil using a continuous fix-bed reactor. They evaluated sulfide NiMo and CoMo catalysts supported on alumina and determined some differences in FTIR spectra and the distribution of liquid products. NiMo catalyst presented satisfactory catalytic properties with advantages in reaction time and selectivity for green diesel production. Another work with triglycerides was done by Han *et al.*[141] They studied the co-hydrotreatment of tire pyrolysis oil and vegetable oil to produce transportation fuels. They proposed an effective technology to convert this feedstock into straight and branched chain aliphatic hydrocarbons. Aliphatic C7-C12 and aromatic C6-C10 were mainly collected in the naphtha cut, aliphatic C9-C12 and aromatic C6-C10 in the kerosene cut, and aliphatic C15-C20 and aromatic C10-C16 for the diesel cut.

Lv *et al.*[142] evaluated the hydrodeoxygenation process with pyrolysis bio-oil and lignin-derived oil at different temperatures (250-350 °C). They concluded that lignin-derived oil is an effective coke suppression agent for pyrolysis oil upgrading because the coke yield during the process was lower when they did cofeeding with lignin-derived oil. Additionally, the oxygen content could be effectively reduced from a mass fraction of 45-50% in the upgrading process.

Han *et al.* [143] studied the co-hydrotreatment of vegetable oil and bio-oil-derived lignin rich oil to identify suitable co-processing conditions for the hydro processed ester and fatty acid process to be used in diesel and jet fuels. Blends of lignin-rich oil and vegetable oil (1:8, 1:4, and 1:1) were prepared and hydrotreated over $CoMo/Al_2O_3$ at 623 K and 500 rpm, with 9.3 MPa of an initial hydrogen pressure for 4 h. Cracking/stabilization studies were also conducted in the presence of butanol and methanol. The best results were obtained with the oils stabilized with butanol, which acts as a hydrogen donor and helps increase the hydrogenation efficiency [143]. The yield of coke decreased from 34.7 wt.% on lignin-rich oil basis to 6.65 wt.%. They also studied the experimental conditions that maximize kerosene yield and reduce coke during the co-processing of yellow grease and water-

insoluble bio-oil, keeping the same vegetable oil/pyrolytic lignin blends. Hydrotreatment was conducted over NiMo/Al$_2$O$_3$; they proposed to conduct it at 380°C, initial H$_2$ pressure of 7 MPa, and 1.3 g of catalyst to improve the kerosene yield to more than 20 wt.% and reduce the yield of coke to 2.0 wt.% approx.

The aim of this work is to evaluate the coke formation in the hydrotreatment process at different concentrations of pyrolytic lignin and yellow grease. The information collected will also be useful to understand the potential of co-hydrotreatment to upgrade pyrolytic lignin into valuable products like transportation fuels.

5.2 Methodology

In this study, co-hydrotreatment studies with different pyrolytic lignin/yellow grease blend ratios (0, 10, 20, 30 and 40 wt.%) were conducted using a NiMo/Al$_2$O$_3$ catalyst at a high temperature (380 °C) and a high hydrogen pressure (7.5 MPa).

5.2.1 Chemicals

The studied pyrolysis bio-oil was purchased from BTG (The Netherlands) and stored in a refrigerator at 268 K. The BTG bio-oil was produced from pine wood using a rotating cone reactor under the following conditions: ambient pressure, reactor temperature of approximately 500 °C, and short gas residence time (<2 s). The bio-oil was fully mixed by hand shaking before use. The pyrolytic lignin was obtained by centrifugating the bio-oil-water mix in a 1:2 mass ratio. The oil phase was collected and mixed again with 1-butanol in a 1:2 mass ratio to mitigate polymerization reactions and enhance the miscibility with the waste cooking oil at the sample mass ratios. The pre-filtered waste cooking oil (yellow grease) was procured from Baker Commodities Inc. and stored at room temperature. The blends were prepared at different concentrations of pyrolignin in vegetable oil (0, 10, 20, 30, and 40 wt.%). The NiMo catalyst was provided by Pacific Northwest National Laboratory (PNNL), and dimethyl sulfide (DMDS) from Sigma Aldrich was used as the sulfur source to activate the catalysts. Nitrogen and hydrogen were obtained from Linde (Germany) and were all analytical grade (>99.99% purity).

5.2.2 Co-hydrotreatment experiments

The blends at different concentrations (0, 10, 20, 30, and 40 wt.%) were hydrotreated in a 250 mL batch autoclave (Parr 4848.) The experimental setup is described elsewhere[53]. In a typical experiment, the reactor was charged with 1.3 g of catalyst and 1 mL of DM. Subsequently, the reactor was flushed 3 times with N$_2$ gas (1.3 MPa) at room temperature to remove the air in the autoclave. Then, H$_2$ gas was pressurized into the reactor until it reached 1.7 MPa to activate the catalyst. Then, desired amounts of yellow grease and PL were blended to obtain a 50 g mixture. The reactor vessel was briefly charged with the blends and flushed 3 times with N$_2$ gas (1.3 MPa) at room temperature to remove the air in

the autoclave. Afterward, H_2 gas was pressurized into the reactor until 7.6 MPa (at room temperature). A leak check was subsequently conducted using a leak detector (catalog number 22655, Restek). Once the leak test was passed, the reactor was heated by the heating mantle and the stirrer was turned on to spin at 500 rpm. It normally took 35 min for the reactor to reach 523 K, and then its temperature was kept constant for 24 h before increasing it to 653 K for 4h. Then, it was cooled off to room temperature using an air blower for 1.5 hours.
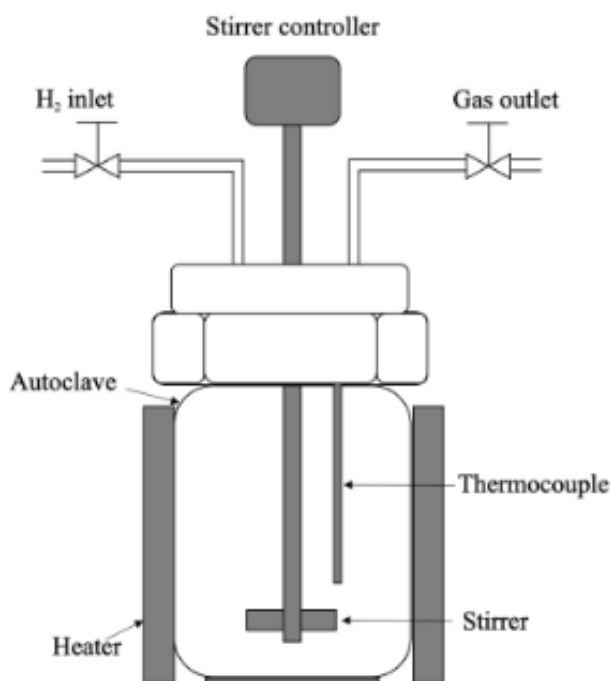
Figure 5-1. Hydrotreatment reactor setup [143].

Once the reactor temperature reached 298 K, the stirring was turned off. After the leftover gases were depressurized to the ventilation system, the reactor was opened and then weighed. The major liquid product in the vessel was transferred to a coned tube for centrifugation (3000 rpm for 30 min). Then, the leftover residue in the reactor vessel was vacuum filtrated over a Whatman grade 42 filter paper using acetone for washing. The solids obtained from centrifugation and filtration were subsequently dried in an oven at 383 K overnight. The combined mass of both solids —after removing the amount of initially added catalyst— was then used to calculate the solid yields. The gas yield was determined by subtracting the mass of "ceiling oil" from the weight difference of the reactor vessel (with samples/products inside) before and after the reaction. The liquid yield was then calculated by subtracting both solid and gas yields from unity.

5.2.3 Analysis of products

Ultraviolet (UV) Fluorescence (Synchronized). The oils were diluted in HPLC-grade dichloromethane at 20 ppm and analyzed on a Shimadzu RF 5301 pc (Panorama Fluorescence 2.1) spectrometer. Synchronous fluorescence spectra at a constant wavelength difference were set. The excitation wavelength was scanned from 250 to 700 nm, and emission wavelengths were recorded with 15 nm difference (from 265 to 715 nm). The excitation slit width and emission slit width were set at 3 nm. Data was collected every 1 nm. Samples at different concentration levels (1, 10, and 100 ppm) had been tested and showed the same profile as with 100 ppm to rule out the self-absorption effect.

Fourier Transform Infrared Spectroscopy (FTIR). FITR spectra were obtained using a Shimadzu IRPrestige 21 spectrometer equipped with a MIRacle single-reflection attenuated total reflection (ATR) Ge probe. A drop of sample was applied to cover the crystal window, and the spectra were acquired (32 scans, 600−4000 cm^{-1} , and resolution of 4 cm^{-1}).

Distillation. A simple distillation setup (ASTM D86-12) was used, and the operation procedure was described in [141]. Around 20 g of hydrotreated oil were loaded into a round flask with 3 grains of carborundum # 12 from Hengar to avoid heterogeneous temperature during the heating. The organic phase samples were distillated in a laboratory batch distillation unit under ambient pressure. During the distillation, the samples were heated to boiling point at 150, 250 and 350°C to obtain the following fractions: <150 °C (gasoline), 150-250 °C (kerosene), 250-350 °C (diesel). The gaseous flow from the flask went through the distillation column, then the flow entered the serpentine condenser, and the condensate liquid drops were collected. The three receiving bottles were switched alternatively to collect the fuels. A solid residue was collected from the round flask after the process, and its yield was reported as the residue.

Two-dimensional Gas Chromatography – FID. The GCxGC-FID analysis was performed on an Agilent 8890 with a SepSolve flow modulator. The first-dimension column is a Restek Rxi-17Sil (60m x 0.32mm x 0.50um), the second-dimension column is a Restek Rxi-1ms (15m x 0.32mm x 0.50um). The carrier gas is grade 5.0 helium with flows of 1.2 mL/min and 48mL/min through the first- and second-dimension columns, respectively. The GC oven starts at 40 °C for 30 seconds and then increases at 1°C/min until 280 °C. The modulation time is 10 seconds. The injection volume is 1uL. The hydrocarbon group type analysis is performed with the method described by Vozka *et al.* [144].

Elemental Analysis (CHN−O). A Leco TruSpec CHN 628 series instrument was used to analyze all of the carbon, hydrogen, and nitrogen contents in all the liquid samples following the ASTM D5373-08 method. The oxygen content was calculated by difference. A total of 0.15 g of the oil sample was weighed into a tin foil cup; then, approximately 0.3 g of Leco's Com-Aid was added on top, and the foil cup was sealed by hand. Three-point calibrations were performed with LECO 502-092 ethylenediaminetetraacetic acid (EDTA).

Density. The density was determined using a cleaned and dried 2-mL Gay-Lussac pycnometer. The pycnometer was weighed and tared. The pycnometer was filled with fuel, closed with a stopper, carefully wiped, and weighed. The density of the sample was calculated by dividing the mass obtained by the volume of the pycnometer [145].

Surface Tension. The surface tension was measured following the Du Noüy Ring Method with a LAUDA TD 2 Tensiometer. The ring dimensions were R=9.55 mm and r=0.2mm. Between measurements, the ring was washed with acetone and heated up with a mini-torch unit to remove impurities. Before the sample analysis, the Du Noüy Ring was tared, and then calibrated using a calibration weight of 500.00 mg (standard deviation = 0.1 mg). Measuring parameters (Mov. Speed = 5; Mov. Opt. = 20%; Pause = 1 min; Max time = 15 min; Points of Stdv = 5; Stdv = 0.01 mN/m). The measurements were conducted at sample temperature of 18 ± 0.5°C. Each fuel sample was analyzed in triplicate, and average and standard deviations were reported (ASTM D1331 (2014)).

Viscosity. The viscosity was measured at four different temperatures (15, 25, 35 and 45 °C). A viscometer with a range covering the estimated viscosity was selected and immersed in a temperature-controlled bath filled with distilled water. 3 mL of sample was inserted into each glass viscometer and time was allowed for the sample to reach bath temperature. Using air to apply pressure, the level of the fuel sample was adjusted to about 7 mm above the first timing mark in the instrument arm. The total time that the sample meniscus took to flow from the first to the second timing mark was measured and recorded. The kinematic viscosity is calculated by multiplying the measured time (in seconds) by the viscometer calibration constant (in mm^2/s^2). The procedure was repeated three times and the kinematic viscosity reported was an average of the three values obtained (ASTM D445, 2015).

Heating value. Heating value was calculated using a Gumz and Channiwala-Parikh model for liquid fuels [146] in Eq. 1 based on the fuel elemental compositions, the model gives the high heating value in KJ/kg.

$$\Delta H = aC + bH + cN + dS + eO \qquad \qquad \text{Eq. 1}$$

Where a, b, c, d, and e, are the improved coefficients with values 328.1, 1091, 81.83, -2513, and -94.73 respectively by Richards [147].ASTM D1655 specifies the lower limit for heating value as 42.8 MJ/kg for Jet1 and Jet 1A fuels.

5.3 Results and Discussion

5.3.1 Catalytic co-hydrotreatment of pyrolignin and yellow grease

The co-hydrotreatment of pyrolytic lignin and yellow grease was performed. The overall composition of the yellow grease and pyrolignin is shown in Table 5-1. A total of 5 PL and yellow grease blends were used in this study, in order to evaluate the effect of the mixture at different concentrations. A liquid phase consisting of two immiscible layers, a top organic

phase and an aqueous bottom phase were obtained after reaction for all different blends. Figure 5-2 shows the distribution of product yields and mass balances obtained.

Table 5-1. Overall composition of yellow grease and pyrolignin [145].

	Yellow grease	Pyrolignin
TAN (mg KOH/g oil)	30.1 ± 0.3	63.9 ± 2.9
Carbonyl content (mmol/g)	-	3.3 ± 0.1
Total phenols (wt. % GAE)	2.3 ± 0.3	37.9 ± 4.6
Water content (wt. %)	0.09 ± 0.0	15.7 ± 0.2
Elemental Analysis		
C (wt.%)	78.0 ± 0.3	69.1 ± 7.3
H (wt.%)	9.3 ± 0.0	6.5 ± 0.9
N (wt.%)	0.2 ± 0.0	0.3 ± 0.1
O (wt.%)	12.5 ± 0.3	24.0 ± 8.2
Proximate analysis		
Volatiles	61.7	77.2 ± 0.3
Ash	0.0	0.0 ± 0.0
Fixed Carbon	38.3	22.8 ± 0.3
HHV (kJ/g)	39.20 ± 0.05	24.98 ± 0.03

Triglycerides present in yellow grease, consist of three chains of fatty acids (linoleic, oleic, and stearic acid) and when these molecules are hydrogenated, all the unsaturated fatty acid are transformed into saturated one, resulting in three chains of stearic acid [148]. After saturation of triglycerides, there is more hydrogen addition since there was a cleavage of the glycerol compound forming propane and a chain of free fatty acids; the carboxylic acid group that remains attached to the free fatty acid must be removed to form straight chain alkanes. This removal can happen in three ways: decarboxylation, decarbonylation and hydrodeoxygenation. The last two pathways can produce the fatty chain and water [149], [150]. The formation of water is indicative of the occurrence of hydrodeoxygenation reactions. The aqueous phase for pure yellow grease represented 0.2 wt.% of the sample. While the water content increase when pyrolytic lignin was used in the blends (2.1 to 11.9 wt.%). The HDO routes for pyrolytic lignin are different since hydrogen radicals from the catalyst interact with the C-O bond, breaking it, to form -OH group or water on one end, and an alkane on the other. Carbonyl groups C=O will be reduced into C-O by hydrogen, followed by the C-O cleavage route. And as result, H_2O, CO; and CO_2 are produced [53]. The increase of water content in the products indicates that the water comes mainly from the pyrolytic lignin hydrotreatment routes during the process.

A break-down of the bonds in the PL is first required during the hydrotreatment process. The breakage of these linkages should generate radicals and these radicals may further break down or be hydrogenated to form stable molecules or recombine to form larger molecules leading the coke formation [151]. The coke concentration value for pure yellow grease was 0.7 wt. %., this value was not expected for triglycerides, however, phenols

content value for yellow grease reported in Table 5-1 was 2.3 wt. %. This suggests that coke formation could be related to unknown phenol pathways during the process.

When PL was added, the solid formation increased from 1.5 to 2.5 wt.%, indicating that coke formation increases with an increasing PL concentration. In this study, the initial hydrogen pressure in the reactor was the same for all blends, which could generate a higher hydrogen consumption and lower HDO rates for blends with higher PL content, since pressure in the hydrotreatment process is associated with the HDO rates [151]. These results suggest that all PL concentrations evaluated in this study can be optimized to get a lower coke formation value increasing the hydrogen feed pressure in batch systems. However, increasing maximum hydrogen pressure in reactor setups is challenging, due to the special characteristics of the required materials and sealings.

The obtained coke values conflict with those reported in the literature [25–27]. The light compounds without aromatics in pyrolysis bio-oil are composed of O-containing active functional groups that can take part in cracking and polymerization under high temperatures [28, 29]. Hydrotreating reactions are also carried out at high temperatures; therefore, the use of bio-oil fractions with a low content of oxygenated compounds such as PL could reduce the coke content. It supports the idea that the formation of solids is strongly related to the sugar fraction as reported in [15, 30], which used the same catalyst and pyrolytic lignin. These results indicate that PL has potential to reduce coke formation in the operation of the upgrading process. However, the blend at 10 % of PL is recommended because it has the closer value (1.6 %) to the accepted coke formation (1%) in the process due to the obstruction that can occur.

a)

b)
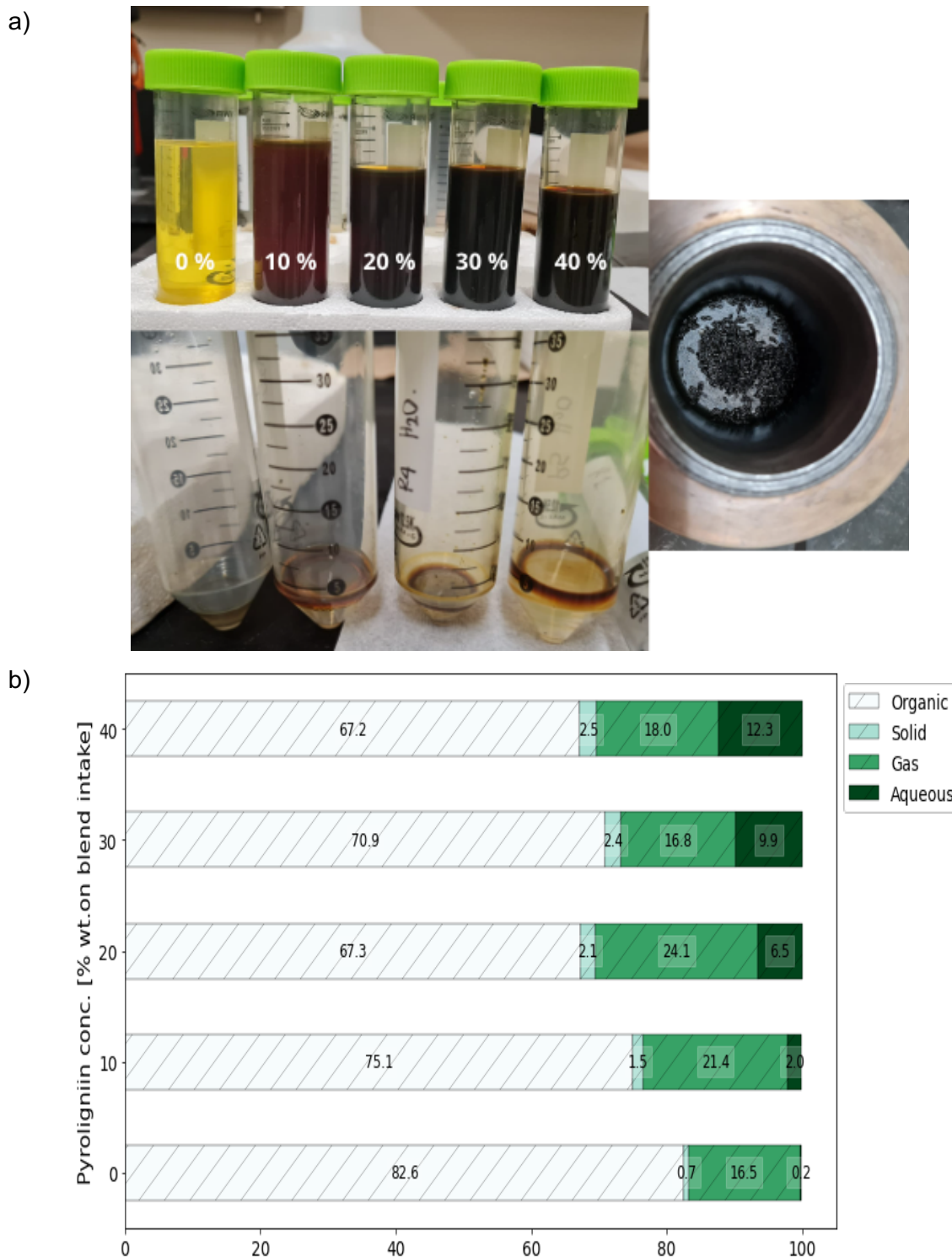
Figure 5-2. a) Solid, organic, and aqueous product, b) Product yields and mass balances (% values) obtained for the co-hydrotreatment of pyrolignin and yellow grease at different concentrations.

The organic phase yield for pure yellow grease was 82.6 wt.%, while for blends with pyrolytic lignin, it ranged between 78.1 and 65.7 wt.%. In the hydrotreatment process, the main product is the organic phase because it is the precursor of fuels. However, in addition to having a good organic phase yield during the HDO process, it is important to analyze the quality of the phase, the yields in the distillation stage, and the standards of the obtained fuels. To examine the effect of the PL concentration on the upgraded blends, PL's FTIR spectra and upgraded blends were obtained (Figure 5-2).

IR spectra of yellow grease and raw pyrolignin are presented. Yellow grease showed absorbance bands at 1170 cm^{-1} (ester C-O-C), 1742 cm^{-1} (ester C=O), and above 3000 cm^{-1} (alkene =C-H) as characteristic of triglycerides[158]. Ester groups in yellow grease belonging to fatty acids C=O groups were reduced during the hydrotreatment [159]. This peak was not observed in samples with 0, 10, and 20 wt.% PL and had a much lower intensity for the rest of the co-hydrotreated blends. Thus, it showed the process effectivity to remove oxygen from lower PL concentrations. This supports the idea that the hydrogen requirements must be high to get high hydrodeoxygenation rates. PL has a broad peak around 3419 cm^{-1} related to O-H stretching, which disappeared in all hydrotreated samples, thus suggesting a successful oxygen remotion during the HDO process. Peaks at 2860 and 3000 cm^{-1} are attributed to aliphatic C-H stretch in PL and fatty acids in yellow grease. The aliphatic -CH$_2$OH groups of the alkyl side chains in PL tend to be released as volatile products[32]. However, all blends show these peaks, thus indicating a contribution of aliphatic chains from yellow grease to the upgraded blends. Disappearing peaks above 3000 cm^{-1} belonging to alkene (=C-H groups) show that the final products are saturated alkanes [160].
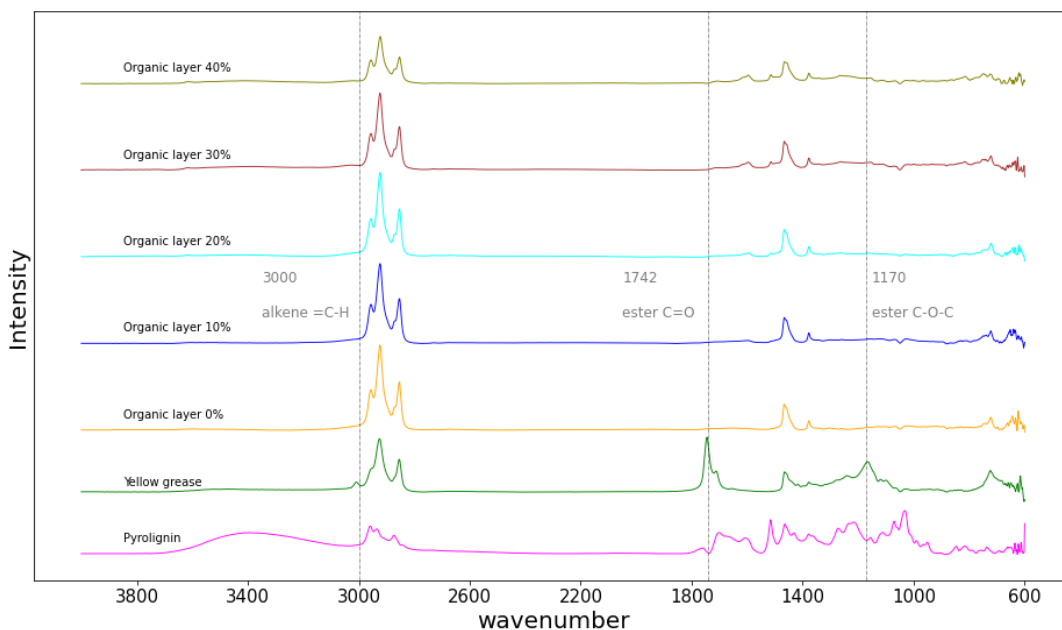
Figure 5-3. FTIR spectra for the feedstock and organic layer products.

The intensities of unconjugated C=O stretching at 1704 cm^{-1} and conjugated C=O with aromatic rings at 1612 cm^{-1} in PL also decrease with the hydrotreatment process. The existence of unconjugated C=O bands in PL can be attributed to the breakage of ether bonds in the PL structure [161]. It suggests that the carbonyl groups and carboxylic acids are eliminated from the blend structures. There is still a signal related to conjugated C=O at higher PL concentrations in the blends. This may happen because these groups with aromatic structures have better thermal stability than unconjugated groups [162] and supports the hypothesis about the HDO rate being limited by the hydrogen pressure in the process.

The distribution of heavy molecules after the hydrotreatment process was also studied. Figure 5-3 shows the UV-fluorescence spectra of the feedstock and the hydrotreated samples. Three characteristic regions can be distinguished: monophenols before 285 nm, dimers and short conjugated systems between 285 and 320 nm, and the polycondensed structures after 320 nm[130]. The results in Figure 5-3 show that PL mainly contains aromatic structure with dimers, short conjugated systems, and polycondensed structures while YG does not show aromatic structures as expected since it is an aliphatic structure.
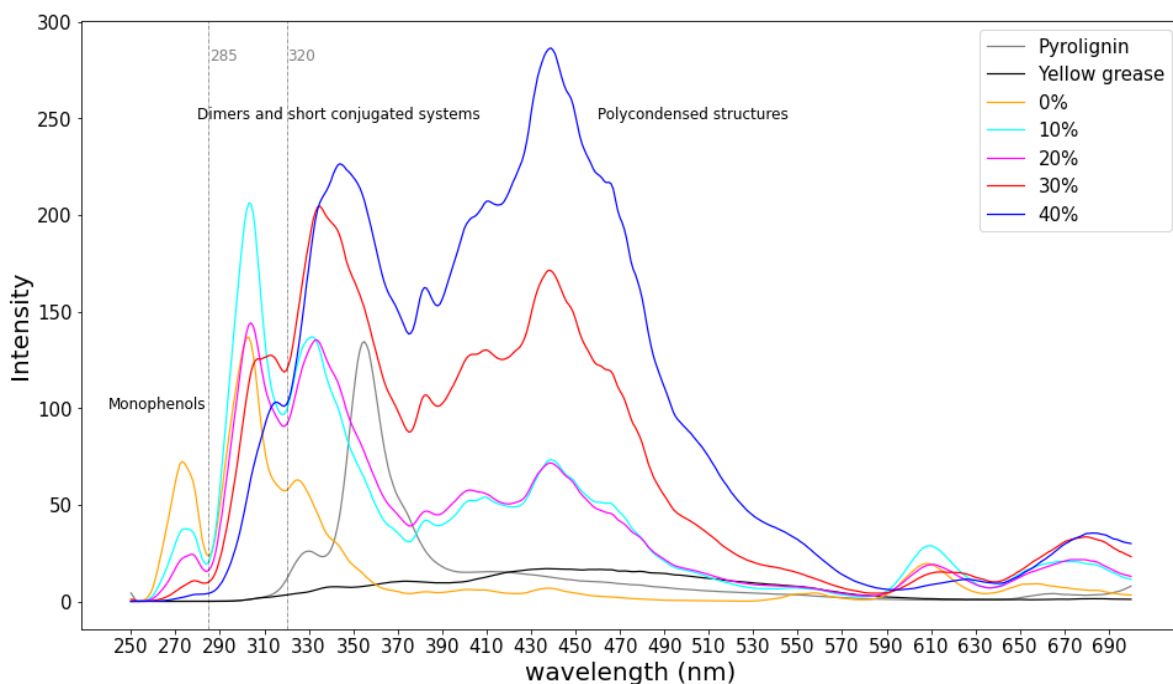
Figure 5-4. Synchronous UV-fluorescence spectra for the feedstocks and organic phase product.

It can be observed that after the hydrotreatment process, the intensity in all regions shifts towards larger aromatic ring structures, especially for hydrotreated samples with 30 and 40 wt.% PL. This suggests that the hydrotreated samples structures at higher PL concentrations form conjugated systems before coke, i.e., 2.4 and 2.5 wt. %, respectively. The interpretation of this data must take into consideration the importance of intra-molecular energy transfer to the observed fluorescence intensity for this type of samples. Due to this

energy, large aromatic ring systems in large molecules in bio-oil could be not well represented by the observed fluorescence[163]. However, Gholizadeh *et al.* [164] mentioned that during hydrocracking, the efficiency of intramolecular transfer decreases, and these results could be a better representation of these large aromatic systems in the observed fluorescence.

5.3.2 Chemical Characterization

The distribution of fuels in the liquid products at different PL and yellow grease concentrations is presented in Figure 5-4. Gasoline contained C9 to C14, considered as hydrocracked light molecules; kerosene, C15 to C18 as the desired paraffin products, and C19 to C30 as the oligomerized heavy fraction. The formation of light molecules can be attributed to hydrocracking, while the formation of heavier molecules is caused by the oligomerization reactions [165].
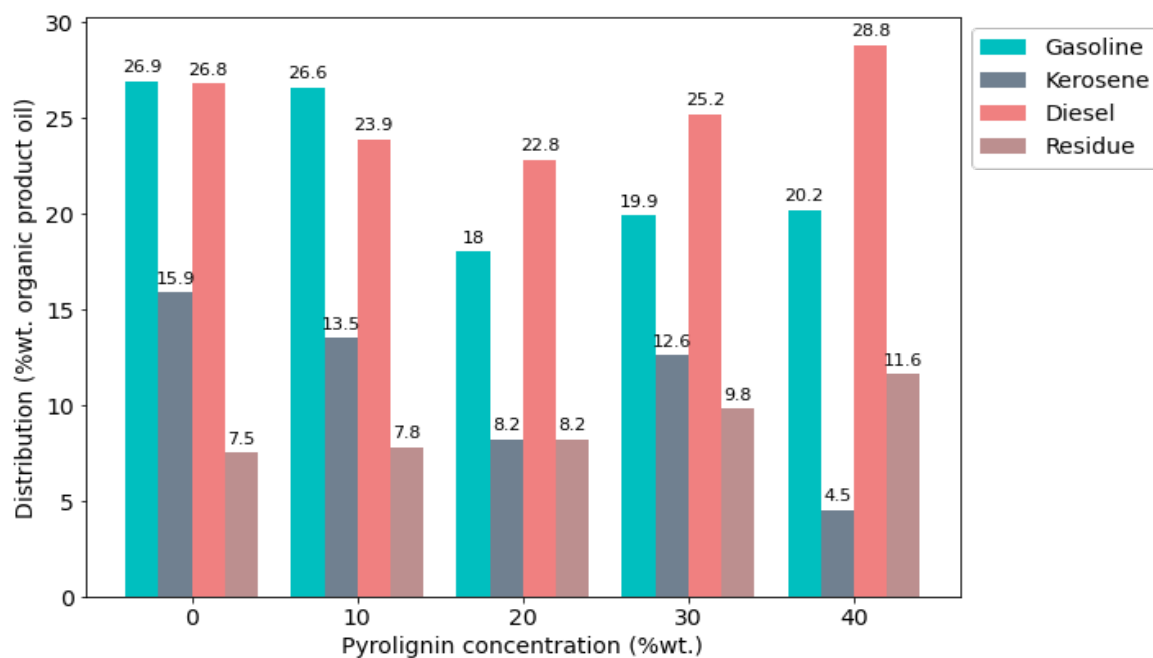
Figure 5-5. Fuels distribution for the distillation of organic product oil.

The results in Figure 5-5 indicate that gasoline and kerosene yields decreased when the PL concentration increases, while the diesel yield has a smooth increasing trend when the amount of pyrolignin is higher in the blend. This suggests that oligomerization reactions are prevalent over hydrocracking reactions at higher concentrations of PL in the mix. The oligomeration reactions generate oils with bigger conjugated systems as can be seen in Figure 5-4.

5.3.3 Fuels Properties

Density. Table 5-2 shows the density of the tested fuels. The density is an important property to quantify weight in transportation systems. Density was measured at 15 °C according to [145]. As per Table 5-2, the density of gasoline shows values between 0.717 and 0.751 g/mL while kerosene has densities between 0.791 and 0.802 g/mL, and for diesel the values are between 0.786 and 0.808 g/mL. The density for kerosene complies with ASTM D1655 and IATA specifications, which mention that the density for Jet A/Jet A-1 kerosene must be in the range from 0.775 to 0.840 g/mL [145].

Table 5-2. Density of fuels at room temperature.

Pyrolignin conc. (%)	Gasoline (g/mL)	Kerosene (g/mL)	Diesel (g/mL)
0	0.717	0.791	0.792
10	0.735	0.791	0.808
20	0.728	0.790	0.786
30	0.741	0.797	0.810
40	0.751	0.802	0.808

Viscosity. High viscosity can cause filter plugging and problems in fuel pumpability. Besides, viscosity is related to the droplet size in sprays generated by burner nozzles. Table 5-3 presents the kinematic viscosity of the fuels obtained in this work at different temperatures. The kinematic viscosity was measured at four different temperatures (15, 25, 35 and 45 °C). Then, the value at -20 °C was extrapolated with the collected data. The viscosity decreases with the increase in temperature for all fuels.

Table 5-3. Kinematic viscosity of fuels at different temperatures (*extrapolated data).

Pyrolignin conc. (wt. %)	Fuel	-20℃ (mm²/s)	15℃ (mm²/s)	25℃ (mm²/s)	35℃ (mm²/s)	45℃ (mm²/s)
0	Gasoline	8.62	0.97	0.86	0.77	0.70
	Kerosene	3.93	2.68	2.22	1.87	1.55
	Diesel	1.28	5.60	4.38	3.51	2.88
10	Gasoline	8.21	0.93	0.83	0.75	0.68
	Kerosene	5.50	5.40	4.07	3.39	2.77
	Diesel	1.20	3.63	3.07	2.43	2.04
20	Gasoline	8.02	1.01	0.87	0.80	0.72
	Kerosene	4.20	2.86	2.34	1.95	1.66
	Diesel	1.32	5.23	4.09	3.29	2.70
30	Gasoline	7.82	0.93	0.83	0.74	0.67
	Kerosene	5.49	3.40	2.73	2.24	1.55
	Diesel	1.22	5.50	4.14	3.63	2.78
40	Gasoline	7.86	0.88	0.80	0.72	0.65
	Kerosene	3.57	2.45	2.12	1.77	1.50
	Diesel	1.15	5.46	4.12	3.26	3.10

Also, the values increase when the fuel has more carbon chains in its structure. This supports [166] that mentioned that the value of viscosity is directly related to the number of carbons or to the molecular weight. ASTM D1655 establishes a viscosity limit at -20°C of 8 mm²/s for Jet A/Jet A-1, and 8.5 mm²/s for JP-5. In this study all obtained kerosene samples presented viscosity values below 8 mm²/s, which indicates that the samples comply with the mentioned standards.

Surface tension. Surface tension has an important effect in atomization and ignition characteristics of jet fuels. Table 5-4 shows the average measured surface tension of the obtained fuels.

Table 5-4. Surface tension of fuels at room temperature.

Pyrolignin conc. (%)	Gasoline (mN/m)	Kerosene (mN/m)	Diesel (mN/m)
0	22.02 ± 0.11	24.61 ± 0.15	27.53 ± 0.20
10	21.81 ± 0.07	23.68 ± 0.24	26.95 ± 0.09
20	22.03 ± 0.07	24.86 ± 0.03	25.30 ± 0.30
30	21.74 ± 0.11	23.96 ± 0.06	23.22 ± 0.05
40	21.39 ± 0.03	23.53 ± 0.35	23.48 ± 0.28

The values for surface tension were in the range between 21.39 and 22.03, 23.53 and 24.86, and 23.22 and 27.53 for gasoline, kerosene and diesel respectively. There is no standard specification for surface tension, however, the reported average is 23.5 mN/m at 22 °C [145].

5.4 Conclusions

This study demonstrates that yellow grease and pyrolytic lignin can be successfully co-hydrotreated over a NiMo/Al$_2$O$_3$ catalyst. All blends obtained good coke formation results (0.7-2.5 wt. %), indicating that the formation of solids in bio-oil hydrotreatment is strongly related to oligomers from the sugar fraction and that PL has potential to reduce coke formation in the process. However, the overall fuel distribution of the organic product was shown to be strongly dependent on the pyrolytic lignin concentration. Diesel has a high yield when pyrolytic lignin concentration increases, while kerosene presents high yield when it is lower, according to the results. Fuel properties of gasoline, kerosene and diesel were evaluated to compare with those of transportation fuels. Results for viscosity and surface tension comply with the standards for these fuels in transportation applications. As such, It can be concluded that pyrolytic lignin obtained from fast pyrolysis of biomass is an potential feed for the synthesis of important biobased transportation fuels.

6. Conclusions and recommendations

6.1 Conclusions

The results of this thesis provide new insights for the development of a pyrolysis process. In the second chapter, we created a review of lignin reactions involved during pyrolysis and hydrotreatment process, involving lignin structure, reactions in pyrolysis of lignin, reactions in upgrading process and composition of the upgraded pyrolytic lignin. Then in the **third chapter**, we elucidated the pyrolytic lignin oligomers structures through electronic structure calculation using Density Functional Theory. These results proposed 18 oligomer structures of the heavy fraction of bio-oil. In **the fourth chapter** we focused on separating the pyrolytic lignin through fractionation by liquid – liquid extraction and solid – liquid chromatography, presenting a strategie for the separation of the heavy fraction of bio-oil. Furthermore, we evaluated the co-hydrotreatment of pyrolytic lignin and yellow grease in **the fifth chapter**. We provided an analysis of the coke formation at different pyrolytic lignin and yellow grease blends over a $NiMo/Al_2O_3$ catalyst, suggesting that the formation of solids in bio-oil hydrotreatment is strongly related to oligomers from the sugar fraction.

A summary of the major findings is shown below.

1. Structures for dimer, trimer and tetramer oligomers from pyrolytic lignin are suggested based on the demethylation reaction.
2. The structures were evaluated through two different pathways taking hydrogen radicals on the media and using intramolecular hydrogen using electronic structure calculation depending on the Gibbs free energies of the reaction.
3. The formation of quinone methides is relevant in all the proposed oligomer structures.
4. The FTIR and NMR simulated spectra were obtained for all proposed oligomer structures from pyrolytic lignin.
5. The oligomers D5, T3* and OG13 have a more similar structure if compared with the experimental pyrolytic lignin used in this study according to the FTIR results.
6. The properties of the proposed structure were analyzed, distributed, and calculated according to GCM.
7. The pyrolytic lignin was separated into various fractions of chemical compounds using combined techniques of liquid-liquid and solid-liquid extraction.
8. The ethyl acetate fraction from pyrolytic lignin is composed of phenolic compounds with methoxyl substituents while acetone and isopropanol are mainly composed of aliphatic compounds.
9. The coke formation value for the blends, suggest that the pyrolytic lignin has potential to reduce coke formation during the upgrading process.
10. Hydrodeoxygenation process was done at different pyrolytic lignin concentrations (10-40%), increasing the concentration reported on literature.

11. The overall fuel distribution of the organic product was shown strongly dependent on the pyrolytic lignin concentration, the production of diesel increased when the pyrolytic lignin concentration was increased.
12. Fuel properties were evaluated with transportation fuels. Viscosity and surface tension values comply with the standards for fuels in transportation applications.

6.2 Recommendations and future research

The elucidation of the oligomers structures for the pyrolytic lignin were proposed considering the demethylation reaction that could happen after depolymerization of lignin. Another way to analyze these structures is to evaluate other reactions such as demethoxylation due to methanol being another important gas produced from the pyrolysis of lignin.

The study of the spatial distribution of the oligomer molecules in different media (solvents) could facilitate the interaction between the catalyst and the oligomers in hydrotreating processes. The use of Molecular Dynamics techniques can be useful if working with dimers due to the high computational cost that the system requires to simulate the size of the oligomers in the hydrotreating conditions.

Co-hydrotreatment of pyrolytic lignin and yellow grease blends at different concentrations were evaluated in order to reduce coke formation. The solid formation increased from 1.5 to 2.5 wt. %, indicating that coke formation increases with an increasing pyrolytic lignin concentration. We suggested that all pyrolytic lignin blends can be optimized to get a lower coke formation value increasing the hydrogen feed pressure in batch systems. However, a gas chromatography analysis at different concentrations is important to verify if the hydrogen pressure in the reactor is enough for all reactions in the blends. In addition, different catalysts can be investigated to improve the fuel quality.

The oligomers proposed in this thesis could be used for the evaluation of properties using phase equilibria models for pyrolysis bio-oil. These structures also can be used to evaluate the desoxygenation mechanism over NiMo/Al$_2$O$_3$ catalyst through DFT modeling to understand the desoxygenation and probably the coke formation in the heavy fraction of the pyrolysis bio-oil.

The analysis of the use of nanoparticles in hydrotreating processes to improve the solubility between pyrolytic lignin and vegetable oil could increase the yield of the organic phase, allowing to increase the yield of liquid fuels.

Due to the high complexity of the chemical composition of pyrolignin, the separation and isolation of certain compounds is a task that requires the use of several separation

techniques together and multiple steps, such as liquid-liquid extraction and column chromatograpy.

References

[1]   L. F. Cabeza, A. Palacios, S. Serrano, D. Ürge-Vorsatz, and C. Barreneche, "Comparison of past projections of global and regional primary and final energy consumption with historical data," *Renewable and Sustainable Energy Reviews*, vol. 82. Elsevier Ltd, pp. 681–688, 2018. doi: 10.1016/j.rser.2017.09.073.

[2]   A. K. Vuppaladadiyam *et al.*, "Biomass pyrolysis: A review on recent advancements and green hydrogen production," *Bioresource Technology*, vol. 364. Elsevier Ltd, Nov. 01, 2022. doi: 10.1016/j.biortech.2022.128087.

[3]   J. Cai *et al.*, "Review of physicochemical properties and analytical characterization of lignocellulosic biomass," *Renewable and Sustainable Energy Reviews*, vol. 76. Elsevier Ltd, pp. 309–322, 2017. doi: 10.1016/j.rser.2017.03.072.

[4]   Unidad de Planeación Minero Energética, "Atlas del Potencial Energético de la Biomasa en Colombia," Bogota D.C, 2008. [Online]. Available: http://www1.upme.gov.co/sites/default/files/article/1768/files/Atlas de Biomasa Residual Colombia__.pdf

[5]   V. Duc Bui *et al.*, "Techno-economic assessment and logistics management of biomass in the conversion progress to bioenergy," *Sustainable Energy Technologies and Assessments*, vol. 55, Feb. 2023, doi: 10.1016/j.seta.2022.102991.

[6]   V. Dhyani and T. Bhaskar, "A comprehensive review on the pyrolysis of lignocellulosic biomass," *Renew Energy*, vol. 129, pp. 695–716, Dec. 2018, doi: 10.1016/j.renene.2017.04.035.

[7]   W. Yin, R. H. Venderbosch, and H. J. Heeres, *8 - Recent developments in the catalytic hydrotreatment of pyrolysis liquids*. Elsevier Ltd., 2017. doi: 10.1016/B978-0-08-101029-7.00007-2.

[8]   X. Li *et al.*, "Upgrading of bio-oil into advanced biofuels and chemicals. Part III. Changes in aromatic structure and coke forming propensity during the catalytic hydrotreatment of a fast pyrolysis bio-oil with Pd/C catalyst," *Fuel*, vol. 116, pp. 642–649, 2014, doi: 10.1016/j.fuel.2013.08.046.

[9]   S. Kadarwati *et al.*, "Coke formation during the hydrotreatment of bio-oil using NiMo and CoMo catalysts," *Fuel Processing Technology*, vol. 155, pp. 261–268, 2017, doi: 10.1016/j.fuproc.2016.08.021.

[10]   W. Laosiripojana, W. Kiatkittipong, and C. Sakdaronnarong, "Catalytic hydrotreatment of pyrolysis-oil with bimetallic Ni-Cu catalysts supported by several mono-oxide and mixed-oxide materials," *Renew Energy*, vol. 135, pp. 1048–1055, 2019, doi: 10.1016/j.renene.2018.12.069.

[11]   S. Kadarwati *et al.*, "Polymerization and cracking during the hydrotreatment of bio-oil and heavy fractions obtained by fractional condensation using Ru/C and NiMo/Al 2 O 3 catalyst," *J Anal Appl Pyrolysis*, vol. 118, pp. 136–143, 2016, doi: 10.1016/j.jaap.2016.01.011.

[12]   B. Scholze and D. Meier, "Characterization of the water-insoluble fraction from pyrolysis oil (pyrolytic lignin). Part I. PY-GC/MS, FTIR, and functional groups," *J Anal Appl Pyrolysis*, vol. 60, no. 1, pp. 41–54, 2001, doi: 10.1016/S0165-2370(00)00110-8.

[13]   K. Iisa, A. C. Johansson, E. Pettersson, R. J. French, K. A. Orton, and H. Wiinikka, "Chemical and physical characterization of aerosols from fast pyrolysis of biomass," *J Anal Appl Pyrolysis*, vol. 142, no. February, pp. 1–9, 2019, doi: 10.1016/j.jaap.2019.04.022.

[14]   A. P. Pinheiro Pires *et al.*, "Challenges and opportunities for bio-oil refining: A review," *Energy and Fuels*, vol. 33, no. 6, pp. 4683–4720, 2019, doi: 10.1021/acs.energyfuels.9b00039.

[15]   M. Matos *et al.*, "Acetone:Water fractionation of pyrolytic lignin improves its antioxidant and antibacterial activity," *J Anal Appl Pyrolysis*, vol. 156, Jun. 2021, doi: 10.1016/j.jaap.2021.105175.

[16]   M. B. Figueirêdo, "Valorization Strategies for Pyrolytic Lignin," University of Groningen, 2020.

[17]   X. Zhang, H. Ma, T. Li, and S. Wu, "Oligomers obtained from sequential fractionation of lignin pyrolysis oil," *Energy Convers Manag*, vol. 201, no. July, p. 112181, 2019, doi: 10.1016/j.enconman.2019.112181.

[18]   A. P. Pinheiro Pires *et al.*, "Challenges and opportunities for bio-oil refining: A review," *Energy and Fuels*, vol. 33, no. 6, pp. 4683–4720, 2019, doi: 10.1021/acs.energyfuels.9b00039.

[19]   M. U. Garba, U. Musa, A. G. Olugbenga, Y. S. Mohammad, M. Yahaya, and A. A. Ibrahim, "Catalytic upgrading of bio-oil from bagasse: Thermogravimetric analysis and fixed bed pyrolysis," *Beni Suef Univ J Basic Appl Sci*, vol. 7, no. 4, pp. 776–781, 2018, doi: 10.1016/j.bjbas.2018.11.004.

[20]   J. Lehto, A. Oasmaa, Y. Solantausta, M. Kytö, and D. Chiaramonti, "Fuel oil quality and combustion of fast pyrolysis bio-oils," *VTT Publications*, no. 87, p. 79, 2013, doi: http://dx.doi.org/10.1016/j.apenergy.2013.11.040.

[21]   I. Hita, E. Rodríguez, M. Olazar, J. Bilbao, J. M. Arandes, and P. Castaño, "Prospects for Obtaining High Quality Fuels from the Hydrocracking of a Hydrotreated Scrap Tires Pyrolysis Oil," *Energy & Fuels*, vol. 29, no. 8, pp. 5458–5466, Aug. 2015, doi: 10.1021/acs.energyfuels.5b01181.

[22]   A. H. Zacher, M. v. Olarte, D. M. Santosa, D. C. Elliott, and S. B. Jones, "A review and perspective of recent bio-oil hydrotreating research," *Green Chemistry*, vol. 16, no. 2, pp. 491–515, 2014, doi: 10.1039/c3gc41382a.

[23]   A. Abbas, Z. Wang, Y. Zhang, P. Peng, and D. She, "Lignin-based controlled release fertilizers: A review," *Int J Biol Macromol*, Oct. 2022, doi: 10.1016/j.ijbiomac.2022.09.265.

[24]   A. J. Ragauskas *et al.*, "Lignin valorization: Improving lignin processing in the biorefinery," *Science*, vol. 344, no. 6185. American Association for the Advancement of Science, 2014. doi: 10.1126/science.1246843.

[25]   M. Saidi, F. Samimi, D. Karimipourfard, T. Nimmanwudipong, B. C. Gates, and M. R. Rahimpour, "Upgrading of lignin-derived bio-oils by catalytic hydrodeoxygenation," *Energy and Environmental Science*, vol. 7, no. 1. Royal Society of Chemistry, pp. 103–129, 2014. doi: 10.1039/c3ee43081b.

[26]   A. Agarwal, M. Rana, and J. H. Park, "Advancement in technologies for the depolymerization of lignin," *Fuel Processing Technology*, vol. 181. Elsevier B.V., pp. 115–132, Dec. 01, 2018. doi: 10.1016/j.fuproc.2018.09.017.

[27]   J. C. del Río, J. Rencoret, A. Gutiérrez, T. Elder, H. Kim, and J. Ralph, "Lignin Monomers from beyond the Canonical Monolignol Biosynthetic Pathway: Another Brick in the Wall," *ACS Sustainable Chemistry and Engineering*, vol. 8, no. 13. American Chemical Society, pp. 4997–5012, Apr. 06, 2020. doi: 10.1021/acssuschemeng.0c01109.

[28]   M. M. Campbell and R. R. Sederoff, "Variation in Lignin Content and Composition' Mechanisms of Control and Implications for the Genetic Improvement of Plants." [Online]. Available: https://academic.oup.com/plphys/article/110/1/3/6068918

[29]   L. Zhang, A. Larsson, A. Moldin, and U. Edlund, "Comparison of lignin distribution, structure, and morphology in wheat straw and wood," *Industrial Crops and Products*, vol. 187. Elsevier B.V., Nov. 01, 2022. doi: 10.1016/j.indcrop.2022.115432.

[30]   Y. Pu, D. Zhang, P. M. Singh, and A. J. Ragauskas, "The new forestry biofuels sector," *Biofuels, Bioproducts and Biorefining*, vol. 2, no. 1. pp. 58–73, Jan. 2008. doi: 10.1002/bbb.48.

[31]   S. Sethupathy *et al.*, "Lignin valorization: Status, challenges and opportunities," *Bioresource Technology*, vol. 347. Elsevier Ltd, Mar. 01, 2022. doi: 10.1016/j.biortech.2022.126696.

[32] S. Wang *et al.*, "Comparison of the pyrolysis behavior of lignins from different tree species," *Biotechnol Adv*, vol. 27, no. 5, pp. 562–567, Sep. 2009, doi: 10.1016/j.biotechadv.2009.04.010.

[33] R. Md Salim, J. Asik, and M. S. Sarjadi, "Chemical functional groups of extractives, cellulose and lignin extracted from native Leucaena leucocephala bark," *Wood Sci Technol*, vol. 55, no. 2, pp. 295–313, Mar. 2021, doi: 10.1007/s00226-020-01258-2.

[34] H. Yang, R. Yan, H. Chen, D. H. Lee, and C. Zheng, "Characteristics of hemicellulose, cellulose and lignin pyrolysis," *Fuel*, vol. 86, no. 12–13, pp. 1781–1788, Aug. 2007, doi: 10.1016/j.fuel.2006.12.013.

[35] S. Wang, H. Lin, B. Ru, W. Sun, Y. Wang, and Z. Luo, "Comparison of the pyrolysis behavior of pyrolytic lignin and milled wood lignin by using TG-FTIR analysis," *J Anal Appl Pyrolysis*, vol. 108, pp. 78–85, 2014, doi: 10.1016/j.jaap.2014.05.014.

[36] C. Chio, M. Sain, and W. Qin, "Lignin utilization: A review of lignin depolymerization from various aspects," *Renewable and Sustainable Energy Reviews*, vol. 107. Elsevier Ltd, pp. 232–249, Jun. 01, 2019. doi: 10.1016/j.rser.2019.03.008.

[37] H. B. Goyal, D. Seal, and R. C. Saxena, "Bio-fuels from thermochemical conversion of renewable resources: A review," *Renewable and Sustainable Energy Reviews*, vol. 12, no. 2, pp. 504–517, 2008, doi: 10.1016/j.rser.2006.07.014.

[38] R. E. Guedes, A. S. Luna, and A. R. Torres, "Operating parameters for bio-oil production in biomass pyrolysis: A review," *J Anal Appl Pyrolysis*, vol. 129, no. July 2017, pp. 134–149, 2018, doi: 10.1016/j.jaap.2017.11.019.

[39] Y. Shen and K. Yoshikawa, "Recent progresses in catalytic tar elimination during biomass gasification or pyrolysis - A review," *Renewable and Sustainable Energy Reviews*, vol. 21. pp. 371–392, 2013. doi: 10.1016/j.rser.2012.12.062.

[40] H. Yang, R. Yan, H. Chen, D. H. Lee, and C. Zheng, "Characteristics of hemicellulose, cellulose and lignin pyrolysis," *Fuel*, vol. 86, no. 12–13, pp. 1781–1788, 2006, doi: 10.1016/j.fuel.2006.12.013.

[41] M. Brebu and C. Vasile, "THERMAL DEGRADATION OF LIGNIN-A REVIEW," 2010.

[42] H. Kawamoto, "Lignin pyrolysis reactions," *Journal of Wood Science*, vol. 63, no. 2, pp. 117–132, 2017, doi: 10.1007/s10086-016-1606-z.

[43] C. A. Mullen and A. A. Boateng, "Catalytic pyrolysis-GC/MS of lignin from several sources," *Fuel Processing Technology*, vol. 91, no. 11, pp. 1446–1458, 2010, doi: 10.1016/j.fuproc.2010.05.022.

[44] M. Asmadi, H. Kawamoto, and S. Saka, "Thermal reactions of guaiacol and syringol as lignin model aromatic nuclei," *J Anal Appl Pyrolysis*, vol. 92, no. 1, pp. 88–98, 2011, doi: 10.1016/j.jaap.2011.04.011.

[45] T. Kotake, H. Kawamoto, and S. Saka, "Mechanisms for the formation of monomers and oligomers during the pyrolysis of a softwood lignin," *J Anal Appl Pyrolysis*, vol. 105, pp. 309–316, 2014, doi: 10.1016/j.jaap.2013.11.018.

[46] T. Kotake, H. Kawamoto, and S. Saka, "Pyrolytic formation of monomers from hardwood lignin as studied from the reactivities of the primary products," *J Anal Appl Pyrolysis*, vol. 113, pp. 57–64, May 2015, doi: 10.1016/j.jaap.2014.09.029.

[47] S. Saka, M. Asmadi, and H. Kawamoto, "Gas- and solid/liquid-phase reactions during pyrolysis of softwood and hardwood lignins," *J Anal Appl Pyrolysis*, vol. 92, no. 2, pp. 417–425, 2011.

[48] M. Asmadi, H. Kawamoto, and S. Saka, "Thermal reactions of guaiacol and syringol as lignin model aromatic nuclei," *J Anal Appl Pyrolysis*, vol. 92, no. 1, pp. 88–98, 2011, doi: 10.1016/j.jaap.2011.04.011.

[49] E. B. Ledesma, N. D. Marsh, A. K. Sandrowitz, and M. J. Wornat, "AN EXPERIMENTAL STUDY ON THE THERMAL DECOMPOSITION OF CATECHOL," 2002.

[50] K. Lopez Camas and A. Ullah, "Depolymerization of lignin into high-value products," *Biocatal Agric Biotechnol*, vol. 40, Mar. 2022, doi: 10.1016/j.bcab.2022.102306.

[51] T. Hosoya, H. Kawamoto, and S. Saka, "Role of methoxyl group in char formation from lignin-related compounds," *J Anal Appl Pyrolysis*, vol. 84, no. 1, pp. 79–83, 2009, doi: 10.1016/j.jaap.2008.10.024.

[52] Y. Han *et al.*, "Hydrotreatment of pyrolysis bio-oil: A review," *Fuel Processing Technology*, vol. 195, no. July, p. 106140, 2019, doi: 10.1016/j.fuproc.2019.106140.

[53] Y. Han *et al.*, "Hydrotreatment of pyrolysis bio-oil: A review," *Fuel Processing Technology*, vol. 195, no. July, 2019, doi: 10.1016/j.fuproc.2019.106140.

[54] F. Stankovikj, A. G. McDonald, G. L. Helms, and M. Garcia-Perez, *Quantification of Bio-Oil Functional Groups and Evidences of the Presence of Pyrolytic Humins*, vol. 30, no. 8. 2016. doi: 10.1021/acs.energyfuels.6b01242.

[55] M. Garcia-Perez, S. Wang, J. Shen, M. Rhodes, W. J. Lee, and C. Z. Li, "Effects of temperature on the formation of lignin-derived oligomers during the fast pyrolysis of

Mallee woody biomass," *Energy and Fuels*, vol. 22, no. 3, pp. 2022–2032, 2008, doi: 10.1021/ef7007634.

[56]   M. Garcia-Perez *et al.*, "Fast pyrolysis of oil mallee woody biomass: Effect of temperature on the yield and quality of pyrolysis products," *Ind Eng Chem Res*, vol. 47, no. 6, pp. 1846–1854, 2008, doi: 10.1021/ie071497p.

[57]   F. Stankovikj and M. Garcia-Perez, "TG-FTIR Method for the Characterization of Bio-oils in Chemical Families," *Energy and Fuels*, vol. 31, no. 2, pp. 1689–1701, 2017, doi: 10.1021/acs.energyfuels.6b03132.

[58]   F. Stankovikj, A. G. McDonald, G. L. Helms, M. V. Olarte, and M. Garcia-Perez, *Characterization of the Water-Soluble Fraction of Woody Biomass Pyrolysis Oils*, vol. 31, no. 2. 2017. doi: 10.1021/acs.energyfuels.6b02950.

[59]   S. Li, Z. Luo, W. Wang, K. Lu, Y. Yang, and X. Liang, "Characterization of pyrolytic lignin and insight into its formation mechanisms using novel techniques and DFT method," *Fuel*, vol. 262, Feb. 2020, doi: 10.1016/j.fuel.2019.116516.

[60]   Z. Sun, B. Fridrich, A. de Santi, S. Elangovan, and K. Barta, "Bright Side of Lignin Depolymerization: Toward New Platform Chemicals," *Chemical Reviews*, vol. 118, no. 2. American Chemical Society, pp. 614–678, Jan. 24, 2018. doi: 10.1021/acs.chemrev.7b00588.

[61]   L. Fan *et al.*, "Bio-oil from fast pyrolysis of lignin: Effects of process and upgrading parameters," *Bioresource Technology*, vol. 241. Elsevier Ltd, pp. 1118–1126, 2017. doi: 10.1016/j.biortech.2017.05.129.

[62]   Y. H. Chan *et al.*, "Fractionation and extraction of bio-oil for production of greener fuel and value-added chemicals: Recent advances and future prospects," *Chemical Engineering Journal*, vol. 397. Elsevier B.V., Oct. 01, 2020. doi: 10.1016/j.cej.2020.125406.

[63]   Q. Cai, T. Gong, T. Yu, and S. Zhang, "Comparison of hydrocracking and cracking of pyrolytic lignin over different Ni-based catalysts for light aromatics production," *Fuel Processing Technology*, vol. 240, p. 107564, Feb. 2023, doi: 10.1016/j.fuproc.2022.107564.

[64]   X. Zhu, L. L. Lobban, R. G. Mallinson, and D. E. Resasco, "Bifunctional transalkylation and hydrodeoxygenation of anisole over a Pt/HBeta catalyst," *J Catal*, vol. 281, no. 1, pp. 21–29, Jul. 2011, doi: 10.1016/j.jcat.2011.03.030.

[65]   S. Chen, "Green Oil Production by Hydroprocessing," *International Journal of Clean Coal and Energy*, vol. 01, no. 04, pp. 43–55, 2012, doi: 10.4236/ijcce.2012.14005.

[66]   Y. He, Y. Bie, J. Lehtonen, R. Liu, and J. Cai, "Hydrodeoxygenation of guaiacol as a model compound of lignin-derived pyrolysis bio-oil over zirconia-supported Rh

catalyst: Process optimization and reaction kinetics," *Fuel*, vol. 239, no. August 2018, pp. 1015–1027, 2019, doi: 10.1016/j.fuel.2018.11.103.

[67] M. Auersvald *et al.*, "Hydrotreatment of straw bio-oil from ablative fast pyrolysis to produce suitable refinery intermediates," *Fuel*, vol. 238, no. June 2018, pp. 98–110, 2019, doi: 10.1016/j.fuel.2018.10.090.

[68] M. B. Figueirêdo, P. J. Deuss, R. H. Venderbosch, and H. J. Heeres, "Catalytic hydrotreatment of pyrolytic lignins from different sources to biobased chemicals: Identification of feed-product relations," *Biomass Bioenergy*, vol. 134, no. January, 2020, doi: 10.1016/j.biombioe.2020.105484.

[69] C. Amen-Chen, H. Pakdel, and C. Roy, "Production of monomeric phenols by thermochemical conversion of biomass: a review."

[70] X. Zhang, Q. Chen, Q. Zhang, C. Wang, L. Ma, and Y. Xu, "Conversion of pyrolytic lignin to aromatic hydrocarbons by hydrocracking over pristine MoO3 catalyst," *J Anal Appl Pyrolysis*, vol. 135, pp. 60–66, Oct. 2018, doi: 10.1016/j.jaap.2018.09.020.

[71] B. Hu *et al.*, "Advances on the fast pyrolysis of biomass for the selective preparation of phenolic compounds," *Fuel Processing Technology*, vol. 237. Elsevier B.V., Dec. 01, 2022. doi: 10.1016/j.fuproc.2022.107465.

[72] S. Wang, G. Dai, H. Yang, and Z. Luo, "Lignocellulosic biomass pyrolysis mechanism: A state-of-the-art review," *Prog Energy Combust Sci*, vol. 62, pp. 33–86, 2017, doi: 10.1016/j.pecs.2017.05.004.

[73] S. Wang *et al.*, "Pyrolysis of wood/biomass for bio-oil: a critical review.," *Prog Energy Combust Sci*, vol. 62, no. 4, pp. 848–889, 2017, doi: 10.1021/ef0502397.

[74] L. Zhang, S. Zhang, X. Hu, and M. Gholizadeh, "Progress in application of the pyrolytic lignin from pyrolysis of biomass," *Chemical Engineering Journal*, vol. 419. Elsevier B.V., Sep. 01, 2021. doi: 10.1016/j.cej.2021.129560.

[75] V. K. Ponnusamy *et al.*, "A review on lignin structure, pretreatments, fermentation reactions and biorefinery potential," *Bioresour Technol*, vol. 271, no. September 2018, pp. 462–472, 2019, doi: 10.1016/j.biortech.2018.09.070.

[76] J. Ralph, C. Lapierre, and W. Boerjan, "Lignin structure and its engineering," *Current Opinion in Biotechnology*, vol. 56. Elsevier Ltd, pp. 240–249, Apr. 01, 2019. doi: 10.1016/j.copbio.2019.02.019.

[77] E. Rosini *et al.*, "Cascade enzymatic cleavage of the β-O-4 linkage in a lignin model compound," *Catal Sci Technol*, vol. 6, no. 7, pp. 2195–2205, Apr. 2016, doi: 10.1039/c5cy01591j.

[78] T. Hosoya, H. Kawamoto, and S. Saka, "Role of methoxyl group in char formation from lignin-related compounds," *J Anal Appl Pyrolysis*, vol. 84, no. 1, pp. 79–83, 2009, doi: 10.1016/j.jaap.2008.10.024.

[79] X. Jiang, Q. Lu, B. Hu, J. Liu, C. Dong, and Y. Yang, "Intermolecular interaction mechanism of lignin pyrolysis: A joint theoretical and experimental study," *Fuel*, vol. 215, pp. 386–394, Mar. 2018, doi: 10.1016/j.fuel.2017.11.084.

[80] B. Hu *et al.*, "Hydroxyl-Assisted Hydrogen Transfer Interaction in Lignin Pyrolysis: An Extended Concerted Interaction Mechanism," *Energy and Fuels*, vol. 35, no. 16, pp. 13170–13180, Aug. 2021, doi: 10.1021/acs.energyfuels.1c01606.

[81] Y. Huang, H. Wang, X. Zhang, Q. Zhang, C. Wang, and L. Ma, "CO2 pyrolysis kinetics and characteristics of lignin-rich hydrolysis residue produced from a tandem process of steam-stripping and acid hydrolysis," *Fuel*, vol. 316, May 2022, doi: 10.1016/j.fuel.2022.123361.

[82] L. Wang *et al.*, "Fast pyrolysis of guaiacyl-syringyl (GS) type milled wood lignin: Product characteristics and CH4 formation mechanism study," *Science of the Total Environment*, vol. 838, Sep. 2022, doi: 10.1016/j.scitotenv.2022.156395.

[83] E. Terrell and M. Garcia-Perez, "Vacuum Pyrolysis of Hybrid Poplar Milled Wood Lignin with Fourier Transform-Ion Cyclotron Resonance Mass Spectrometry Analysis of Feedstock and Products for the Elucidation of Reaction Mechanisms," *Energy and Fuels*, vol. 34, no. 11, pp. 14249–14263, Nov. 2020, doi: 10.1021/acs.energyfuels.0c02928.

[84] X. Fu, Q. Li, and C. Hu, "Identification and structural characterization of oligomers formed from the pyrolysis of biomass," *J Anal Appl Pyrolysis*, vol. 144, Nov. 2019, doi: 10.1016/j.jaap.2019.104696.

[85] V. Dhyani and T. Bhaskar, "A comprehensive review on the pyrolysis of lignocellulosic biomass," *Renew Energy*, vol. 129, pp. 695–716, 2018, doi: 10.1016/j.renene.2017.04.035.

[86] J. Huang, C. Liu, H. Tong, W. Li, and D. Wu, "A density functional theory study on formation mechanism of CO, CO2 and CH4 in pyrolysis of lignin," *Comput Theor Chem*, vol. 1045, pp. 1–9, Oct. 2014, doi: 10.1016/j.comptc.2014.06.009.

[87] I. Fonts *et al.*, "Thermodynamic and physical property estimation of compounds derived from the fast pyrolysis of lignocellulosic materials," *Energy and Fuels*, vol. 35, no. 21, pp. 17114–17137, Nov. 2021, doi: 10.1021/acs.energyfuels.1c01709.

[88] E. Terrell, "Estimation of Hansen solubility parameters with regularized regression for biomass conversion products: An application of adaptable group contribution," *Chem Eng Sci*, vol. 248, Feb. 2022, doi: 10.1016/j.ces.2021.117184.

[89]   E. Leng, Y. Guo, J. Chen, S. Liu, J. E, and Y. Xue, "A comprehensive review on lignin pyrolysis: Mechanism, modeling and the effects of inherent metals in biomass," *Fuel*, vol. 309, no. October 2021, p. 122102, 2022, doi: 10.1016/j.fuel.2021.122102.

[90]   P. F. Britt, A. C. Buchanan, M. J. Cooney, and D. R. Martineau, "Flash vacuum pyrolysis of methoxy-substituted lignin model compounds," *Journal of Organic Chemistry*, vol. 65, no. 5, pp. 1376–1389, Mar. 2000, doi: 10.1021/jo991479k.

[91]   P. F. Britt, A. C. Buchanan, and E. A. Malcolm, "Thermolysis of Phenethyl Phenyl Ether: A Model for Ether Linkages in Lignin and Low Rank Coal," 1995. doi: https://doi.org/10.1021/jo00125a044.

[92]   S. Zhou, B. Pecha, M. van Kuppevelt, A. G. McDonald, and M. Garcia-Perez, "Slow and fast pyrolysis of Douglas-fir lignin: Importance of liquid-intermediate formation on the distribution of products," *Biomass Bioenergy*, vol. 66, pp. 398–409, 2014, doi: 10.1016/j.biombioe.2014.03.064.

[93]   Y. Fan *et al.*, "Elucidating radical-mediated pyrolysis behaviors of preoxidized lignins," *Bioresour Technol*, vol. 350, Apr. 2022, doi: 10.1016/j.biortech.2022.126908.

[94]   M. Lei, S. Wu, J. Liang, and C. Liu, "Comprehensive understanding the chemical structure evolution and crucial intermediate radical in situ observation in enzymatic hydrolysis/mild acidolysis lignin pyrolysis," *J Anal Appl Pyrolysis*, vol. 138, pp. 249–260, Mar. 2019, doi: 10.1016/j.jaap.2019.01.004.

[95]   J. M. Younker, A. Beste, and A. C. Buchanan, "Computational study of bond dissociation enthalpies for substituted β-O-4 lignin model compounds," *ChemPhysChem*, vol. 12, no. 18, pp. 3556–3565, 2011, doi: 10.1002/cphc.201100477.

[96]   Y. Ünal, W. Nassif, B. C. Özaydin, and K. Sayin, "Scale factor database for the vibration frequencies calculated in M06-2X, one of the DFT methods," *Vib Spectrosc*, vol. 112, Jan. 2021, doi: 10.1016/j.vibspec.2020.103189.

[97]   F. Stankovikj and M. Garcia-perez, "TG-FTIR Method for the Characterization of Bio-oils in Chemical Families," *Energy & Fuels*, vol. 30, no. 8, pp. 1689–1701, 2017, doi: 10.1021/acs.energyfuels.6b03132.

[98]   S. E. Stein and R. L. Brown, "Estimation of Normal Boiling Points from Group Contributions," 1994. doi: https://doi.org/10.1021/ci00019a016.

[99]   M. Satou, D. Itoh, H. Hattori, and T. Yoshida, "Evaluation of ring size distribution in a heavy oil based on boiling point and molecular weight distributions," 2000. doi: https://doi.org/10.1016/S0016-2361(99)00168-4.

[100]   W. Yuan, A. C. Hansen, and Q. Zhang, "Vapor pressure and normal boiling point predictions for pure methyl esters and biodiesel fuels," *Fuel*, vol. 84, no. 7–8, pp. 943–950, May 2005, doi: 10.1016/j.fuel.2005.01.007.

[101]   Al. L. Lydersen, R. A. Greenkorn, and O. A. Hougen, "Estimation of critical properties of organic compounds," Madison, 1955. Accessed: Feb. 06, 2023. [Online]. Available: https://scholar.google.com/scholar_lookup?hl=en&publication_year=1955&author=A.+L.+Lydersen&author=R.+A.+Greenkorn&author=O.+A.+Hougen&title=Estimation+of+Critical+Properties+of+Organic+Compounds

[102]   K. G. Joback, "A unified approach to physical property estimation using multivariate statistical techniques." 1984.

[103]   E. Stefanis and C. Panayiotou, "Prediction of Hansen Solubility Parameters with a New Group-Contribution Method," *Int J Thermophys*, vol. 29, pp. 568–585, 2008, doi: 10.1007/s10765-008-0415-z.

[104]   C. F. Chueh and A. C. Swanson, "Estimation of Liquid Heat Capacity," *Can J Chem Eng*, vol. 51, 1973.

[105]   J. E. Hurst and B. K. Harrison, "Estimation of liquid and solid heat capacities using a modified kopp's rule," *Chem Eng Commun*, vol. 112, no. 1, pp. 21–30, 1992, doi: 10.1080/00986449208935989.

[106]   B. Keith Harrison and W. H. Seaton, "Solution to Missing Group Problem for Estimation of Ideal Gas Heat Capacities," *Ind Eng Chem Res*, vol. 27, no. 8, pp. 1536–1540, 1988, doi: 10.1021/ie00080a031.

[107]   I. Fonts *et al.*, "Thermodynamic and Physical Property Estimation of Compounds Derived from the Fast Pyrolysis of Lignocellulosic Materials," *Energy and Fuels*, 2021, doi: 10.1021/acs.energyfuels.1c01709.

[108]   M. Lei, S. Wu, C. Liu, J. Liang, and R. Xiao, "Revealing the pyrolysis behavior of 5-5′ biphenyl-type lignin fragment. Part I: A mechanistic study on fragmentation via experiments and theoretical calculation," *Fuel Processing Technology*, vol. 217, Jun. 2021, doi: 10.1016/j.fuproc.2021.106812.

[109]   D. Chen, K. Cen, X. Cao, F. Chen, J. Zhang, and J. Zhou, "Insight into a new phenolic-leaching pretreatment on bamboo pyrolysis: Release characteristics of pyrolytic volatiles, upgradation of three phase products, migration of elements, and energy yield," *Renewable and Sustainable Energy Reviews*, vol. 136, Feb. 2021, doi: 10.1016/j.rser.2020.110444.

[110] C. Li *et al.*, "Quantification of Nanoplastic Uptake in Cucumber Plants by Pyrolysis Gas Chromatography/Mass Spectrometry," *Environ Sci Technol Lett*, vol. 8, no. 8, pp. 633–638, Aug. 2021, doi: 10.1021/acs.estlett.1c00369.

[111] Z. Pan, A. Puente-Urbina, A. Bodi, J. A. van Bokhoven, and P. Hemberger, "Isomer-dependent catalytic pyrolysis mechanism of the lignin model compounds catechol, resorcinol and hydroquinone," *Chem Sci*, vol. 12, no. 9, pp. 3161–3169, Mar. 2021, doi: 10.1039/d1sc00654a.

[112] Q. Zhou, Z. Luo, G. Li, and S. Li, "EPR detection of key radicals during coking process of lignin monomer pyrolysis," *J Anal Appl Pyrolysis*, vol. 152, Nov. 2020, doi: 10.1016/j.jaap.2020.104948.

[113] G. Paul and J. Gajewski, "Benzoquinone Methide: An Intermediate in the Gas-Phase Pyrolysis of Chroman," *J. Org. Chem*, vol. 58, pp. 5060–5062, 1993.

[114] T. Kotake, H. Kawamoto, and S. Saka, "Pyrolytic formation of monomers from hardwood lignin as studied from the reactivities of the primary products," *J Anal Appl Pyrolysis*, vol. 113, pp. 57–64, May 2015, doi: 10.1016/j.jaap.2014.09.029.

[115] E. Terrel and M. Garcia-Perez, "Novel Strategy to analyze FT-ICR MS data of biomass pyrolysis oil for oligomeric structure assignment," 2020.

[116] N. Aktaş, N. Şahiner, Ö. Kantoğlu, B. Salih, and A. Tanyolaç, "Biosynthesis and Characterization of Laccase Catalyzed Poly(Catechol)," *J Polym Environ*, vol. 11, no. 3, pp. 123–128, 2003, doi: 10.1023/A:1024639231900.

[117] P. W. Hsieh, S. A. Al-Suwayeh, C. L. Fang, C. F. Lin, C. C. Chen, and J. Y. Fang, "The co-drug of conjugated hydroquinone and azelaic acid to enhance topical skin targeting and decrease penetration through the skin," *European Journal of Pharmaceutics and Biopharmaceutics*, vol. 81, no. 2, pp. 369–378, Jun. 2012, doi: 10.1016/j.ejpb.2012.03.006.

[118] Y. Wang, S. Wang, F. Leng, J. Chen, L. Zhu, and Z. Luo, "Separation and characterization of pyrolytic lignins from the heavy fraction of bio-oil by molecular distillation," *Sep Purif Technol*, vol. 152, pp. 123–132, Aug. 2015, doi: 10.1016/j.seppur.2015.08.011.

[119] S. Wang, Y. Wang, Q. Cai, X. Wang, H. Jin, and Z. Luo, "Multi-step separation of monophenols and pyrolytic lignins from the water-insoluble phase of bio-oil," *Sep Purif Technol*, vol. 122, pp. 248–255, Feb. 2014, doi: 10.1016/j.seppur.2013.11.017.

[120] J. Y. Kim, H. Hwang, S. Oh, Y. S. Kim, U. J. Kim, and J. W. Choi, "Investigation of structural modification and thermal characteristics of lignin after heat treatment," *Int*

J Biol Macromol, vol. 66, pp. 57–65, May 2014, doi: 10.1016/j.ijbiomac.2014.02.013.

[121]   B. Scholze, C. Hanser, and D. Meier, "Characterization of the water-insoluble fraction from fast pyrolysis liquids (pyrolytic lignin) Part II. GPC, carbonyl goups, and 13 C-NMR," 2001. [Online]. Available: www.elsevier.com/locate/jaap

[122]   A. R. Teixeira *et al.*, "Aerosol generation by reactive boiling ejection of molten cellulose," *Energy Environ Sci*, vol. 4, no. 10, pp. 4306–4321, 2011, doi: 10.1039/c1ee01876k.

[123]   M. B. Pecha *et al.*, "Effect of Pressure on Pyrolysis of Milled Wood Lignin and Acid-Washed Hybrid Poplar Wood," *Ind Eng Chem Res*, vol. 56, no. 32, pp. 9079–9089, Aug. 2017, doi: 10.1021/acs.iecr.7b02085.

[124]   S. E. Stein and R. L. Brown, "Estimation of Normal Boiling Points from Group Contributions," 1994. [Online]. Available: https://pubs.acs.org/sharingguidelines

[125]   C. Stephan, M. Dicko, P. Stringari, and C. Coquelet, "Liquid-liquid equilibria of water + solutes (acetic acid/ acetol/furfural/guaiacol/methanol/phenol/propanal) + solvents (isopropyl acetate/toluene) ternary systems for pyrolysis oil fractionation," *Fluid Phase Equilib*, vol. 468, pp. 49–57, Jul. 2018, doi: 10.1016/j.fluid.2018.04.016.

[126]   Y. Wang, S. Wang, F. Leng, J. Chen, L. Zhu, and Z. Luo, "Separation and characterization of pyrolytic lignins from the heavy fraction of bio-oil by molecular distillation," *Sep Purif Technol*, vol. 152, pp. 123–132, Aug. 2015, doi: 10.1016/j.seppur.2015.08.011.

[127]   R. V. S. Silva, V. B. Pereira, K. T. Stelzer, T. A. Almeida, G. A. Romeiro, and D. A. Azevedo, "Comprehensive study of the liquid products from slow pyrolysis of crambe seeds: Bio-oil and organic compounds of the aqueous phase," *Biomass Bioenergy*, vol. 123, pp. 78–88, Apr. 2019, doi: 10.1016/j.biombioe.2019.02.014.

[128]   B. Scholze and D. Meier, "Characterization of the water-insoluble fraction from pyrolysis oil (pyrolytic lignin). Part I . PY – GC / MS , FTIR , and functional groups," vol. 60, pp. 41–54, 2001.

[129]   A. Oasmaa, I. Fonts, M. R. Pelaez-Samaniego, M. E. Garcia-Perez, and M. Garcia-Perez, *Pyrolysis Oil Multiphase Behavior and Phase Stability: A Review*, vol. 30, no. 8. 2016. doi: 10.1021/acs.energyfuels.6b01287.

[130]   F. Stankovikj, A. G. McDonald, G. L. Helms, M. V. Olarte, and M. Garcia-Perez, "Characterization of the Water-Soluble Fraction of Woody Biomass Pyrolysis Oils," *Energy and Fuels*, vol. 31, no. 2, pp. 1650–1664, Feb. 2017, doi: 10.1021/acs.energyfuels.6b02950.

[131] J. Shi, D. Xing, and J. Li, "FTIR studies of the changes in wood chemistry from wood forming tissue under inclined treatment," in *Energy Procedia*, Elsevier Ltd, 2012, pp. 758–762. doi: 10.1016/j.egypro.2012.01.122.

[132] T. Kishimoto, Y. Uraki, and M. Ubukata, "Synthesis of β-O-4-type artificial lignin polymers and their analysis by NMR spectroscopy," *Org Biomol Chem*, vol. 6, no. 16, pp. 2982–2987, 2008, doi: 10.1039/b805460f.

[133] B. Sukhbaatar, P. H. Steele, and M. G. Kim, "Bio-oil lignin for OSB binder," 2009.

[134] X. Dong, M. Dong, Y. Lu, A. Turley, T. Jin, and C. Wu, "Antimicrobial and antioxidant activities of lignin from residue of corn stover to ethanol production," *Ind Crops Prod*, vol. 34, no. 3, pp. 1629–1634, Nov. 2011, doi: 10.1016/j.indcrop.2011.06.002.

[135] X. Huang, T. I. Korányi, M. D. Boot, and E. J. M. Hensen, "Ethanol as capping agent and formaldehyde scavenger for efficient depolymerization of lignin to aromatics," *Green Chemistry*, vol. 17, no. 11, pp. 4941–4950, Jun. 2015, doi: 10.1039/c5gc01120e.

[136] F. Leng, Y. Wang, J. Chen, S. Wang, J. Zhou, and Z. Luo, "Characterization of pyrolytic lignins with different activities obtained from bio-oil," *Chin J Chem Eng*, vol. 25, no. 3, pp. 324–329, Mar. 2017, doi: 10.1016/j.cjche.2016.06.015.

[137] B. Panchal *et al.*, "Synthesis of Generation-2 polyamidoamine based ionic liquid: Efficient dendrimer based catalytic green fuel production from yellow grease," *Energy*, vol. 219, Mar. 2021, doi: 10.1016/j.energy.2020.119637.

[138] L. Zhang, S. Zhang, X. Hu, and M. Gholizadeh, "Progress in application of the pyrolytic lignin from pyrolysis of biomass," *Chemical Engineering Journal*, vol. 419. Elsevier B.V., Sep. 01, 2021. doi: 10.1016/j.cej.2021.129560.

[139] X. Hu *et al.*, "Polymerization on heating up of bio-oil: A model compound study," *AIChE Journal*, vol. 59, no. 3, pp. 888–900, Mar. 2013, doi: 10.1002/aic.13857.

[140] A. Afshar Taromi and S. Kaliaguine, "Green diesel production via continuous hydrotreatment of triglycerides over mesostructured Γ-alumina supported NiMo/CoMo catalysts," *Fuel Processing Technology*, vol. 171, pp. 20–30, Mar. 2018, doi: 10.1016/j.fuproc.2017.10.024.

[141] Y. Han, F. Stankovikj, and M. Garcia-Perez, "Co-hydrotreatment of tire pyrolysis oil and vegetable oil for the production of transportation fuels," *Fuel Processing Technology*, vol. 159, pp. 328–339, 2017, doi: 10.1016/j.fuproc.2017.01.048.

[142] D. C. Lv, K. Jiang, K. Li, Y. Q. Liu, D. Wang, and Y. Y. Ye, "Effective suppression of coke formation with lignin-derived oil during the upgrading of pyrolysis oils," *Biomass Bioenergy*, vol. 159, Apr. 2022, doi: 10.1016/j.biombioe.2022.106425.

[143] Y. Han, A. P. P. Pires, and M. Garcia-Perez, "Co-hydrotreatment of the Bio-oil Lignin-Rich Fraction and Vegetable Oil," *Energy and Fuels*, vol. 34, no. 1, pp. 516–529, Jan. 2020, doi: 10.1021/acs.energyfuels.9b03344.

[144] P. Vozka and G. Kilaz, "How to obtain a detailed chemical composition for middle distillates via GC × GC-FID without the need of GC × GC-TOF/MS," *Fuel*, vol. 247, pp. 368–377, Jul. 2019, doi: 10.1016/j.fuel.2019.03.009.

[145] A. P. P. Pires, Y. Han, J. Kramlich, and M. Garcia-Perez, "Alternative jet fuel properties," 2018.

[146] S. A. Channiwala and P. P. Parikh, "A unified correlation for estimating HHV of solid, liquid and gaseous fuels." [Online]. Available: http://www.fuel

[147] A. P. Richards, D. Haycock, J. Frandsen, and T. H. Fletcher, "A review of coal heating value correlations with application to coal char, tar, and other fuels," *Fuel*, vol. 283. Elsevier Ltd, Jan. 01, 2021. doi: 10.1016/j.fuel.2020.118942.

[148] S. G. Sourelis, "The hydrogenation process," *J Am Oil Chem Soc*, vol. 33, no. 10, pp. 488–494, 1956, doi: 10.1007/BF02612307.

[149] M. C. Vásquez, E. E. Silva, and E. F. Castillo, "Hydrotreatment of vegetable oils: A review of the technologies and its developments for jet biofuel production," *Biomass and Bioenergy*, vol. 105. Elsevier Ltd, pp. 197–206, 2017. doi: 10.1016/j.biombioe.2017.07.008.

[150] Z. Zhang *et al.*, "LDH derived Co-Al nanosheet for lipid hydrotreatment to produce green diesel," *Fuel*, vol. 333, Feb. 2023, doi: 10.1016/j.fuel.2022.126341.

[151] S. Kadarwati *et al.*, "Coke formation during the hydrotreatment of bio-oil using NiMo and CoMo catalysts," *Fuel Processing Technology*, vol. 155, pp. 261–268, Jan. 2017, doi: 10.1016/j.fuproc.2016.08.021.

[152] R. H. Venderbosch, A. R. Ardiyanti, J. Wildschut, A. Oasmaa, and H. J. Heeres, "Stabilization of biomass-derived pyrolysis oils," *Journal of Chemical Technology and Biotechnology*, vol. 85, no. 5, pp. 674–686, May 2010, doi: 10.1002/jctb.2354.

[153] Z. Tang, Y. Zhang, and Q. Guo, "Catalytic hydrocracking of pyrolytic lignin to liquid fuel in supercritical ethanol," *Ind Eng Chem Res*, vol. 49, no. 5, pp. 2040–2046, Mar. 2010, doi: 10.1021/ie9015842.

[154] C. C. Schmitt *et al.*, "Hydrotreatment of Fast Pyrolysis Bio-oil Fractions Over Nickel-Based Catalyst," *Top Catal*, vol. 61, no. 15–17, pp. 1769–1782, Oct. 2018, doi: 10.1007/s11244-018-1009-z.

[155] T. A. Al-Attas *et al.*, "Recent Advances in Heavy Oil Upgrading Using Dispersed Catalysts," *Energy and Fuels*, vol. 33, no. 9, pp. 7917–7949, Sep. 2019, doi: 10.1021/acs.energyfuels.9b01532.

[156] Y. W. Chua, Y. Yu, and H. Wu, "Thermal decomposition of pyrolytic lignin under inert conditions at low temperatures," *Fuel*, vol. 200, pp. 70–75, 2017, doi: 10.1016/j.fuel.2017.03.035.

[157] M. B. Figueirêdo, Z. Jotic, P. J. Deuss, R. H. Venderbosch, and H. J. Heeres, "Hydrotreatment of pyrolytic lignins to aromatics and phenolics using heterogeneous catalysts," *Fuel Processing Technology*, vol. 189, pp. 28–38, Jun. 2019, doi: 10.1016/j.fuproc.2019.02.020.

[158] A. Afshar Taromi and S. Kaliaguine, "Green diesel production via continuous hydrotreatment of triglycerides over mesostructured Γ-alumina supported NiMo/CoMo catalysts," *Fuel Processing Technology*, vol. 171, pp. 20–30, Mar. 2018, doi: 10.1016/j.fuproc.2017.10.024.

[159] G. Zhou *et al.*, "Preparation and characterization of NiW-nHA composite catalyst for hydrocracking," *Nanoscale*, vol. 4, no. 24, pp. 7698–7703, 2012, doi: 10.1039/c2nr31486j.

[160] L. M. Orozco, D. A. Echeverri, L. Sánchez, and L. A. Rios, "Second-generation green diesel from castor oil: Development of a new and efficient continuous-production process," *Chemical Engineering Journal*, vol. 322, pp. 149–156, 2017, doi: 10.1016/j.cej.2017.04.027.

[161] S. Zhou, M. Garcia-Perez, B. Pecha, A. G. McDonald, S. R. A. Kersten, and R. J. M. Westerhof, "Secondary vapor phase reactions of lignin-derived oligomers obtained by fast pyrolysis of pine wood," *Energy and Fuels*, vol. 27, no. 3, pp. 1428–1438, Mar. 2013, doi: 10.1021/ef3019832.

[162] S. Wang, H. Lin, B. Ru, W. Sun, Y. Wang, and Z. Luo, "Comparison of the pyrolysis behavior of pyrolytic lignin and milled wood lignin by using TG-FTIR analysis," *J Anal Appl Pyrolysis*, vol. 108, pp. 78–85, 2014, doi: 10.1016/j.jaap.2014.05.014.

[163] C.-Z. Li, F. Wu, H.-Y. Cai, and R. Kandiyoti, "UV-Fluorescence Spectroscopy of Coal Pyrolysis Tars," 1994. [Online]. Available: https://pubs.acs.org/sharingguidelines

[164] M. Gholizadeh *et al.*, "Different reaction behaviours of the light and heavy components of bio-oil during the hydrotreatment in a continuous pack-bed reactor," *Fuel Processing Technology*, vol. 146, pp. 76–84, Jun. 2016, doi: 10.1016/j.fuproc.2016.01.026.

[165] R. K. Sharma *et al.*, "Jatropha-oil conversion to liquid hydrocarbon fuels using
       mesoporous titanosilicate supported sulfide catalysts," *Catal Today*, vol. 198, no. 1,
       pp. 314–320, Dec. 2012, doi: 10.1016/j.cattod.2012.05.036.

[166] L. M. Balster, S. Zabarnick, R. C. Striebich, L. M. Shafer, and Z. J. West, "Analysis
       of polar species in jet fuel and determination of their role in autoxidative deposit
       formation," *Energy and Fuels*, vol. 20, no. 6, pp. 2564–2571, Nov. 2006, doi:
       10.1021/ef060275l.